T.C.
REPUBLIC OF TURKEY
HACETTEPE UNIVERSITY
INSTITUTE OF HEALTH SCIENCES

ELECTROPHYSIOLOGICAL EFFECTS OF ESLICARBAZEPINE ON SELECTED $Na_v1.6$ VARIANTS ASSOCIATED WITH DEVELOPMENTAL AND EPILEPTIC ENCEPHALOPATHIES

Erva BAYRAKTAR, MPharm

Medical Pharmacology Program

DOCTOR OF PHILOSOPHY THESIS

ANKARA

2020

ABSTRACT

Bayraktar, E., Electrophysiological effects of Eslicarbazepine on selected $Na_v1.6$ variants associated with developmental and epileptic encephalopathies, Hacettepe University Graduate School of Health Sciences Medical Pharmacology Doctor of Philosophy Thesis, Ankara, 2020. Major problems with the current anti-epileptic drugs (AED) are resistance, inability to modify the course of the disease and side effects profiles, which rises the need for improved AEDs for all age group of patients. Eslicarbazepine acetate is a sodium channel blocker AED and is superior to some other well-known AEDs in terms of selectivity, safety, efficacy and effects on sodium channels. In our study, to assess eslicarbazepine (S-Lic) effects, we chose wild-type $Na_v1.6$ channels along with three *SCN8A* gene variants known to be causing developmental and epileptic encephalopathies (DEE), (M1760I, G1475R, and A1622D). Electrophysiological analyses were performed by using two heterologous expression systems (neuroblastoma cell line (ND7/23) for voltage-clamp recordings, and primary neuronal cultures for current-clamp recordings). 300 µM of S-Lic reduced maximal firing rates in neurons having wild-type $Na_V1.6$ channels. S-Lic enhanced slow inactivation kinetics in all DEE variants tested, but also displayed variant-specific effects by modifying biophysical properties of tested variant channels. S-Lic treatment increased the kinetics of fast inactivation and reduced the persistent current in A1622D variant. Additionally, S-Lic decreased neuronal firing rate to that of wild-type in M1760I variant. Those findings emphasize the significance of individualized therapy, and prompt the potential use of Eslicarbazepine acetate, -taking into account its unique effects on epileptogenesis and slow inactivation, and its better safety and therapeutic index – as an alternative option against some *SCN8A* ($Na_V1.6$) variants causing DEE.

Key Words: Epilepsy, Developmental and Epileptic encephalopathies, Eslicarbazepine acetate, $Na_v1.6$, M1760I, A1622D, G1475R, Sodium channel blockers, Voltage-clamp, Current-clamp.

Supporting Organizations: This work will was supported by BIAL – Portela & Ca, S.A.

ÖZET

Bayraktar, E., Gelişimsel ve epileptik ensefalopatilerle ile ilişkili seçilmiş $Na_v1.6$ varyantlarında eslikarbazepinin elektrofizyolojik etkileri, Hacettepe Üniversitesi Sağlık Bilimleri Enstitüsü Tıbbi Farmakoloji Doktora Tezi, Ankara, 2020. Günümüz kullanımında yer alan antiepileptik ilaçların (AEİ) direnç gelişimi, hastalık seyrini modifiye etmedeki yetersizliği ve yan etki profilinin geniş olması gibi problemlerinin bulunması tüm yaş gruplarındaki hastalarda daha gelişmiş AEİ seçeneklerine ihtiyacı doğurmaktadır. Eslikarbazepin asetat sodyum kanal blokajı yapan bir AEİ olup seçicilik, güvenlilik, etkililik ve sodyum kanallarına etki açılarından iyi bilinen diğer sodyum kanal blokörü AEİ'lere nazaran daha üstündür. Çalışmamızda eslikarbazepinin (S-Lic) etkilerini incelemek amacıyla yabanıl tip $Na_v1.6$ kanallarınının yanı sıra gelişimsel ve epileptik ensefalopatilere (GEE) neden olduğu bilinen üç farklı *SCN8A* gen varyantı (M1760I, G1475R ve A1622D) seçilmiştir. Seçilen varyantlarda elektrofizyolojik çalışmalar iki heterolog ekspresyon sisteminde gerçekleştirildi (voltaj kenetleme kayıtları için neuroblastom hücre serileri (ND7/23), akım kenetleme kayıtları için primer nöron kültürleri). 300 µM S-Lic yabanıl tip $Na_v1.6$ kanallarına sahip nöronlarda maksimum ateşleme hızını azalttı. S-Lic yavaş inaktivasyon kinetiğini test edilen tüm GEE varyantlarında güçlendirdi, aynı zamanda test edilen bazı varyant kanallarının biyofiziksel özelliklerini modifiye ederek varyant spesifik etkiler gösterdi. S-Lic tedavisi A1622D varyantında hızlı inaktivasyon kinetiklerini artırırken kalıcı akımı azalttı. Ek olarak, S-Lic M1760I varyantında nöronal ateşleme hızını yabanıl tip seviyesine indirdi. Bu bulgular kişiselleştirilmiş tedavinin önemini vurgulamanın yanında; epileptogenez ve yavaş inaktivasyon üzerine benzersiz etkisi, terapötik indeks genişliği ve güvenliliği ile eslikarbazepin asetatın GEE'ye neden olan bazı *SCN8A* varyantlarında alternatif tedavi olarak kullanılmasını desteklemektedir.

Anahtar Kelimeler: Epilepsi, gelişimsel ve epileptik ensefalopatiler, eslikarbazepin asetat, $Na_v1.6$, M1760I, A1622D, G1475R, Sodyum kanal blokörleri, Voltaj kenetleme, Akım kenetleme.

Destekleyen kurum: Bu çalışma BIAL – Portela & Ca, S.A tarafından desteklenmiştir.

TABLE OF CONTENTS

SYMBOLS AND ABBREVIATIONS

AED	Antiepileptic drug
AP	Action potential
AUC	Area under the curve
CAMKII	Calcium/calmodulin-dependent kinase II
CBZ	Carbamazepine
cDNA	Complementary DNA
CNS	Central nervous system
CYP3A4	Cytochrome P450 3A4
DEE	Developmental and epileptic encephalopathy
DMEM	Dulbecco's Modified Eagle Medium
DMSO	Dimethyl sulfoxide
FBS	Fetal bovine serum
FI	Fast inactivation
GAD67	Glutamic Acid Decarboxylase 67 Kd
GFP	Green-florescent protein
g_{max}	Maximum conductance
GOF	Gain of function
h	Hour
HBSS	Hank's Balanced Salt Solution
I-Clamp	Current-clamp
I_{max}	Maximal current amplitude
kg	Kilogram
kHz	Kilohertz
k_V	Slope factor
LOF	Loss of function
min	Minute
ms	Millisecond

mM	Milli molar
mOsm	Milliosmole
mV	Millivolt
MΩ	Mega ohm
nA	Nano ampere
Na^+	Sodium
OXC	Oxcarbazepine
PBS	Phosphate buffered saline
PHT	Phenytoin
PNS	Peripheral nervous system
RT	Room temperature
s	Second
SCB	Sodium channel blocker
SEM	Standard error of the mean
SI	Slow inactivation
S-Lic	Eslicarbazepine
S-Lic-A	Eslicarbazepine acetate
TTX	Tetrodotoxin
UGT	Uridine 5'diphospoglucuronosyl transferase
V-Clamp	Voltage-clamp
VGSC	Voltage-gated sodium channels
V_{rev}	Reversal potential of Na^+
$V_{1/2}$	Voltage at half-maximum
WT	Wild-type
α	Alpha
β	Beta
τ	Time constant
µM	Micro molar

LIST OF FIGURES

LIST OF TABLES

1. INTRODUCTION

The voltage-gated sodium channels (VGSC) consist mainly of an alpha (α) subunit and auxiliary beta (β) subunits (1). The α-subunit in those channels forms the ion pore and is accountable for the voltage sensitivity of the channel, whereas the auxiliary β subunits act in a regulatory manner (2, 3). The human genome comprises ten paralogous genes that encode the α-subunit of the VGSC (4). Among those genes, the *SCN8A* gene encodes $Na_v1.6$. This sodium (Na^+) channel is expressed following birth, and is distributed across the hippocampus, cortex, brainstem, cerebellum, heart, as well as lower motor neurons, which gives $Na_v1.6$ a crucial importance (5). In recent times, some pathogenic *de novo* variants of this channel have been recognized in epileptic patients displaying phenotypes ranging from mild to severe and devastating developmental and epileptic encephalopathies (DEEs) (6, 7).

There are some major challenges that face the current treatment options for epilepsy. First, the treatment is 'symptomatic' since epileptic seizures usually return after discontinuation of the treatment, as the underlying cause of the seizures is still present (8). Second, a percentage exceeding 30% of adolescent and adult patients face drug-resistant epilepsy, which is defined as continuing to have seizures, despite receiving treatment with at least two or more agents of the antiepileptic drugs (AEDs) (9). This situation is further complicated by the neurological implications and side-effect profile of antiepileptic drugs, giving that sedation, distractibility, memory and attention problems along with other mood disturbances such as anxiety and depression are frequently reported as the most common adverse effects of antiepileptic therapies (10, 11). To sum up, there is an urgent need for improved antiepileptic therapies for adult patients (12) as well as for children and neonates (13).

Eslicarbazepine acetate (S-Lic-A) is a sodium channel blocker (SCB) that has been found to be superior to some other established SCB AEDs in terms of selectivity, safety, efficacy, and kinetics of binding to Na^+ channels, which makes it a good candidate for epilepsy treatment. In order to assess S-Lic-A effects in our study, we

chose wild-type (WT) $Na_v1.6$ channels along with three *SCN8A* gene variants known to be causing DEEs (M1760I, G1475R and A1622D). In this study, electrophysiological analyses for the chosen variants were performed *in vitro* using the main metabolite of S-Lic-A: Eslicarbazepine (S-Lic). We employed two heterologous expression systems (neuroblastoma cell line for voltage-clamp (V-Clamp) recordings, and primary neuronal cultures for current-clamp (I-Clamp) recordings), in order to assess the effects of S-Lic on both the biophysical and neuronal properties on those variants and compare them to the recordings of WT *SCN8A* channels.

2. GENERAL INFORMATION

2.1. Voltage-gated sodium channels

The VGSCs are heteromeric transmembrane proteins that exist in excitable cells (neurons for instance), and control the transmembrane transport of Na^+ (2). VGSCs take a major role in action potentials (APs) in neurons, as well as in the majority of electrically excitable tissues. The VGSCs contain of an α-subunit with a size of 240-260 kDa and highly glycosylated that forms the channel pore, and an 1-4 auxiliary β-subunits with a size of 30.4-45 kDa (14, 15). A representation of VGSCs can be seen in Figure 2.1.

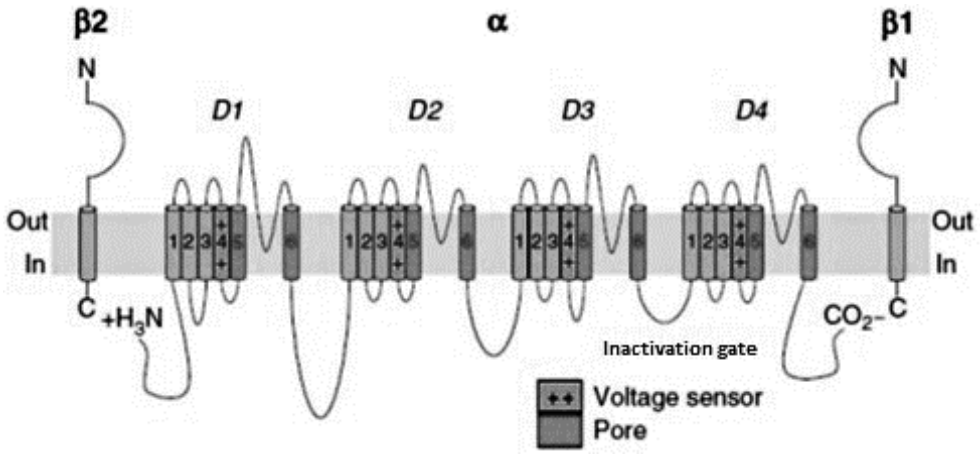

Figure 2.1 The general structure of the VGSC. ^+H_3N represents the N-terminal and CO_{2^-} the C-terminal (15).

2.1.1. VGSC α-subunits

All eukaryotic VGSCs share a similar structure topology of α-subunits; four domains (DI-DIV) connected by large intra-cellular loops and each domain of those encompassing six transmembrane segments (S1-S6). The voltage sensitivity of VGSCs lies within the voltage-sensing domain (S1–S4 segments) that controls the gating with S4 acting chiefly as the voltage sensor. On the other hand, S5–S6 in each repeat constitute the pore (Figure 2.1). The pore loops, (supported by helices P1 and P2) act

chiefly as a selectivity filter (16, 17). The loop joining DIII and DIV is crucial for channel inactivation since it forms the inactivation gate (15). In mammals, there are nine distinct isoforms of α-subunits ($Na_v1.1$–$Na_v1.9$). Those isoforms are respectively encoded by the genes *SCN1A, SCN2A, SCN3A, SCN4A, SCN5A, SCN8A, SCN9A, SCN10A, and SCN11A*. Those isoforms harbor significant differences in their coding gene, structure, sensitivity to tetrodotoxin (TTX), electrophysiological parameters, and tissue distribution (Table 2.1) (14). For example, $Na_v1.1$, $Na_v1.2$, $Na_v1.3$, and $Na_v1.6$ are chiefly present in the central nervous system (CNS) with various distribution patterns (Table 2.2). Whereas in skeletal muscles Nav1.4 is common, and in cardiac muscle Nav1.5 is prevalent. Lastly, in the peripheral nervous system (PNS), Nav1.7, Nav1.8 and Nav1.9 are prevalent (18).

Table 2.1. Diversity of VGSC α- subunits

Type	Gene	Tissue expression	TTX sensitive
$Na_V1.1$	*SCN1A*	CNS and PNS	+
$Na_V1.2$	*SCN2A*	CNS and PNS	+
$Na_V1.3$	*SCN3A*	CNS and PNS	+
$Na_V1.4$	*SCN4A*	Skeletal muscle	+
$Na_V1.5$	*SCN5A*	Cardiac muscle	-
$Na_V1.6$	*SCN8A*	CNS and PNS	+
$Na_V1.7$	*SCN9A*	PNS	+
$Na_V1.8$	*SCN10A*	PNS	-
$Na_V1.9$	*SCN11A*	PNS	-

Adapted from (19, 20).

Table 2.2. Distribution of VGSCs α- subunits in neurons of CNS.

Na_v isoforms	Cell body	Proximal process	Proximal AIS	Distal AIS	Nodes of Ranvier
$Na_v1.1$	+	+	+		+
$Na_v1.2$			+		
$Na_v1.3$	+	+			
$Na_v1.5$	+	+			
$Na_v1.6$	+	+		+	+

AIS: axon initial segment (14).

2.1.2. The auxiliary β subunits

β-subunits are transmembrane proteins. They principally consist of an α-helix that is bound to the α-subunit either covalently or non-covalently (16). There are four known β-subunit genes (*Scn1b, Scn2b, Scn3b* and *Scn4b*) encoding the proteins (β1, β2, β3, and β4) (21). Each β-subunit has an extracellular N-terminal domain, a transmembrane α-helix, and an intracellular C-terminal domain (Figure 2.1) (18). The distribution pattern of VGSC β-subunits in neurons varies between different isoforms (Table 2.3). The β-subunits are known to modulate some properties of VGSCs, such as, membrane trafficking and expression, voltage-dependence, and gating kinetics (17). Additionally, the β subunits have been thought to take a part in the regulation of cell migration and aggregation through acting as adhesion molecules interacting with cytoskeleton proteins and cytokines (14).

Table 2.3. The distribution of VGSC β subunits in neurons.

$Na_v\beta$ isoforms	Distribution in neurons
β1	Mainly in large or medium (>30 μm) dorsal root ganglion neurons, less in smaller neurons (<25 μm).
β2	Widely distributed in CNS and PNS neurons, including cerebral and dorsal root ganglion neurons.
β3	Mainly in small (<25 μm) and medium (25–45 μm) neurons, less in large (>45 μm) neurons.
β4	Mainly in large neurons, less in medium and small neurons.

Adapted from (14).

2.1.3. Functioning of VGSCs

Characteristically, at least three principal states are known to exist for VGSCs: resting, activated, and inactivated, whereby the state in which the channels reside is mainly controlled by the voltage sensors in the S4 helices (Figure. 2.2) (18). VGSCs play a key role in shaping APs. They exist in mixed states (closed, inactivated or open) at the resting membrane potential (RMP) but only closed channels take a part in the generation of an AP. In short, membrane depolarization leads to the opening of VGSCs and a rapid transient (<1 ms) influx of Na^+ ions causing a further depolarizing the membrane and subsequently initiating the rising phase of an AP. Following that, VGSCs inactivate within milliseconds of opening due to the closing of the intracellular inactivation gate resulting in a rapid decay of Na^+ current and henceforth the corresponding falling phase of an AP; a phenomenon known as fast inactivation (FI). Simultaneously, another phenomenon called slow inactivation (SI) takes place in response to long-term changes in the RMP or repetitive AP firing (Figure 2.3). Nevertheless, the structural basis for SI are still not well understood but thought to involve some conformational changes in VGSCs. Notably, the inactivation of VGSCs is

known to be imperfect; causing a small Na^+ current lasting for a period of seconds (19). Upon membrane repolarization, VGSCs recover from FI (by the movement of the inactivating gate back to its initial position) and deactivate (the activation gate closes) (14, 18). When neurons fire at a low frequency during normal physiological conditions, they undergo mainly FI (where they can rapidly return to the closed state), with only a small portion of VGSCs going through the slow inactivated state. Nevertheless, in some pathophysiological conditions when neurons are depolarized and have a sustained AP firing they become more prone to enter the slow inactivated state (Figure 2.4).

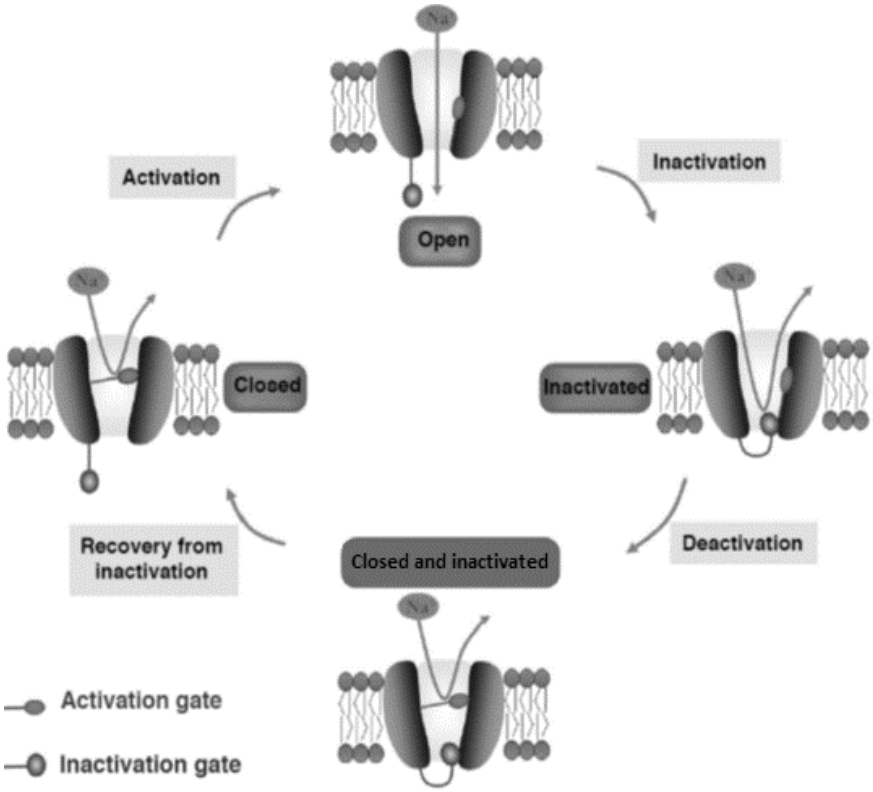

Figure 2.2. **The main conformational states of VGSCs.** Adapted from (18).

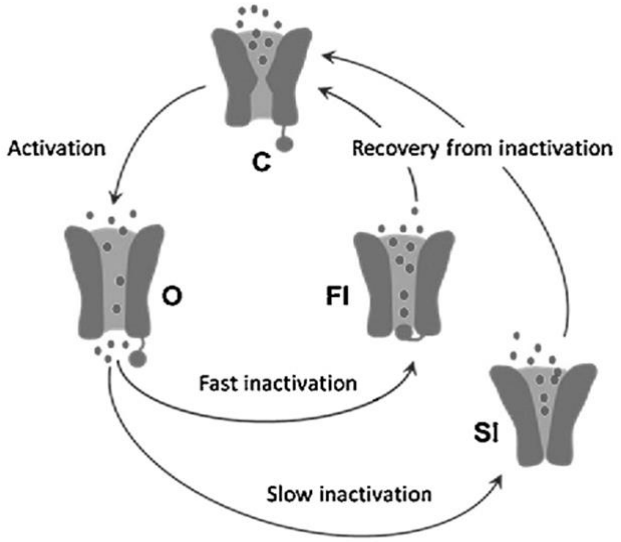

Figure 2.3. Inactivation of VGSCs. (C), closed state. (O), open state. (FI), fast inactivation. (SI), slow inactivation. Adapted from (22).

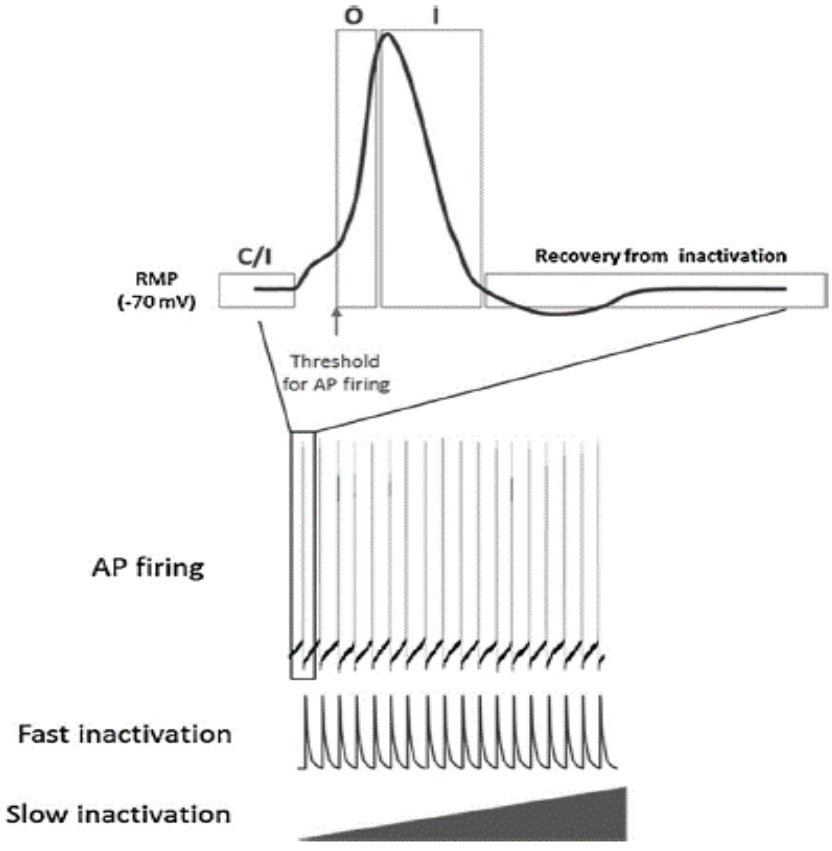

Figure 2.4. The role of VGSCs in neuronal firing. (RMP), resting membrane potential. (O), open state. (I), inactivated state. (C/I), closed and inactivated channels. (AP), action potential. Adapted from (22).

2.2. $Na_v1.6$ channels

The gene responsible for encoding the Na^+ channel $Na_v1.6$ (*SCN8A*), was identified in 1995 (Figure 2.5). $Na_v1.6$ is one of the chief VGSCs existing in brain neurons and is considered as the most abundant isoform in the CNS (14). This channel's expression starts shortly after birth. $Na_v1.6$ is known to be widely distributed across the brain (cortex, hippocampus, brainstem, and cerebellum), along with other locations such as the heart and lower motor neurons (5). $Na_v1.6$ is chiefly located at the axial initial segment, making this isoform accountable for initiating and propagating the neuronal APs (23). Moreover, $Na_v1.6$ is the main channel at the nodes of Ranvier located in mature myelinated axons. The node of Ranvier is essential for impulse propagation via saltatory conduction in myelinated fibers. Additionally, this channel is also present at lower abundance in presynaptic and postsynaptic membranes, as well as non-myelinated axons and dendrites of the neurons for the CNS (24).

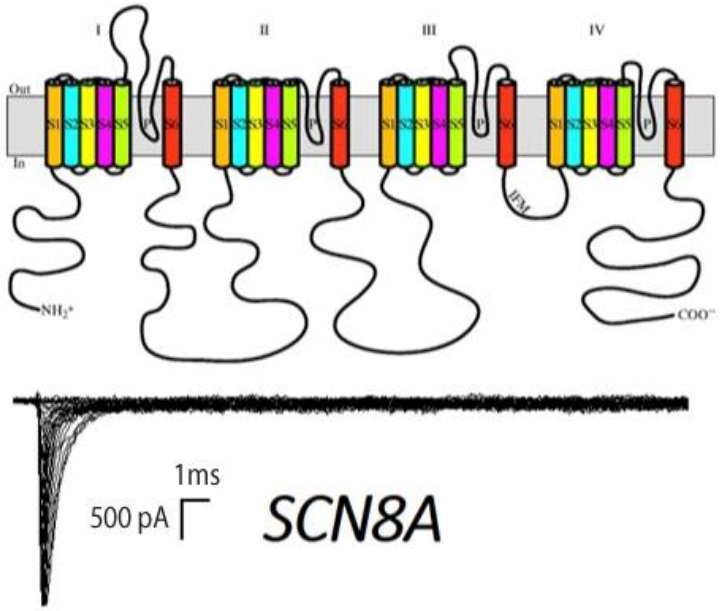

Figure 2.5. Schematic representation of the Na^+ channel $Na_v1.6$ α- subunit along with a representative trace of $Na_v1.6$ channels Na^+ current. Na^+ currents were recorded in the presence of TTX in transfected ND7/23 cells. The top part of the figure is adapted and modified from (25).

2.2.1. Function and importance of $Na_v1.6$

The importance of $Na_v1.6$ in regulating neuronal excitability has been linked to three distinguished features of this channel: 1- AP generation and propagation considering its special location in the initial segment of the axon and in the nodes of Ranvier, 2- its voltage-dependence of activation, and finally 3- its involvement in the generation of persistent and resurgent current (26). Persistent current is a current (around 1% of peak Na^+ current) that persists after firing due to the incomplete inactivation of VGSCs (Figure2.6). Regardless of its small magnitude, this current can influence some neuronal properties such as repetitive firing, synaptic integration, as well as alter the threshold for AP generation (especially when membrane voltages are near the firing threshold). For instance, this current is vital for the generation of repetitive firing in cerebellar Purkinje neurons (27). Resurgent current, on the other hand, is a small, transient current that takes place due to membrane depolarization shortly after the initial AP. It is a voltage- and time-dependent feature that allows neurons to fire rapidly and repetitively. The resurgent current is thought to be a result of an intracellular, positively charged particles clogging the open Na^+ channels in a voltage-dependent fashion causing a strong blockade at depolarized voltages but exiting when the membrane is hyperpolarized and consequently resulting in a fleeting flow of resurgent current at these voltages (Figure2.7) (28).

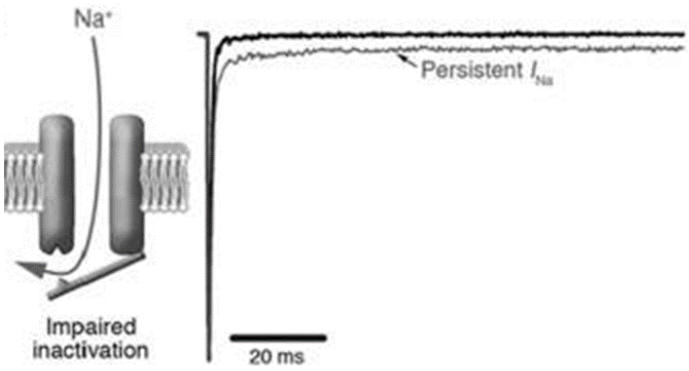

Figure 2.6. A conceptual model of Na^+ channel gating and neuron firing during flow of persistent Na^+ current. Representation of persistent Na^+ current crossing a channel with incomplete inactivation along with current traces showing both the transient Na^+ current (downward spike) and the persistent Na^+ current (27).

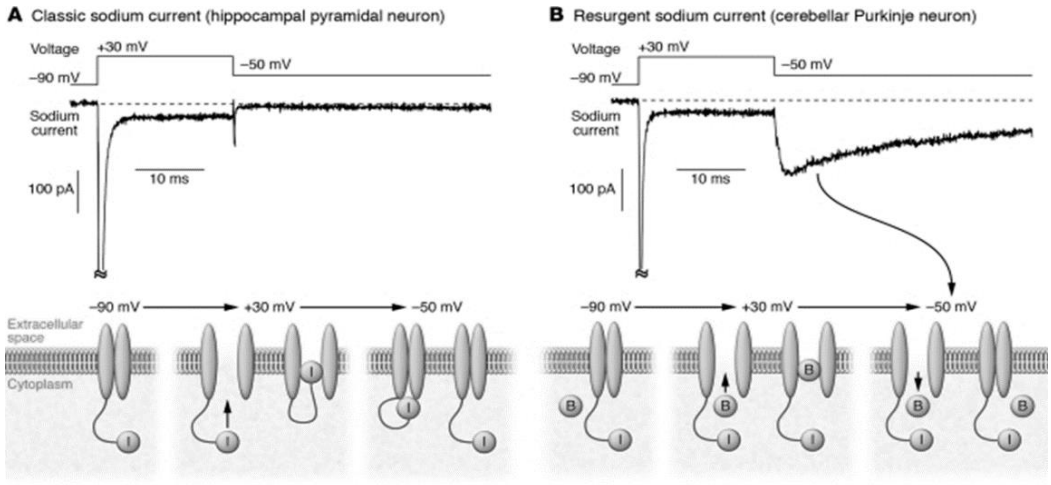

Figure 2.7. Some conceptual models of Na^+ channel gating throughout the flow of both classic and resurgent Na^+ current. A) Classical Na^+ current kinetics: current trace from a hippocampal CA1 pyramidal neuron along with an interpretation of channel gating. **B)** Resurgent Na^+ current kinetics: current trace from a cerebellar Purkinje neuron exposed to a similar voltage step given in A along with an interpretation of channel gating. (B), blocking particle (28).

2.2.2. Pathogenic *de novo SCN8A* mutations and their connection to DEEs

In 2012, *SCN8A* gene has been formally recognized as an epilepsy-associated gene (29). Following that, many pathogenic *de novo SCN8A* variants have been isolated in epileptic patients displaying phenotypes ranging from mild (benign familial infantile seizures, infantile convulsions, paroxysmal choreoathetosis, treatable epilepsy with neurological anomalies) to severe and devastating DEEs with poor prognosis and a high rate of early mortality (Figure 2.8) (5). The term DEEs refers to a group of heterogeneous rare neurodevelopmental conditions manifested by early-onset seizures refractory to standard AEDs, electroencephalographic anomalies, behavioral disturbances, developmental delay or regression, resulting in early death in some cases (30-32). Interestingly, some pathogenic variants in *SCN8A* have been found to be responsible for around 1-3% of DEEs cases (6). On the other hand, some variants in this gene have been associated with intellectual disability among other defects (behavioral or movement issues) (26, 33). Typically in *SCN8A*-related encephalopathy, seizures of various types (tonic, clonic, focal, myoclonic, and

absence seizures) emerge around 4 to 5 months early in life. Those seizures are usually refractory to treatment and cause developmental regression and cognitive disabilities (Table 2.4). Some individuals have been also found to suffer from motor manifestations such as hypotonia, dystonia, hyperreflexia, and ataxia (6, 34). In literature, more than 60 *de novo* missense mutations of *SCN8A* have since been isolated by exome and genome sequencing (Figure 2.9) (35). Such mutations can functionally cause either gain of function or loss of function effects (GOF/LOF) in Na^+ channels (36, 37). Notably, the majority of epilepsy-associated variants in this gene are GOF variants and show a response to high-dose SCBs. On the other hand, LOF variants associated with intellectual incapacities, autism spectrum disorder, or movement conditions without seizures have been also identified lately (6, 15, 38).

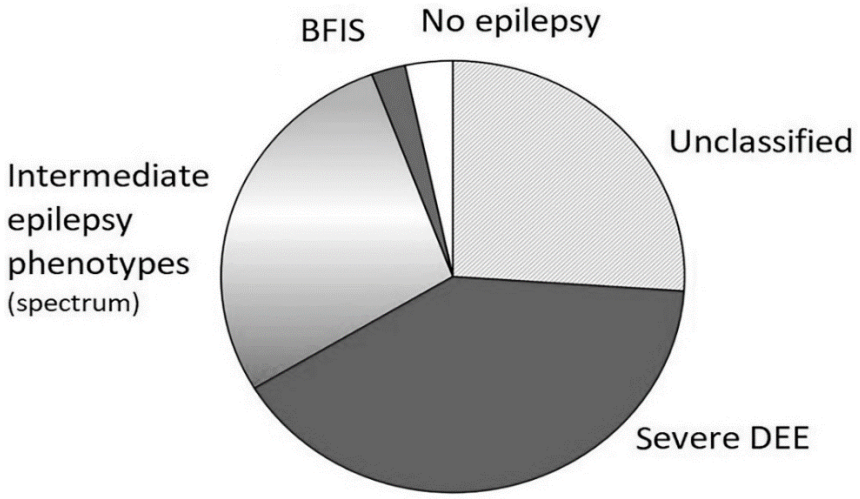

	No epilepsy	7	3.3%
	BFIS	5	2.4%
DEE	Intermediate	59	28%
DEE	Severe	85	40.3%
DEE	Unclassified	55	26%

Figure 2.8. The spectrum of *SCN8A*-related channelopathies. (DEE), developmental and epileptic encephalopathy. (BFIS), benign familial infantile seizures (38).

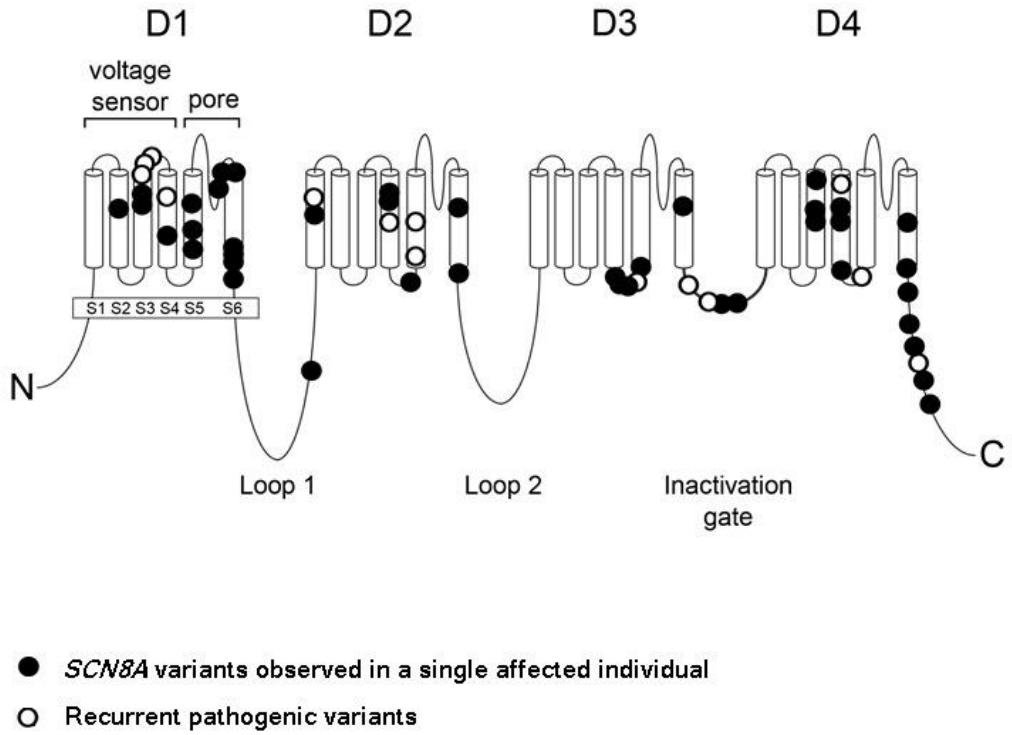

Figure 2.9. Positions of some *SCN8A* missense pathogenic variants. Adapted from (35).

Table 2.4. Clinical features of some patients with *SCN8A* channelopathies

Patient identification (sex)	Current age	Seizure onset	Seizure type at onset	Other seizure types	Seizure outcome	Development before seizure onset	Development after seizure onset	Intellect	MRI	Diagnosis at clinical assessment	Additional features
Patient A (F)	Deceased (3 y)	5.5 mo	GTC during afebrile gastroenteritis	C, T, AA, M	Continuing sz until death	Normal	Delayed with regression	Severe ID	At onset: normal	Unclassified EE	No speech, loss of eye contact from 30 mo, hypotonia, dystonia, wheelchair-bound
Patient B (F)	6 y	2.5 mo	FC	C, GTC, A, E, AA	T, FC evolving to BC	Normal	Delayed with regression	Severe ID	At onset: normal; 5 y: diffuse atrophy	Unclassified EE	No speech, loss of eye contact from 24 mo, hypotonia, dystonic cerebral palsy, stereotypies, wheelchair-bound
Patient C (M)	4 y	3 mo	F, GTC, E with eye deviation	F, T, E, GTC preceded by apnea and deep cyanosis, FC evolving to BC, G, SE	F, GTC, SE, FO	Normal	Delayed with regression	Severe ID	At onset: normal; 15 mo: cerebral atrophy	Dravet-like	No speech, loss of eye contact, generalized hypotonia, fatigable muscle weakness and ptosis, dyskinesia, stereotypic hand movements, not sitting, autistic features
Patient D (F)	16 y	7 mo	FC evolving to BC	C, GTC, A, AA, rare myoclonic jerks, F, SE	FC evolving to BC	Normal	Delayed	Moderate ID	NA	Dravet-like	Repetitive language, macrocephaly, generalized hyperreflexia, clumsiness, autistic features
Patient E (F)	4 y	9 mo	Nocturnal BC with cyanosis	BC with cyanosis	Sz-free for 6 mo, except for a single short sz	Delayed	Delayed	Moderate ID	NA	Unclassified EE	Speaks single words, moderate hypotonia, ADHD
Patient F (F)	8 mo	1 d	Nocturnal M	Nocturnal T, SE, perioral cyanosis	T	NA	Delayed	Moderate ID	2.5 mo: circumscript hypoplasia of corpus callosum	Unclassified EE	Hypotonic, movement disorder
Patient G (F)	Deceased (5 y)	4 mo	T with SE and cyanosis	GTC with SE, T with cyanosis, AB with myoclonic jerks, E	Until death continuing sz	Normal	Delayed	Severe ID	At onset and follow-up: normal	EIEE	No speech, loss of eye contact, hypertonia, generalized hyperreflexia, wheelchair-bound
Patient H (M)	12 y	18 mo	GTC with SE	FD, M, SE, T	GTC, FD	Delayed	Delayed with regression	Moderate ID	Nonspecific foci of high signal in white matter of frontal lobes	Unclassified EE	Ataxia, autistic features
Patient I (F)	10 y	4 mo	Clusters of GTC	T, GTC, FD, focal M	GTC, A, FD	Normal	Delayed with regression	Moderate ID	At onset and follow-up: normal	Dravet-like	Speaks short sentences, ataxic gait
Patient J (M)	44 y	4 mo	T	GTC	Sz-free for 17 y	Normal	Delayed	Mild ID	Bilateral reduction in cerebellar volume	"Vaccine encephalopathy"	None
Patient K (F)	7 y	4 mo	FC evolving to BC	GTC, SE, T	Ongoing	Normal	Delayed with regression	Moderate to severe ID	Normal	Unclassified EE	Reflex component to seizures with fall or pain, autistic features
Patient L (M)	19 mo	4 mo	E	None	E	Delayed	Delayed	Severe ID	5 mo: myelination delayed, residual superficial hemosiderin with frontal predominance	Unclassified EE	No speech, loss of eye contact, severe hypotonia, secondary microcephaly
Patient M (F)	4 y	10 mo	Clonic alternating	BC with tonic posture, prolonged BC with vomiting	Ongoing	Delayed	Delayed	Severe ID	17 mo: normal	EIEE	No speech, loss of eye contact, severe extrapyramidal movement disorder, severe dystrophy, gastroparesis, microcephaly
Patient N (F)	NA	3 mo	FC evolving to BC	SE, asymmetric T, AA	Asymmetric F, asymmetric C	Delayed	Delayed	Severe ID	NA	EOEE	Quadriparesis with dystonic posturing, dystonic-dyskinetic movement disorder, hypotonia, wheelchair-bound
Patient O (F)	7 y	6 mo	E	Episodes of prolonged starring	Sz-free for 3 y	Normal	Delayed	Severe ID	Infancy: normal	Rett-like syndrome	No speech, loss of eye contact, hand stereotypies similar to Rett syndrome but superimposed by general chorea involving arms, legs, and body, wheelchair-bound
Patient P (F)	8 mo	5 mo	FO with eye deviation, lip smacking, apnea, perioral cyanosis	None	Sz-free on oxcarbazepine for 6 wk	Normal	Delayed	NA	At onset: mild diffuse white matter volume loss with prominent frontal arachnoid spaces	Unclassified EE	Hypotonia
Patient Q (F)	6 y	1 mo	Prolonged T	FO evolving to BC, M, TC, SE, nonconvulsive SE	Ongoing	Normal	Delayed with regression	Severe ID	Normal	EOEE	Dystonia, intention tremor with some spasticity

Abbreviations: A = atonic seizures; AA = atypical absence seizures; AB = absence seizures; ADHD = attention deficit hyperactivity disorder; BC = bilateral convulsive seizures; C = clonic seizures; E = epileptic spasms; EE = epileptic encephalopathy; EIEE = early infantile epileptic encephalopathy; EOEE = early onset epileptic encephalopathy; F = febrile seizures; FC = focal clonic seizures; FD = focal dyscognitive seizures; FO = focal seizures; G = gelastic seizures; GTC = generalized tonic-clonic seizures; ID = intellectual disability; M = myoclonic seizures; NA = not available; SE = status epilepticus; sz = seizure; T = tonic seizures; TC = tonic-clonic seizures.

Adapted and modified from (38).

2.2.2.1. M1760I

The M1760I variant is result of a point mutation (Methionine 1760 → to Isoleucine) positioned in the S6 transmembrane segment of domain IV of *SCN8A* gene (Figure 2.10). This variant manifests a severe phenotype (epileptic encephalopathy, seizures *in utero*, severe intellectual incapacities, blindness and hypotonia). It is a GOF variant, that mainly shifts the activation curve towards hyperpolarizing potentials and delays the conversion from the activated to the fast-inactivated form (39).

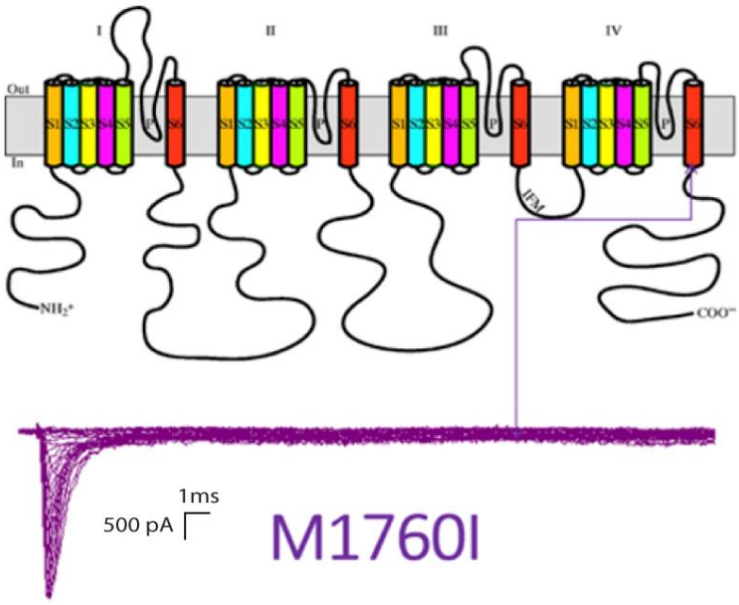

Figure 2.10. The localization of M1760I mutation in $Na_v1.6$ channel α- subunit along with a representative Na^+ current traces. Na^+ currents were recorded in transfected ND7/23 cells in the presence of TTX. The top part of the figure is adapted and modified from (25).

2.2.2.2. A1622D

A1622D variant is a result of a point mutation (Alanine 1622 → to Aspartate) positioned in the voltage-responsive S4 transmembrane segment of domain IV of *SCN8A* gene (Figure 2.11). This variant was associated with developmental delay, intellectual disability, autism, and motor manifestations in non-epileptic patients. The electrophysiological analysis of this variant revealed both GOF and LOF features; a huge GOF manifested by a drastic slowing of FI in ND7/24 cells , that induced a 'functional' LOF in neurons (depolarization plateaus) resulting in a neuronal firing comparable to WT contrary to expectations (39).

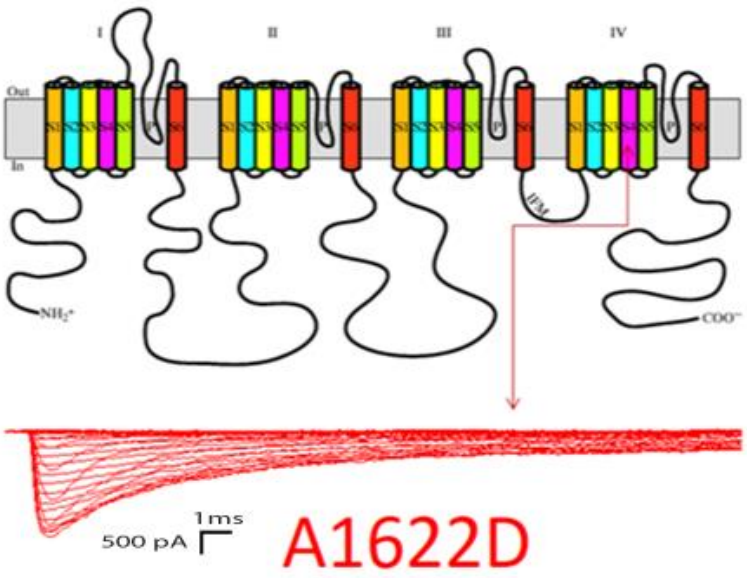

Figure 2.11. The localization of A1622D mutation in $Na_v1.6$ channel α- subunit along with a representative Na^+ current traces. Na^+ currents were recorded in transfected ND7/23 cells in the presence of TTX. The top part of the figure is adapted and modified from (25).

2.2.2.3. G1475R

G1475R variant results from (Glycine 1475 ➞ to Arginine) point mutation located in the DIII-DIV linker of *SCN8A* gene (Figure 2.12). This variant has been reported in different publications (34, 39-43) with various phenotypes ranging from drug-responsive epilepsy to DEEs accompanied by intellectual disabilities and motor problems. The electrophysiological analysis of this variant revealed GOF features, such as a depolarizing shift of the steady-state FI curve and an increase in neuronal firing (39).

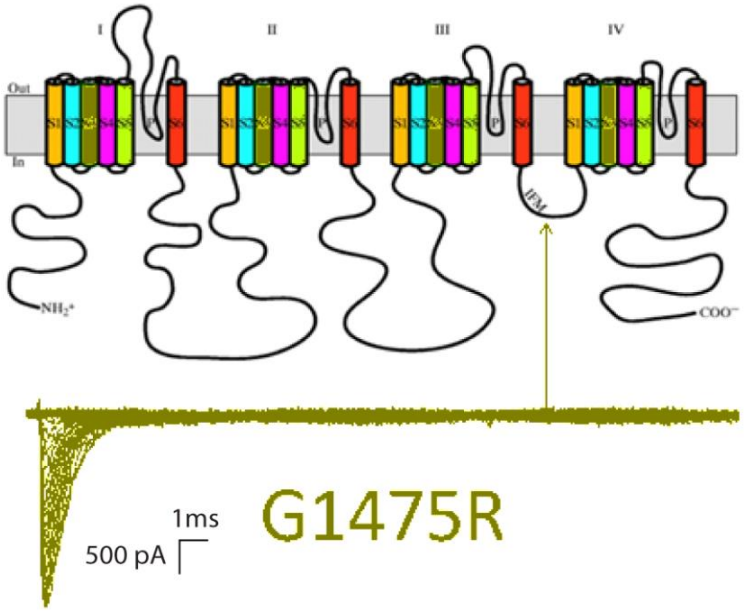

Figure 2.12. The localization of G1475R mutation in $Na_v1.6$ channel α- subunit along with a representative Na^+ current traces. Na^+ currents were recorded in transfected ND7/23 cells in the presence of TTX. The top part of the figure is adapted and modified from (25).

2.3. Sodium channel blockers as antiepileptic drugs

VGSCs have been a valuable target in drug industry since the uncovering of Na^+ channel blocking effects of local anesthetic, antiarrhythmic, and anticonvulsant drugs (44). For more than 70 years, SCBs have been the backbone of the pharmacological management of epilepsy, starting with first-generation AEDs such as phenytoin (PHT), carbamazepine (CBZ), phenobarbitone, and valproic acid (Table 2.5) (9). However, problems such as the narrow therapeutic index of these drugs have raised serious alarms regarding their usage due to severe adverse effects, drug-to-drug interactions and pharmacokinetic variabilities (16). Those complications have led to the development of second- and third-generation AEDs that are dissimilar in some aspects, such as safety profile, mechanism of action and spectrum of activity, and pharmacokinetics. (Table 2.6). The newer generations of AEDs were presented to the market as adjunctive therapy option to established AEDs in patients with uncontrolled seizures, nevertheless, increasing numbers of the newer AEDs have been approved to be used as monotherapy nowadays (45).

The mechanism of SCBs such as PHT and CBZ involves inhibiting high-frequency repetitive neuronal firing (epileptic bursting) in a use-dependent and voltage-dependent manner, since they bind preferentially to depolarized (open) Na^+ channels resulting in a non-conductive state mimicking channel inactivation. Such blockade is comparatively weak at the RPM but strong when the membrane is depolarized. However, once VGSCs become bound to those agents, their recovery is slower than physiological inactivation, allowing this block to accumulate during the repetitive activation of Na^+ channels (46). The binding site of some SCBs such as CBZ, and PHT lies within the amino acid residues in the S6 segment of DI, DIII, DIV located at the internal part of the VGSC pore (Table 2.7 and Figure 2.13).

Nowadays, there is a good evidence supporting for the use of SCBs in some Na^+ channelopathies. For instance, in *SCN8A*-related encephalopathies, the high-dose usage of some SCBs such as PHT and CBZ in epileptic encephalopathy patients carrying GOF mutations in *SCN8A* gene have shown a favorable therapeutic response

(6, 38, 47, 48). However, the use of PHT is problematic, due to its short- and long-term side effects such as cardiac arrhythmias, irreversible cerebellar atrophy and polyneuropathy. Moreover, cognitive impairments in the faculties of attention, memory, and particularly mental speed have also been reported with PHT use (49). Another complicating matter is its narrow therapeutic window due to a steep kinetic profile. CBZ usage, on the other hand, has a wide range of drug-drug interactions and displays serious side effects such as chronic sedation, cognitive impairments, enzyme induction, and hematopoietic abnormalities (aplastic anemia and agranulocytosis, etc.) (50, 51). Wherein the metabolite CBZ-10,11-epoxide is responsible for those adverse effects (52). Such problems can be more prominent in patients with intractable epilepsies since supratherapeutic doses are needed for the management of their seizures, and is of a particular importance since those drugs are often provided to children during their critical brain developmental stages, rising the need for alternative treatment options. Another complicating factor is the poor seizure outcome in *SCN8A* DEEs, which makes the development of new targeted therapies a research main concern (6). The clinical response of Na^+ channelopathies to known SCBs remains complex and understudied. Future investigations in this field must involve profounder assessments of the ion channel dysfunction while evaluating the treatment response (53).

In summary, in spite of having many AEDs in the market, epilepsy management is still faced with problems such as; pharmacoresistance (since 30% of patients continue to experience seizures, despite receiving treatment with at least two or more of the available AEDs), and medication-induced side effects, intensifying the need for new AEDs that are considered both effective and safe. The efforts to identify new SCBs for the management of epilepsy are still going on, leading to various classes of compounds, with a great structural diversity (54).

Table 2.5. Some SCBs along with the year of their initial approval

Sodium channel blocker	Years
Phenytoin	1936
Carbamazepine	1965
Lamotrigine	1991
Oxcarbazepine	2000
Rufinamide	2007
Lacosamide	2008
Eslicarbazepine acetate	2009

Adapted from (9).

Table 2.6. Adverse drug reactions of newer AEDs.

√ Lower :ics	Neurotoxicity/CNS effects				Hepato-toxicity	Terato-genicity	Other important adverse events
	Dizziness	Somnolence	Ataxia	Cognitive impairment			
Second generation							
Fosphenytoin	√	√	√	?	√	√	Nystagmus, paresthesia, pruritis, headache, hypotension, skin rash
Oxcarbazepine	√	√	√	√	√	√ Lower risk than conventional AEDs	Hyponatremia, skin rash
Lamotrigine	√	√	X	√ *	√	√	Steven-Johnson syndrome, toxic epidermal necrolysis, insomnia, acne, nightmares, body aches, dry mouth, damage to tooth enamel
Felbamate	√	√	√	√	√ Severe & fatal		Nausea, vomiting, asplastic anemia, GI complaints, anorexia, headache, diplopia, weight loss, irritability, insomnia
Topiramate	√	√	X	√	√ Only few cases	√	Mood disturbances, occasional renal stones, weight loss, paresthesia
Zonisamide	√	√	√	√	X	√	GI distress, anorexia, tiredness, diplopia, ↓ serum bicarbonate levels, rare cases of oligohydrosis, kidney stones and loss of weight
Third generation							
Eslicarbazepine (BIA-2-093)	√	√	√	√	√ Only few cases	√ Lower risk	Low incidence of rash and hyponatremia
Brivaracetam (UB-34714)	√	√	X	?	?	?	Nausea, vomiting, nasopharyngitis, anorexia, insomnia, pain
Carisbamate	√	√	?	?	√	?	Headache, nausea
Lacosamide	√	√	√	√	X	?	GI distress, nystagmus, diplopia, small ↑ in P–R interval, loss of body weight in some patients
Rufinamide	√	√	?	X	X**	?	Tremor, fatigue, rare cases of lymphadenopathy, rash, status epilepticus
Safinamide	√	?	?	?	?	?	Headache, vertigo, blurred vision, marked decrease in platelet count
Vinpocetine	X	X	X	X*	X***	?	Flushing, rashes, minor GI, distress mild hypotension

√: Adverse events reported with the drug; X: adverse event not reported with the drug; ?: adverse event not studied with the drug *:cognitive improvement also reported in some studies; **: liver abnormalities have been reported in children; ***: hepatoprotection reported in an experimental study; GI: gastrointestinal. Adapted and modified from (45).

Table 2.7. Overview of the binding sites of some SCBs

Site	Neurotoxins	Examples	Peptide	Main binding area known up to date	Result
1	Guanidinium toxins	TTX, STX	–	DI–IV P-loop	Block of Na^+ conduction
	μ-Conotoxins	KIIIA, SIIIA, PIIIA	x		
2	Small lipid-soluble toxins	Batrachotoxin	–	DI DIV S6	Negative shift in voltage-dependency of activation
		Veratridine	–		Slowing down of inactivation
		Grayanotoxins	–		Block of Na^+ conductance
		Aconitine	–		Altering ion selectivity
3	Scorpion α-toxins	AaH II, LqhaIT, BMK M1	x	DIV S3–S4	Slowing down of inactivation
	Sea anemone toxins	ATX-II, AFTII	x		
4	Scorpion β-toxins	Css4, Tsγ, AahIT	x	DII S3–S4	Negative shift in voltage-dependency of activation
	Spider β-toxins	Magi 5, HWTX-IV	x		Block of Na^+ conductance
	μO-conotoxins	MrVIA	x		
5	Cyclic polyether compounds	Brevetoxins	–	DI S6	Negative shift in voltage-dependency of activation
		Ciguatoxins	–		Slowing down of inactivation
6	δ-Conotoxins		x	DIV S4	Slowing down of inactivation
7	Pyrethroids	DDT, Deltamethrin	–	DII–DIII	Slowing down of inactivation
LA	Local anesthetics	Lidocaine	–	DIV S6	Block of Na^+ conduction
	Anticonvulsants		–		
	Antiarrhythmics		–		
	Antidepressants		–		

Adapted from (55)

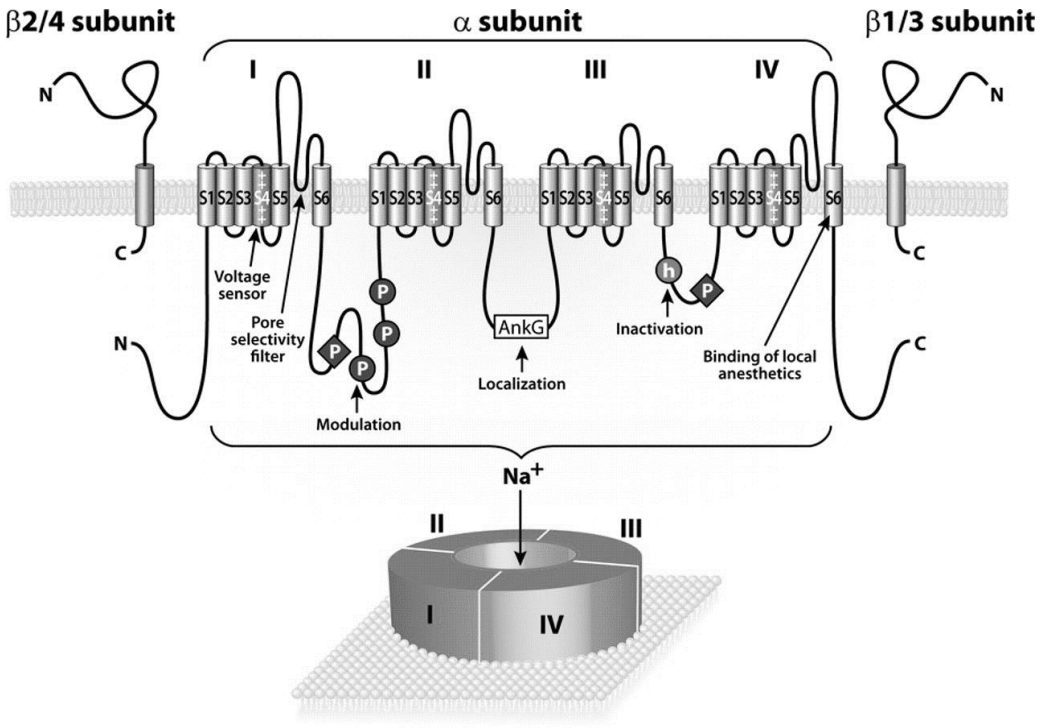

Figure 2.13. A representation of the binding site for some SCBs. The binding site for some SCBs; such as local anesthetics, some antiepileptic and antiarrhythmic drugs, is formed by amino acid residues positioned in the internal part of the pore of VGSCs (in the S6 segment of DI, DIII, DIV). (AnkG), ankyrin G. (h), hinged lid. (P), phosphorylation sites (56).

2.3.1. Eslicarbazepine acetate

S-Lic-A is a new AED that functions as a competitive blocker of the VGSCs. It was licensed in 2009 in Europe, and then in 2013 in the United States for adults as adjunctive treatment for focal onset seizures. Later in 2015, it was approved in the United States for focal onset seizures with or without secondary generalization as monotherapy, and in 2017 it was approved in children and adolescents as an adjunct treatment (57).

2.3.1.1. Pharmacology

S-Lic-A is a third-generation AED that belongs to the dibenzazepine family (Figure 2.14). This family also includes the first generation member CBZ and the second generation member oxcarbazepine (OXC). S-Lic-A is a prodrug that undertakes a fast presystemic (chiefly hepatic and minor intestinal) metabolic hydrolysis to S-Lic, also known as S-licarbazepine. Only a minor part turns into OXC and then to (R)-licarbazepine, with a final ratio of 20:1 (Figure 2.15) (58). The metabolism of OXC results in similar products but with a different ratio (4:1). Which provides S-Lic-A with an advantage having S-Lic as its sole metabolite since it is known to be more effective, less toxic, and can penetrate the blood–brain barrier better than (R)-licarbazepine. When compared to previous agents of the dibenzazepine family, S-Lic-A has distinctive pharmacodynamic and pharmacokinetic features due to the structural dissimilarity at the 10,11 position of the dibenzazepine nucleus (57). This difference leads to improved tolerability, and changes in metabolism and to linear pharmacokinetics (in the 400–1,200 mg dosage range) typically unaffected by age, sex, and food intake (Tables 2.8-2.11). In humans, the oral bioavailability of S-Lic is 94%, and has relatively low affinity to plasma proteins (30%). Its plasma concentration peaks 2–3 h after ingestion, and it reaches a steady state after 4–5 days. S-Lic-A has a half-life of 20-24 h allowing a once daily dosing. Furthermore, S-Lic evades the generation of toxic product and undergoes primarily renal excretion

either unchanged (67%) or as a conjugate with glucuronic acid (33%), thus dose adjustment is needed in patients with renal failure (Figure 2.15). However, mild-to-moderate hepatic damage does not necessitates any dosage adjustments. S-Lic-A does not seem to impact its own metabolism or clearance. It has moderate interactions with the hepatic enzymes, since it weakly induces CYP3A4 and UGT, and inhibits CYP2C19, hence has a low risk for drug-drug interactions (59). S-Lic-A has strong affinity to brain tissues; especially to the organic fraction of the brain with a ratio of 50:1, resulting in concentrations about is 4.6 times higher those detected in total brain volume (Figure 2.16). The recommended maintenance dose of S-Lic-A ranges between 800 mg to 1200 mg once daily. S-Lic-A acts as a competitive blocker of the VGSCs; it reduces their availability by selectively enhancing slow inactivation (contrasting traditional SCBs that interfere with the FI pathway). SI refers to a structural rearrangement of the pore that modifies channel excitability. This unique mechanism results in the reduction of long-term availability of VGSCs, and to a lower tendency to disturb physiological function giving its selectivity to target pathological situations seen in neurons leading to the inhibition of sustained APs firing, and the stabilization of hyper-excitable neuronal membranes (57). Lastly, S-Lic-A inhibits $Ca_v3.2$ T-type Ca^{2+} channels. Those channels are suspected for involvement in the epileptogenesis process. Hence, blocking those channels can enhance the therapeutic potential of S-Lic-A.

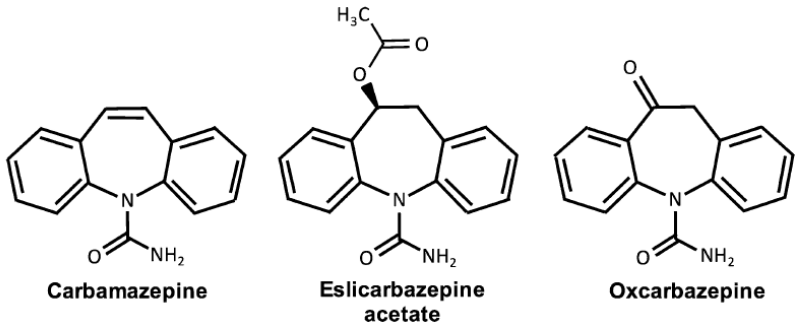

Figure 2.14. Chemical structure of the dibenzazepine family. The difference in S-Lic-A structure lies within the 5-carboxamide attached at the 10, 11 position (60).

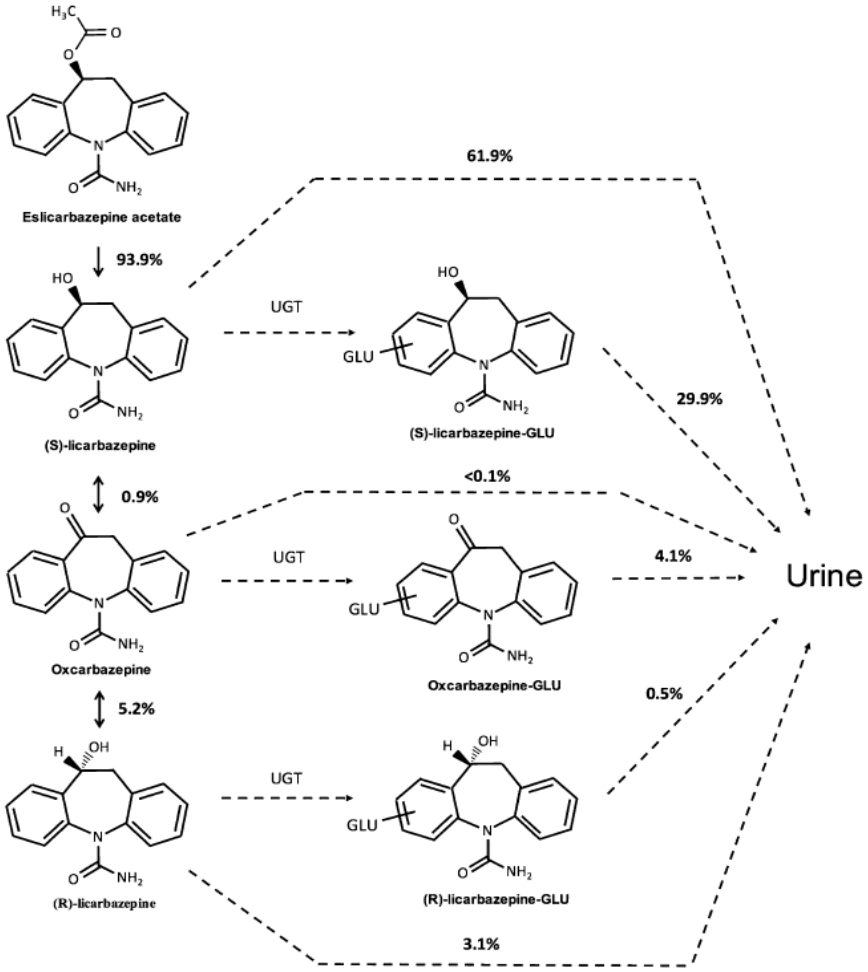

Figure 2.15. Metabolic and elimination pathways of S-Lic-A. S-Lic-A is hydrolyzed mainly to S-Lic. Eventually, S-Lic and its metabolites are excreted in the urine either unchanged or gluconurated. (GLU), glucuronide. (UGT), uridine glucuronosyltransferase (60).

Table 2.8. A summary of some adverse effects commonly reported for S-Lic-A

Adverse event (AE)	Number (%) of patients			
	Placebo (n = 289)	ESL 400 mg/d (n = 196)*	ESL 800 mg/d (n = 284)	ESL 1200 mg/d (n = 280)
Any AE	134 (46.4)	119 (60.7)	178 (62.7)	189 (67.5)
Dizziness	21 (7.3)	26 (13.2)	60 (21.2)	81 (28.9)
Headache	25 (8.7)	17 (8.7)	29 (10.2)	38 (13.6)
Diplopia	5 (1.7)	10 (5.1)	23 (8.1)	24 (8.6)
Nausea	5 (1.7)	8 (4.1)	18 (6.3)	27 (9.6)
Somnolence	27 (9.3)	21 (10.7)	37 (13)	42 (15)
AEs leading to discontinuation	13 (4.5)	16 (8.2)	34 (12)	55 (19.6)

(ESL), eslicarbazepine acetate. Adapted from (61).

Table 2.9. A summary of the pharmacokinetics of S-Lic-A

Bioavailability	Complete
Peak plasma concentration	1–4 h
Plasma protein binding	<40%
Half-life	13–20 h
Serum concentrations	5–9 mcg/ml
"Therapeutic range"	Not established
Plasma clearance	20–30 ml/min
Elimination	Hydroxylation, conjugation –> renal excretion

Adapted from (61).

Table 2.10. Pharmacokinetic parameters of S-Lic-A and OXC following 8-day administration to healthy subjects

Treatment	C_{min} (μM)	C_{max} (μM)	t_{max} (h)	$AUC_{ss,0-\tau}$ (μmol h/L)	$t_{½}$ (h)	Fluctuation (%)	Dose (μmol)	Ratio exposure/ dose (μmol h/L)/ (μmol)
Eslicarbazepine								
ESL 900 mg QD	22.7 (24.1)	87.3 (32.7)	3 (1.5–4)	1156.3 (19.9)	9.12 (13.1)	131.0 (25.6)	3037.3	0.381
ESL 450 mg BID	32.3 (15.6)[a]	65.5 (23.9)[a]	2 (1–3)	1117.6 (18.3)	9.17 (16.2)	69.7 (29.3)	3037.3	0.368
OXC 450 mg BID	31.8 (12.9)[a]	48.0 (16.8)[a]	3 (1.5–6)	968.4 (13.5)	9.24 (35.2)	39.4 (22.9)	3567.6	0.271
(R)-Licarbazepine								
ESL 900 mg QD	1.8 (22.5)	2.7 (27.4)	12 (1.5–18)	53.7 (23.5)	15.0 (24.4)	41.1 (37.4)	3037.3	0.018
ESL 450 mg BID	2.1 (28.3)	2.8 (26.0)	6 (1.5–12)	59.7 (27.4)	14.5 (27.7)	28.6 (27.1)	3037.3	0.020
OXC 450 mg BID	5.8 (24.2) [a,b]	9.8 (14.6) [a,b]	3 (1.5–8)	188.5 (12.3) [a,b]	11.0 (18.7)	50.4 (35.2)	3567.6	0.053
Oxcarbazepine								
ESL 900 mg QD	0.2 (31.4)	0.8 (25.5)	6 (1.5–12)	12.3 (23.0)	13.2 (33.7)	128.0 (33.0)	3037.3	0.004
ESL 450 mg BID	0.3 (31.2)[a]	0.7 (26.0)	3 (1–12)	13.3 (28.2)	11.9 (24.1)	69.4 (38.9)	3037.3	0.004
OXC 450 mg BID	0.4 (22.2)[a]	4.3 (50.7) [a,b]	1 (0.5–3) [c,d]	31.6 (28.1)[a,b]	10.1 (33.7)	278.0 (27.7)	3567.6	0.009

Results are expressed as arithmetic means with coefficient variation (%) in parentheses: t_{max} values are medians with range values in parentheses.
[a]Significantly different from corresponding values for ESL 900 mg QD using one-way ANOVA followed by Tukey's multiple comparison test ($p < 0.05$).
[b]Significantly different from corresponding values for ESL 450 mg QD using one-way ANOVA followed by Tukey's multiple comparison test ($p < 0.05$).
[c]Significantly different from corresponding values for ESL 900 mg QD using Friedman test followed by Dunn's multiple comparison test ($p < 0.05$).
[d]Significantly different from corresponding values for ESL 450 mg QD using Friedman test followed by Dunn's multiple comparison test ($p < 0.05$).

Adapted from (62), n=11. (ESL), eslicarbazepine acetate. (OXC), oxcarbazepine.

Table 2.11. Pharmacokinetic parameters of S-Lic-A following administration of single- or multiple-doses in young and elderly Subjects

	Single Dose		Multiple Dose	
Parameter	Young Group	Elderly Group	Young Group	Elderly Group
C_{max}, ng/mL	9867 ± 1714	9469 ± 2284	17309 ± 3430	15067 ± 2126
t_{max}, h	3.0 ± 1.8	3.0 ± 1.3	2.0 ± 1.6	2.0 ± 0.9
AUC_{0-t}, ng•h/mL	174713 ± 37062	190521 ± 69082	290630 ± 68649	288364 ± 40878
AUC_{0-24}, ng•h/mL	137354 ± 24742	141245 ± 38438	213815 ± 41889	208432 ± 28561
$AUC_{0-\infty}$, ng•h/mL	180899 ± 37624	196030 ± 69152	296702 ± 67577	294290 ± 40356
$t_{1/2}$, h	10.1 ± 1.0	10.9 ± 0.9	10.5 ± 1.4	11.1 ± 1.6
R_0	—	—	1.64 ± 0.21	1.59 ± 0.32

Data presented as Mean ± SD, n=12, dose administered: 600 mg (63).

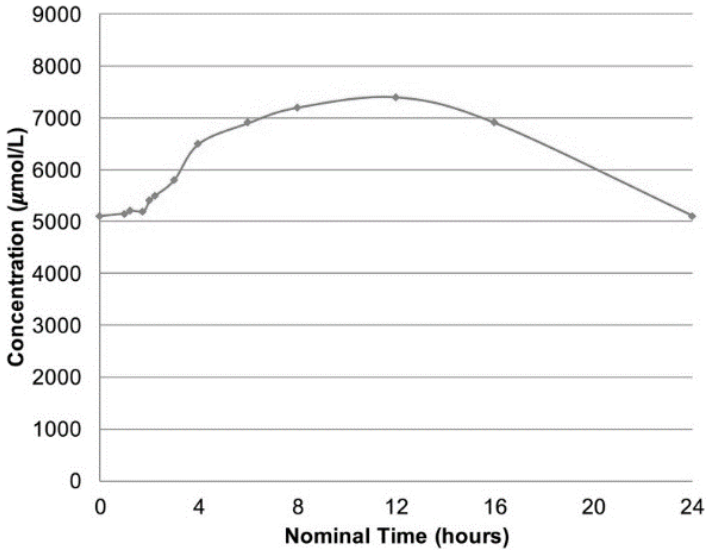

Figure 2.16. Mean concentrations of S-Lic-A in cerebrospinal fluid over time. Following 1200 mg/day dose administration to six healthy volunteers (60).

2.3.1.2. Comparison to older members of the dibenzazepine family

This drug displays some substantial differences when compared to the older agents in its family (CBZ and OXC). Unlike CBZ, toxic epoxides such as CBZ-10,11-epoxide, are not formed from S-Lic-A metabolism, as well as it is not susceptible to auto-induction (64). Additionally, S-Lic-A has lower chances of drug-drug interactions in comparison to the other members like CBZ and OXC. S-Lic has demonstrated a wider therapeutic index (1.5- to 2.5-fold), in comparison to CBZ in some mouse models of epilepsy (62). Furthermore, S-Lic binds more selectively to the inactive state of VGSCs, which is the dominant state of VGSC in speedily firing neurons in comparison to CBZ, OXC and R-licarbazepine, and has a three-fold lesser affinity for the resting state of the VGSC compared to CBZ. Lastly, it was shown that the main mechanism of S-Lic is enhancing the SI of VGSC, unlike CBZ and OXC which mainly act on the FI (65). Occlusion of VGSC pore by a cytoplasmic region is the main mechanism in FI, however, in the SI process conformational changes are believed to take place in the VGSCs. Such data suggest that S-Lic-A can still be an effective AED in patients who had to discontinue the older dibenzazepines for various reasons. Such as, suffering

from adverse events related to CBZ or OXC usage giving the good profile of S-Lic-A with respect to those side effects (cutaneous reactions, hypercholesterolemia, osteoporosis, hyponatraemia, sexual dysfunction, liver disease and cognitive dysfunction), or to the patients who have problems with compliance to two- or three-daily dosing regimens (57).

2.3.1.3. Applications

Both in human and experimental pharmaco-resistant epilepsies, S-Lic-A has been shown to maintain its use-dependent blocking properties. Additionally, substantial add-on effects to CBZ have been also uncovered in tissue samples taken from epileptic patients (66). Likewise, S-Lic-A was well tolerated and effective as an adjunctive therapy for patients suffering from epilepsy resistant to some standard AEDs (67). Moreover, it has been shown that the addition of S-Lic-A to the treatment regimen of epileptic patients had positively influenced their mood and quality of life in a retrospective clinical trial (68). Besides, S-Lic-A was found to be well tolerated in pediatric patients and effective in decreasing seizure frequency. Furthermore, its administration did not significantly influence their neurocognitive and behavioral functioning (69). Finally, S-Lic-A displayed anti-epileptogenic properties in several animal models of epilepsy (65). Those anti-epileptogenic properties are presently investigated in stroke patients who are at high risk for unprovoked seizures (70). The term ‘epileptogenesis‘ describes the process when a brain network that used to be normal is functionally altered leading to a greater likelihood to generate spontaneous recurrent seizures. Epileptogenesis is often used interchangeably with the term ‘latent period’; a term refers to the time period that separates the epileptogenic insult and the occurrence of the first clinical seizure (71). Those findings give a promising role to S-Lic-A as an epilepsy treatment and a powerful alternative to older AEDs.

2.4. Aim and Hypotheses

Hypotheses:

1- S-Lic-A is effective against some GOF variants in $Na_v1.6$ that have a role in the pathophysiology of early onset epileptic encephalopathies.
2- S-Lic-A can be also an effective option against some variants not associated with epilepsy but showing both GOF and LOF features such as A1622D.
3- S-Lic-A can alter more parameters in some $Na_v1.6$ variants with respect to WT $Na_v1.6$ channels.

Aim:

To assess the electrophysiological effects of S-Lic-A on several Na^+ channels variants causing developmental and epileptic encephalopathies using heterologous expression systems such as mouse neuroblastoma cells as well as primary cultured mouse neurons.

3. MATERIALS AND METHODS

3.1. Molecular and cell biology methods

3.1.1. Mutagenesis

The complementary DNA (cDNA) constructs of human $Na_v1.6$ (WT), A1622D, G1475R, and M1760I α-subunit channel were engineered in a TTX-resistant channel isoform (so that the current obtained from the transfected channels can be isolated after the addition of TTX). The constructs of the human VGSC auxiliary β1 with green-florescent protein (GFP) marker gene (pCLH-hβ1-EGFP), and β2 subunits with CD8 as the market gene (pCLH-hβ2-CD8) in their plasmids. Site-directed mutagenesis to engineer the mutations was performed and the constructs were sequenced before being used in the experiments (72, 73).

3.1.2. Cell culture and transfection

3.1.2.1. Culturing of ND7/23 cells

ND7/23 is a cell line that is basically a hybrid of mouse neuroblastoma cells and neonatal rat dorsal root ganglia neurons (Sigma Aldrich). The cells were cultured in 25 ml sterile flasks (Greiner) in Dulbecco's Modified Eagle Medium (DMEM) (Invitrogen) complemented by the addition of 10% fetal bovine serum (FBS) (PANBiothech) and 1% L-glutamine 200 mM (Biochrom) in a cell incubator (IG 150, Germany), at 5% CO_2 humidified atmosphere with 37 °C temperature. The cell line was sub-cultured at least twice weekly. Before splitting, Phosphate Buffered Saline (PBS) solution that is free of Ca^{2+} and Mg^{2+} (PAA Laboratories) was used to wash the cells in order to facilitate the process. Then, the sides of the flask were washed with a new medium in order to create a cell suspension. After that, the suspended cells were pipetted to dissociate cell clumps and to remove attached cells. Following that, the cells were distributed (1:10) into flasks filled with with new medium. The cultures

were monitored microscopically for active growth, and maintained until passage 40 (Figure 3.1).

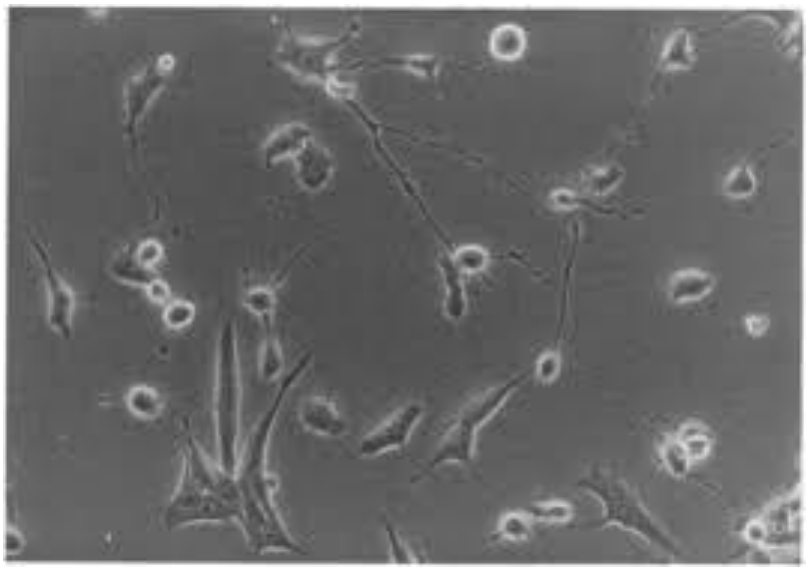

Figure 3.1. Morphology of differentiated ND7/23 cells under light microscopy. Adapted from (74).

3.1.2.2. Transfection and expression in ND7/23 cells

Transfection refers to introducing a foreign DNA into a receiver eukaryotic cell. In transient transfection process, the foreign DNA is not integrated into the nuclear genome, consequently, it is lost when the cells go through mitosis. In this study, the lipofection transient transfection method was performed. Lipofection, otherwise known as 'liposome-based transfection', utilizes a lipid complex in delivering foreign DNA to cells. In this method, a mixture of neutral and cationic liposomes is used in order to form complexes with the foreign DNA. After which, those complexes can pass the cell membrane releasing the nucleotides into the cytoplasm through endocytosis. Following that, those nucleotides can be expressed in the target cells if they manage to escape lysosomal degradation; a critical process that can impact the transfection efficiency greatly (Figure 3.2) (75). To summarize the procedure, the cells were plated in petri dishes (35 mm, Greiner) one day before the

transfection so that cells will be approximately 70% confluent on the next day. At the day of transfection, 4.4 µg of cDNA (4 µg of the TTX- resistant alpha-subunit 'WT or mutant human *SCN8A* cDNAs', and 0.2 µg of each of the human β1- and β2-subunits of VGSCs), along with Lipofectamine 2000 were diluted in 2 separate tubes in Opti-MEM reduced serum medium (250 µl), then mixed gently and incubated for 5 minutes (min) (Invitrogen). Later, the prepared mixtures of DNA and Lipofectamine 2000 were combined then incubated at room temperature (RT) for 20 min, then added dropwise to the dishes. Transfection process was stopped after 48 h by gently changing the medium and splitting the cells at a ratio of 1:4 in preparation for V-Clamp recordings.

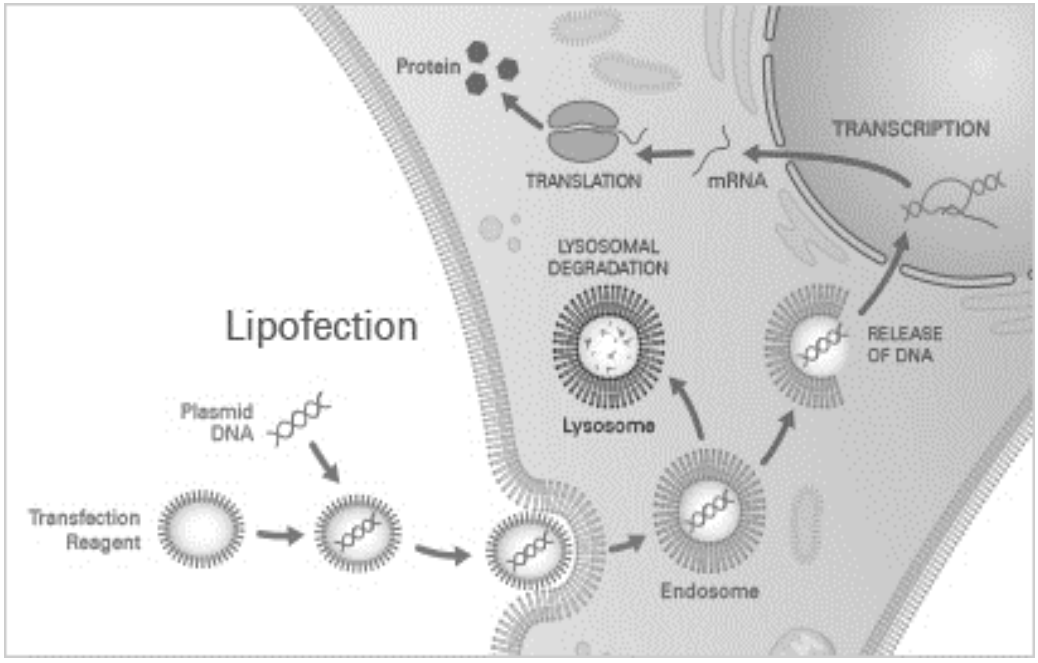

Figure 3.2. The lipofection transient transfection method. A mixture of neutral and cationic liposomes is used in this method in order to form complexes with the nucleotides of interest (75).

3.1.2.3. Culturing of primary mouse hippocampal neurons

Hippocampal neurons from C57BL/6NCrl mouse pups were harvested on embryonic day 18 (76). After rendering the pregnant mice unconscious by CO_2, they were sacrificed by means of cervical dislocation. Then, the embryos were extracted then decapitated and their whole brains were immediately kept in cold with Hank's Balanced Salt Solution (HBSS) that is Ca^{2+}- and Mg^{2+}- free (PAA Laboratories). Then, isolation of the hippocampi was done using fine forceps under the dissecting microscope (Olympus SZ 61, Shinjuku, Japan). After washing the isolated hippocampi for three times with the cold HBSS solution, they were left for 14 min in 2.5% trypsin (Invitrogen) at 37°C in order to get them digested. After the incubation, the digestion process was terminated by washing with DMEM complemented with FBS (Biochrom AG). Following that, the neurons were softly dissociated using mechanical trituration and plated on 13-mm coverslips (poly-D-lysine coated) in 24-well culture plates (Greiner) filled with 500 µl DMEM complemented with FBS and penicillin/streptomycin (Invitrogen) at a density of 80,000 or 60,000 per well. They were left at 37°C in 5% CO_2 humidified atmosphere (Cell incubator IG 150, Jouan, Germany) for 6 h allowing them to settle on the cover slips, and the culture medium was changed after that with Neurobasal culture medium plus B27 and glutamine (Invitrogen) (Figure 3.3). Neurobasal plus medium was changed weekly in order to sustain the osmolality (Figure 3.4). Animals' handling protocols were performed according to 'German National Board for Laboratory Animals' guidelines, by other coworkers in laboratory upon approval granted by 'Regierungspraesidium Tuebingen'; the local Animal Care and Use Committee at Tuebingen, Germany.

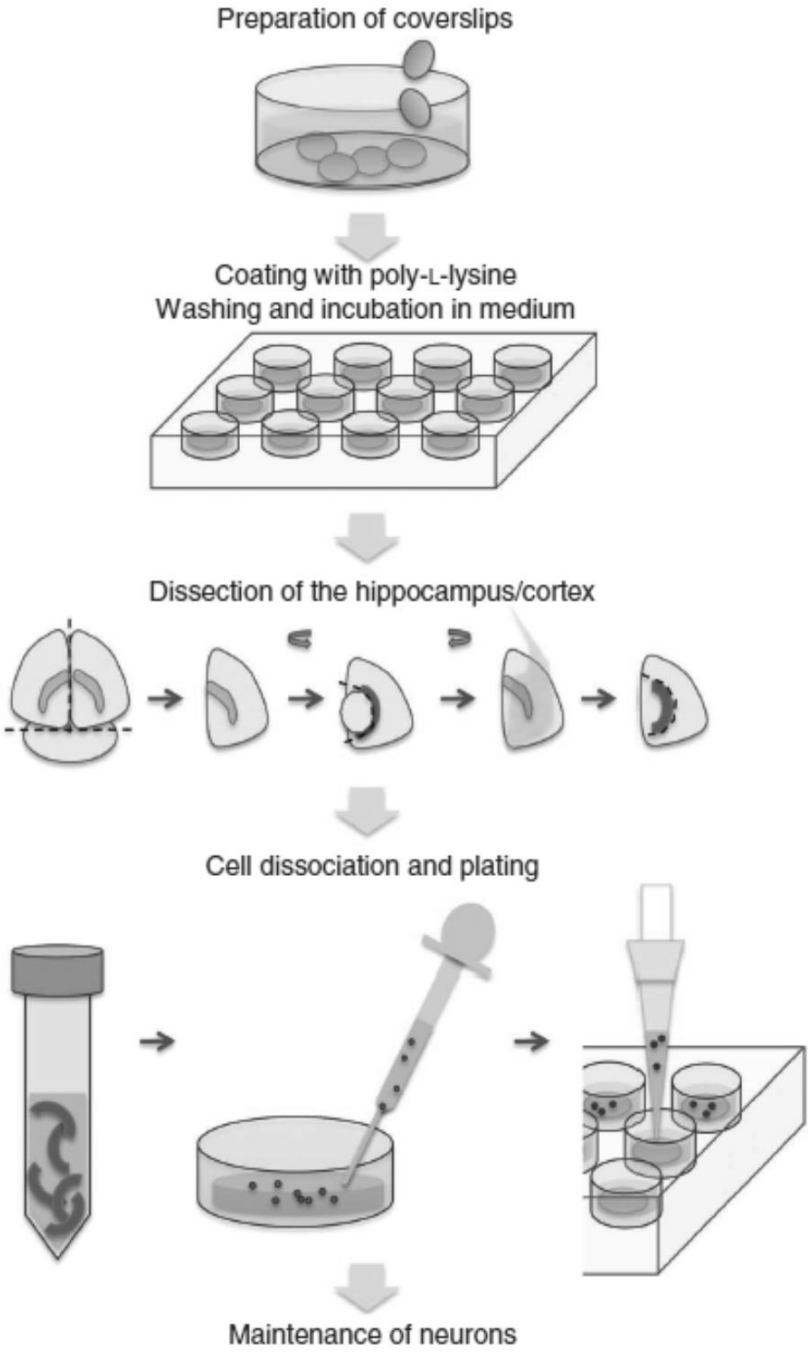

Figure 3.3. Summary of the procedure for culturing primary mouse hippocampal neurons. Adapted from (77).

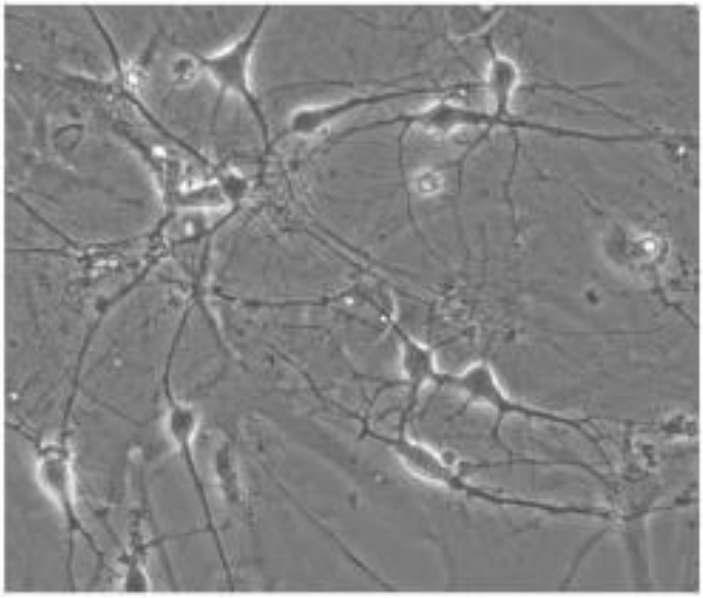

Figure 3.4. Primary hippocampal mouse neurons under light microscopy. Adapted from (78).

3.1.2.4. Transfection and expression in primary neuronal cultures

The lipofection method was performed for transient neuronal transfections. In summary, 6-7 days after initiating the culture, cultured neurons were transfected with either TTX-resistant WT or variant $Na_V1.6$ channels using Optifect (Invitrogen). At the day of transfection, 4 µl of Optifect was combined with 100 µl Opti-MEM reduced-serum medium (Invitrogen), then left at RT for 5 min. After that, 1.08 µg of cDNA (1 µg of human *SCN8A* (WT or variant) cDNA and 0.08 µg of cDNA encoding GFP under Calcium/calmodulin-dependent kinase II (CaMKII) promoter) were added to the mixture then left for 20 min at RT then mixed with the neuronal medium. The pAAV-CaMKII-GFP plasmid with cDNA encoding GFP under α- CaMKII promoter (a gene with expression restricted to excitatory neurons in the neocortex and hippocampus) was chosen in order to identify and measure only the currents from excitatory neurons (Addgene plasmid #64545). An illustration of a primary hippocampal neuron transfected with a GFP can be seen in (Figure 3.5).

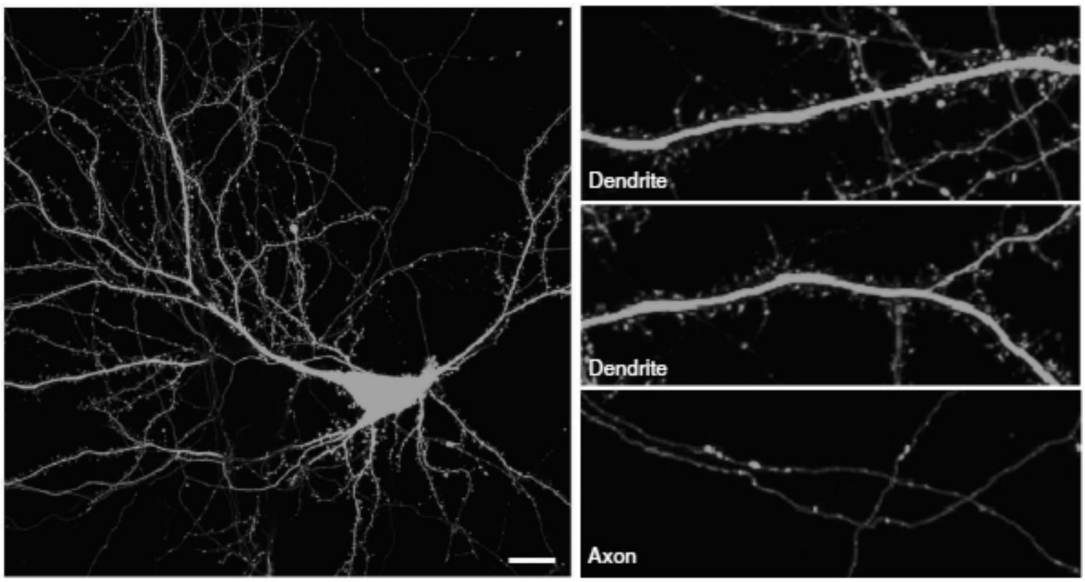

Figure 3.5. Confocal microscope images of a primary hippocampal neuron transfected with a GFP. Scale bar, 20 µm (79).

3.2. Immunohistochemistry

Immunohistochemistry was utilized in this study as a means to confirm that the neurons transfected with GFP under CaMKII promoter were excitatory and exhibited no fluorescence for GAD67 (Glutamic Acid Decarboxylase, 67 Kd), which is a marker for inhibitory neurons. In short, the coverslips plated with cultured hippocampal neurons were fixed for 15 min with 4% paraformaldehyde and then washed with 0.3% Triton X-100 in PBS. After that, the coverslips were left for 1 h at RT with a blocking solution (10 mM Tris solution, 0.15 M NaCl, 0.1% Triton X-100 and 4% non-fat dry milk powder). Then, they were left overnight with a monoclonal anti-GFP antibody at 4°C (rabbit, 1:300, Invitrogen) mixed with a monoclonal anti-GAD67 antibody (mouse, 1:500, Millipore) and a monoclonal anti-MAP2 antibody (chicken, 1:2000, Abcam). On the following day, the coverslips were rinsed with the blocking solution. Then, they were left for 2 h with a secondary Alex Fluor 488-conjugated goat anti-rabbit antibody mixed with an Alex Fluor 647-conjugated goat anti-mouse

antibody and an Alex Fluor 568-conjugated goat anti-chicken antibody at RT, all at a dilution factor of 1:500 (Invitrogen). Later, the coverslips were stained with DAPI (Sigma Aldrich, dilution 1:5000) for 2 min to identify the nuclei and then thoroughly rinsed with PBS and left to dry. Finally, the coverslips were mounted with a mounting medium (Southern Biotech) then left overnight to air-dry preceding their visualization using an Axiovision2 plus Zeiss microscope (Jena, Germany) on the following day.

3.3. Electrophysiology

3.3.1. Patch-clamp technique

Electrophysiology is the branch of physiology designated for studying and investigating the electrical activities taking place in excitable cells such as local field potentials, current flow through ion channels, and APs. Hodgkin and Huxley's studies in the 1950s (80) have recognized the role of ion channels in impulse generation and spreading in excitable cells; marking a milestone in electrophysiology and a foundation for future studies. Within the same period, the principle of voltage-clamping was identified by Cole during his experiments on the squid giant axon (81). In 1976, patch-clamp technique was established by Neher and Sakmann (82) then advanced by Hamill *et al*. (83) to become one of the most common electrophysiological techniques used to study ion channel functions. The patch-clamp technique refers to electrically isolating a patch of the membrane from the external solution, and thus, making the measuring of the current flowing into the patch possible (84). Details such as the configuration of the microelectrode and cell membrane, and the composition of the solutions used for both the pipette and the bath can dictate the nature of the measurements obtained such as whole-cell or single channel level (Figure 3.7-A) (85). The whole-cell configuration is the most common mode applied in the electrophysiological recordings of neuronal cells, cardiac cells and other cell types. There are two major recording modes when it comes to whole-cell configuration. The first one is called the voltage-clamp mode,

wherein the voltage of the cell membrane is modified by the investigator through a feedback circuit, allowing the investigation of ionic currents. The second one is called the current-clamp mode, whereby the current is controlled by the investigator allowing to investigate the changes happening in membrane potential (Figure 3.6B) (86).

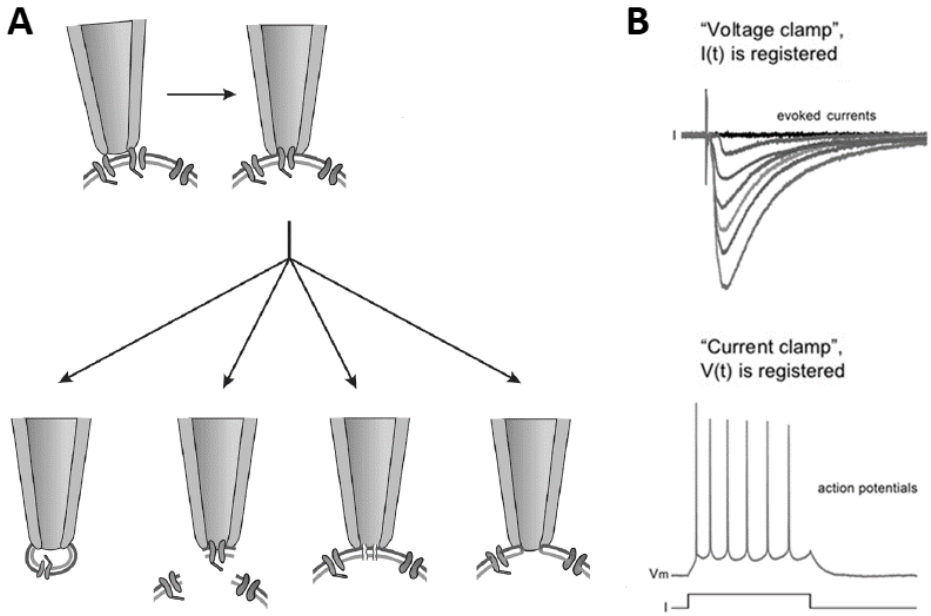

Figure 3.6. Schematic diagram of patch clamp recording configurations. A: top: a low-resistance seal when pipette touches cell which is turned into gigaseal by gentle suction leading to cell-attached patch recording. Bottom from left to right: outside-out excised patch, inside-out excised patch, perforated patch and whole-cell patch clamp configurations. B. Whole-cell configurations: V-Clamp (top) and I-Clamp (bottom). Adapted and modified (87).

3.3.1.1. Setup

Standard whole-cell recordings were applied with a DigiData 1320A digitizer and an Axopatch 200B amplifier. The amplifier head-stage was attached to a LN Unit Junior mini manipulator (Luigs & Neumann, Germany) and an inverted microscope was used to visualize the cells (Axio Vert.A1, Zeiss, Germany) (Figure 3.7). A prepulse protocol (P/4) was used to subtract leakage and capacitive currents. All recordings were performed at RT of 21-24°C.

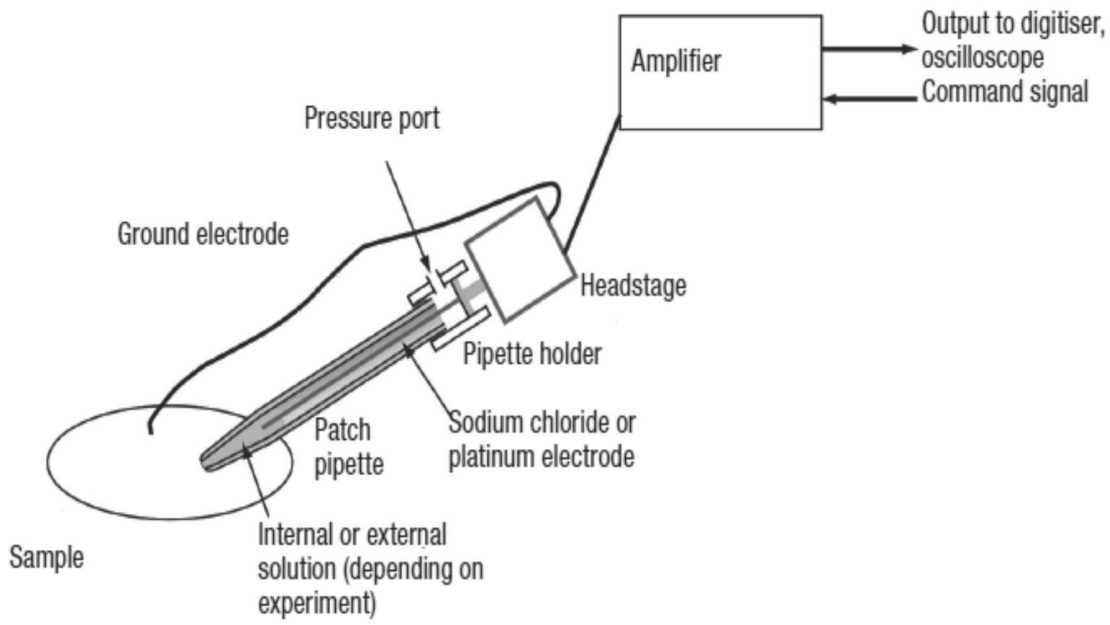

Figure 3.7. Basic patching setup. An illustration of the crucial components of the patching setup (87).

3.3.1.2. Experimental Procedure

In a brief summary, a borosilicate thin wall glass pipettes that has filament (Science Products, Germany) pulled using a horizontal puller (Zeitz Instruments, Germany) in contact with a recording electrode (Ag/AgCl electrodes, Science Products, Germany), was filled with a conductive salt solution, given a slight positive pressure, and brought near to the cell to be investigated. The amplifier was set to V-Clamp the pipette offset was adjusted so the existing currents detected are considered as 0 pA and a seal test was applied via the recording electrode. The pipette was lightly advanced the cell until a dimple was seen on the cell's membrane then pressure was released in order to create the high-resistance seal (gigaseal). Once a Giga Ohm (Ω) seal has been formed, a negative voltage close to RMP (-70 mV) was set and the cells were corrected for fast capacitance. Capacitive currents appear after a voltage step because of the charging of the walls of the glass pipette (fast transients) and the cell membrane (slow transients) representing two capacitors at

this point. Capacitive currents were eliminated by providing additional current to the command stimulus in order to bring the cell to the anticipated voltage value. After that, the membrane patch was disrupted by brief strong suction (negative pressure) to allow intracellular electrical and molecular access. After establishing whole-cell configuration, compensation for whole-cell capacitance and series resistance took place. Series resistance is equivalent to the pipette resistance since it lies in series with the membrane resistance resulting in a voltage drop. Typically, introducing a voltage signal proportional to the membrane current that is scaled fittingly to the command signal and enough to compensate the series resistance. The protocols used in this study contained a P/4 leak and capacitive transient currents subtraction protocols. This sort of compensation took place in order to separate them from the ionic current intended to be measured (84, 86-88).

3.3.1.3. V-Clamp recordings in transfected ND7/23 cells

The recordings took place 48 h following transfection. Picking the cells expressing all the three subunits for the recordings (Figure 3.8). Those cells were recognized by the presence of Na^+ current that is TTX-resistant, green fluorescence; and had some anti-CD8 microbeads (Dynabeads M450, Dynal), (indicating the presence of α-subunit, β1-subunit, and β2-subunit respectively). Recordings took place 10 min after accessing the cell (the whole-cell configuration) (89). Cells were maintained at -100 mV holding potential. Only cells with a peak Na^+ current of at least 1 nA and a maximal voltage error less than 50 mV after 90% compensation were chosen for further evaluation. 500 nM TTX + 300 µM of S-Lic or vehicle 'dimethyl sulfoxide' (DMSO) added to the bath solution. TTX was added in order to block endogenous Na^+ currents. A 5 kHz filter was applied for the currents, they were digitized at 20 kHz, and the pipettes used had a tip resistance of 1.5–3 MΩ.

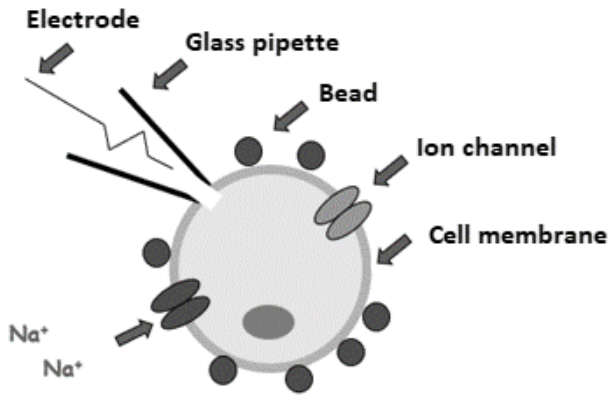

Figure 3.8. V-Clamp recordings were performed using ND7/23 cells expressing all three subunits (α,β1 and β2). Those cells were identified by having: a Na^+ current (TTX-resistant), a green fluorescence; and microbeads on the cell surface (coated with anti-CD8 antibody). Illustration has been provided through the courtesy of Dr. Ulrike Hedrich-Klimosch.

3.3.1.4. I-Clamp recordings in hippocampal neurons

The recordings were performed after 48 h on transfected excitatory neurons that had green fluorescence (expressing GFP under CAMKII promotor). Recordings with hippocampal neurons (Figure 3.9) were performed in presence of 500 nM TTX in the bath solution. Fast I-Clamp mode was activated 2 min after achieving the whole-cell configuration. RMPs were measured then the neurons were left for 5 min before they were maintained at −70 mV RPM by small current injections in order to guarantee uniform conditions. Currents (-50 to +300 pA) with various durations (500-2000 ms) were injected stepwise in order to estimate the input resistance and evoke APs. Following that, the same recordings were repeated again in the same cells but with the presence of 300 µM of S-Lic. The pipettes used had a tip resistance of 2.5-4.5 MΩ. The liquid junction potential due to different ionic distribution of the solutions used at the boundary was estimated to be 15.6 mV and was not corrected. A low-pass filter at 10 kHz was applied for the signals, and they were sampled at 100 kHz.

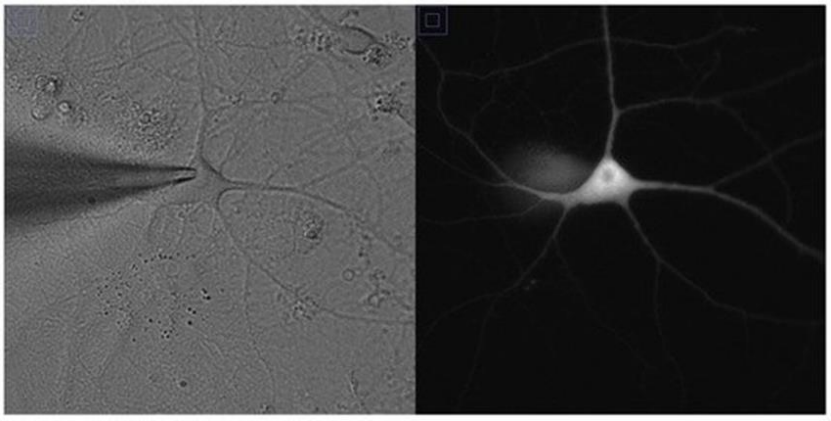

Figure 3.9. A GFP–transfected primary hippocampal neuron during recording. Adapted from (90).

3.4. Solutions

For V-Clamp recordings, the pipette solution had 10 HEPES, 140 CsF, 10 NaCl, 1 EGTA (in mM). This solution had a pH of 7.3 (adjusted with CsOH), and an osmolarity of 310 mOsm/kg (adjusted with mannitol). The bath solution had 10 HEPES, 140 NaCl, 20 TEACl, 3 KCl, 5 CsCl, 0.1 CdCl2, 1 $MgCl_2$ and 1 $CaCl_2$. This solution had a pH of 7.3 (adjusted with CsOH), and an osmolarity of 320 mOsm/kg (adjusted with mannitol). For I-Clamp recordings, the pipette solution had 10 HEPES, 0.3 GTP-Na, 5 KCl, 10 phosphocreatine, 4 ATP-Mg, 10 EGTA, 2 $MgCl_2$ and 125 K-gluconate. This solution had a pH of 7.2 (adjusted with KOH), and an osmolarity of 290 mOsm/kg (adjusted with mannitol). The bath solution had 2.5 KCl, 125 NaCl, 1.25 NaH_2PO_4, 10 glucose, 5 HEPES, 25 $NaHCO_3$, 2 $CaCl_2$ and 1 $MgCl_2$. This solution had a pH of 7.4 (adjusted with HCL), and an osmolarity of 305 mOsm/kg (adjusted with mannitol).

3.5. Drugs and chemicals

S-Lic (BIA 2-194, BIAL - Portela and Ca) was dissolved in DMSO. The recordings for the control groups had equal amounts of DMSO (0.1%) in all experiments. The chemicals -unless otherwise stated- were acquired from Sigma Aldrich.

3.6. Data acquisition and analysis

3.6.1. V-Clamp protocols

3.6.1.1. Voltage-dependence of activation

The activation curve (conductance versus voltage) was acquired by determining the peak Na^+ current at several depolarization steps (Figure 3.10). The data was fitted by a Boltzmann function:

$$g/g_{max}\,(V) = 1/(1+\exp[(V-V_{1/2})/k_V]),$$

Where the conductance (g) = $I/(V-V_{rev})$, V_{rev} the reversal potential of Na^+, $V_{1/2}$ the voltage of activation at half-maximum, k_V is a slope factor and g_{max} is the maximal conductance.

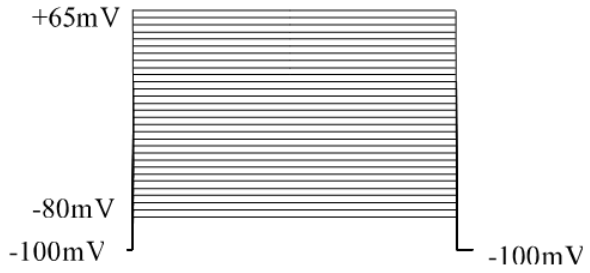

Figure 3.10. The voltage step protocol applied to assess the voltage-dependence of activation.

3.6.1.2. Steady-state FI

Steady-state inactivation was evaluated by assessing the peak of the current obtained using 100 ms conditioning pulses to various potentials (starting from -110 mV up to -20 mV) then a test pulse to -10 mV (Figure 3.11). The peak current obtained in this protocol reflects the ratio of non-inactivated channels. The data obtained was fitted by a standard Boltzmann function:

$$I/I_{max}\,(V) = 1/(1+\exp[(V-V_{1/2})/k_V]),$$

Where k_V as a slope factor, I_{max} is the amplitude of the maximal current and $V_{1/2\ is}$ the voltage of half-maximal inactivation.

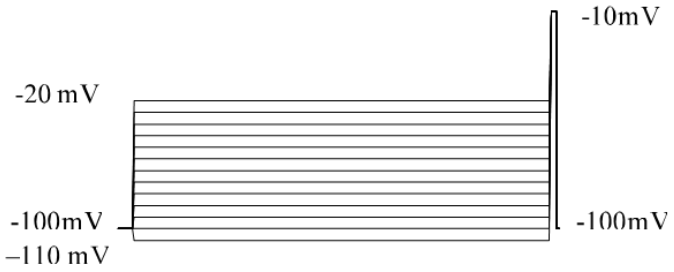

Figure 3.11. The voltage step protocol applied to assess the steady-state FI.

3.6.1.3. Kinetics of FI

The data acquired from the protocol assessing the voltage-dependence of activation was also utilized to determine the time constants of FI. To fit to the time course of FI, a second-order exponential function was used resulting in two time constants. However, only the fast time constant (major time constant of the FI, named τ_h), was considered for analysis since the effect of the other one was minor.

3.6.1.4. Recovery from FI

Cells were maintained at -100 mV, then depolarized for 100 ms to -20 mV (in order to inactivate all VGSCs). The cells were then repolarized to either -80 mV or -100 mV for increasing durations then a second depolarizing step to -20 mV for 5 ms was applied. To fit the time course of recovery from inactivation, a first-order exponential function with an initial delay was used yielding the time constant τ_{rec} for the variants tested with the exception of the A1622D variant, since a second-order exponential function with an initial delay was considered more fitting ($\tau_{rec\ fast}$).

3.6.1.3. Steady-state SI

Cumulative protocols were used to assess both entry into- and steady-state-SI (91). Conditioning pulses (30 s) beginning at –110 mV and stepped gradually (by 10 mV) up to 0 mV were applied. Then, a hyperpolarization to –100 mV for 100 ms took place (to allow recovery from FI). Lastly, a test pulse (5 ms) at -25 mV was applied (Figure 3.12). The data was fitted to the Boltzmann function previously mentioned in FI.

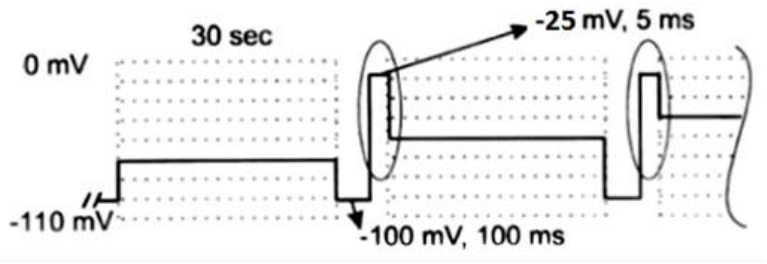

Figure 3.12. The cumulative protocol applied to assess the steady-state SI.

3.6.1.6. Entry into SI

The cells were depolarized (from the holding potential of –100 mV) to 0 mV for various durations, then repolarized again to –100 mV for 100 ms permitting their recovery from FI. Then, the cells were depolarized again to 0 mV briefly for 3 ms in order to assess the fraction of the channels that are slow inactivated. A first order exponential function was used for fitting the time course of entry into SI.

3.6.2. Descriptions of some action potential parameters

1- Rheobase: The minimal injected current that elicits an AP.

2- Input Resistance: The slope of a linear regression fit applied for the plot of voltage responses versus current injections (-110 to -10 pA).

3- Threshold: The maximum negative voltage that has to be reached through the current injection in order to elicit an AP, the voltage at 50% of the maximal dV/dt was assessed (92).

4- Spike height: The peak relative to the maximum negative voltage achieved during after hyperpolarization directly after the spike.

5- Spike half-width: AP width at the membrane voltage in the middle of AP threshold and AP peak.

6- Spike half-height width (Spike width): The width at half-maximal spike height (Figure 3.13).

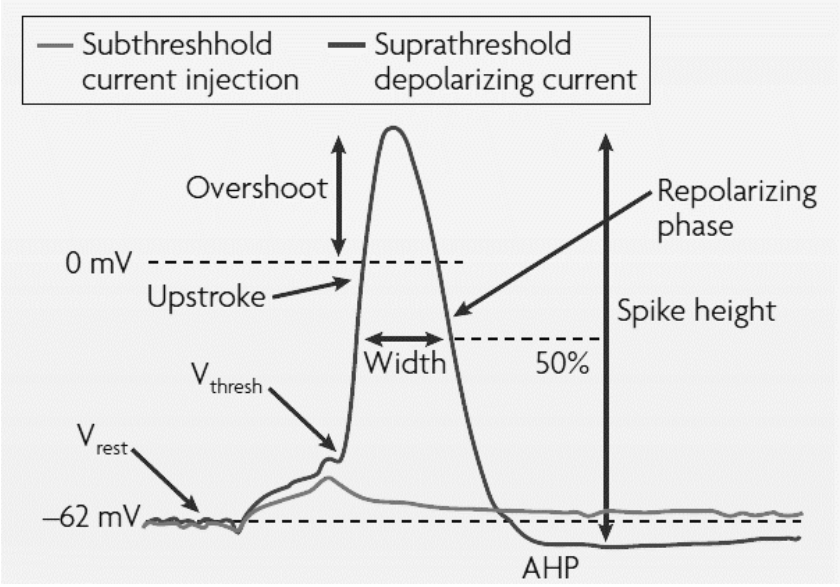

Figure 3.13. Illustration of some commonly measured parameters of an action potential. (Vrest), resting potential. (Vthresh), voltage threshold. (Upstroke), the depolarizing phase of the action potential. (AHP), after hyperpolarization (79).

3.7. Statistical analysis

Data was recorded using pCLAMP 8 (Molecular Devices) and analyzed in Clampfit 11.0.3 (Axon Instruments), Microsoft Excel (USA) and GRAFIT 3.01 (Erithacus UK). Statistial analyses were done in Graphpad software V7 (Graphpad prism, USA). Shapiro-Wilk normality test was used to assess the data for normal distribution. For comparison between two groups, un-paired *t*-test (paired *t*-test for neuronal experiments) or Wilcoxon Signed Rank Test were used. For comparison between multiple groups, ANOVA (one-way or two-way) with Tukey's *post-hoc* test (Dunnett´s *post-hoc* test for neuronal firing experiments) were applied for that data that was normally distributed. For the data that was not distributed normally ANOVA on ranks with Dunn's *post-hoc* test were used, n was used to indicate the number of cells measured. Statistical significance necessitates the p value to be less than 0.05.

4. RESULTS

4.1. Eslicarbazepine effects on $Na_V1.6$ WT channels

4.1.1. V-Clamp recordings in ND7/23 cells

After administration of 300 µM S-Lic, we observed roughly a 22% reduction of peak transient I_{Na} conductance in the averaged curve of $Na_V1.6$ WT channels at a holding potential of -100 mV (Figures 4.1 and 4.2 A). We observed a slight decrease in the conductance of persistent I_{Na} (ramp current peaks normalized to I_{peak} after -100 to + 40 mV ramp stimuli with a duration of 800 ms) in our results (Figure 4.2 B). The $V_{1/2}$ of activation of transient Na^+ current was also not altered by S-Lic treatment (Figure 4.3 A). As for the $V_{1/2}$ of inactivation, S-Lic caused a hyperpolarizing shift (Vehicle, $V_{1/2}$= -63.21±1.2 mV, 300 µM S-Lic, $V_{1/2}$ = -66.98±1.08 mV, $p<0.05$) in the $V_{1/2}$ of FI (Figure 4.3 B). The time course of recovery from FI was generally not affected by S-Lic (Figure 4.4), as well as the voltage-dependence of the τ_h of FI (Figure 4.5 A). However, administration of 300 µM S-Lic accelerated the entry into SI state (τ_{entry}=2847.06±208.4 ms, n=11) when compared to vehicle (τ_{entry}=3500.26±170.8 ms, n=10), $p<0.05$, Figure 4.5 B). In addition, S-Lic caused a hyperpolarizing shift of the steady-state SI (Vehicle, $V_{1/2}$= -55.96±1.16 mV, n = 7; 300 µM S-Lic, $V_{1/2}$ = -72.06±0.71 mV, n = 7; $P<0.0001$), and decreased the slope of the steady-state SI curve when compared to vehicle group (Vehicle, k = 7.69±0.44, n = 7; 300 µM S-Lic, k = 6.05±0.54, n = 7, $p<0.05$), (Figure 4.6 A, B and C).

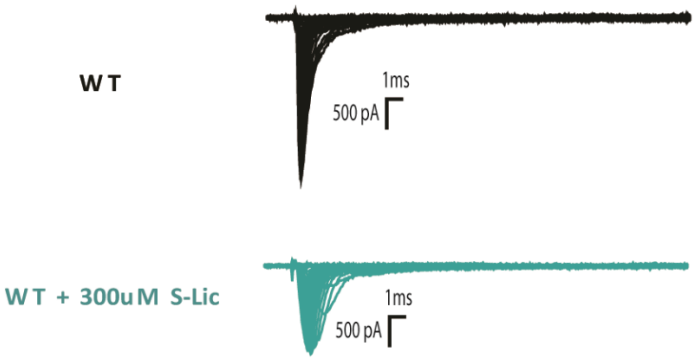

Figure 4.1. Representative Na^+ current traces from WT and WT+300 µM S-Lic in ND7/23 cells. (WT), wild-type. (S-Lic), eslicarbazepine.

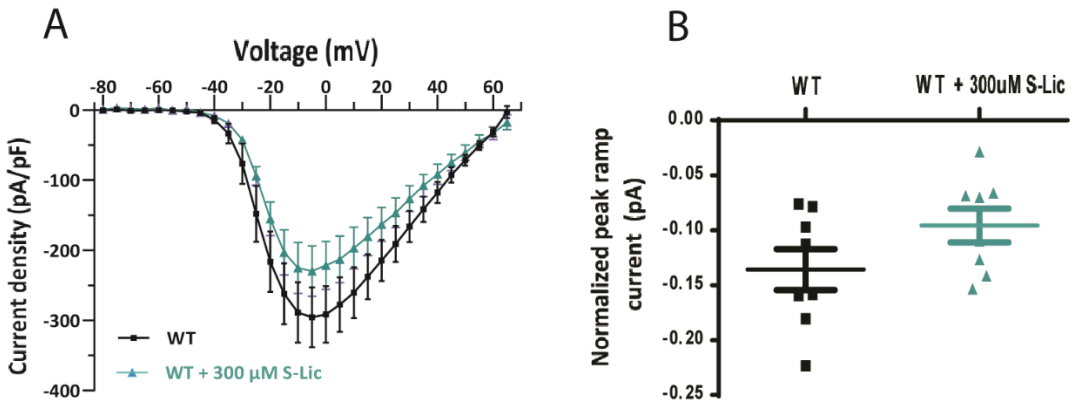

Figure 4.2. Effects of S-Lic on transient and persistent current in WT $Na_v1.6$ Na^+ channels. (A) Peak transient Na^+ currents (normalized to cell capacitances) versus voltage. WT, n=14. WT+300 µM S-Lic, n=9. **(B)** Ramp current peaks (persistent current) normalized to I_{peak}, n=8. Means ± SEM for the data points are displayed. n, number of recorded cells.

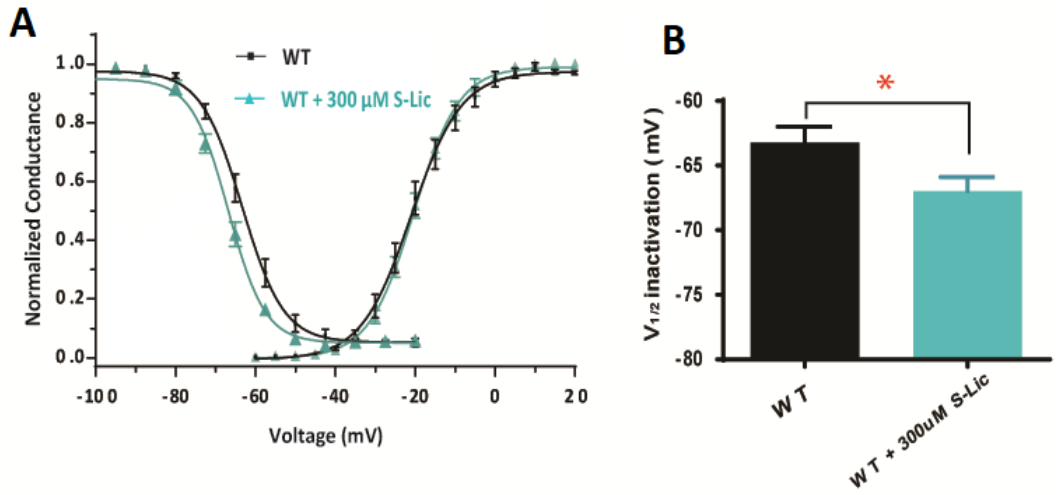

Figure 4.3. Steady-state activation and FI curves in WT $Na_v1.6$ Na^+ channels in the presence of 300 µM of S-Lic (turquoise) or vehicle (black). (A) A Boltzmann function was applied to fit the data points. Administration of 300 µM of S-Lic does not alter the $V_{1/2}$ of activation but a significant hyperpolarizing shift can be seen in **(B)** the $V_{1/2}$ of FI. Activation: n=10 for WT, and n=9 for WT+300 µM S-Lic. Inactivation: n=10 for WT, and n=7 for WT+300 µM S-Lic. Means ± SEM for the data points are displayed. n, number of recorded cells, *p<0.05 (un-paired *t*-test).

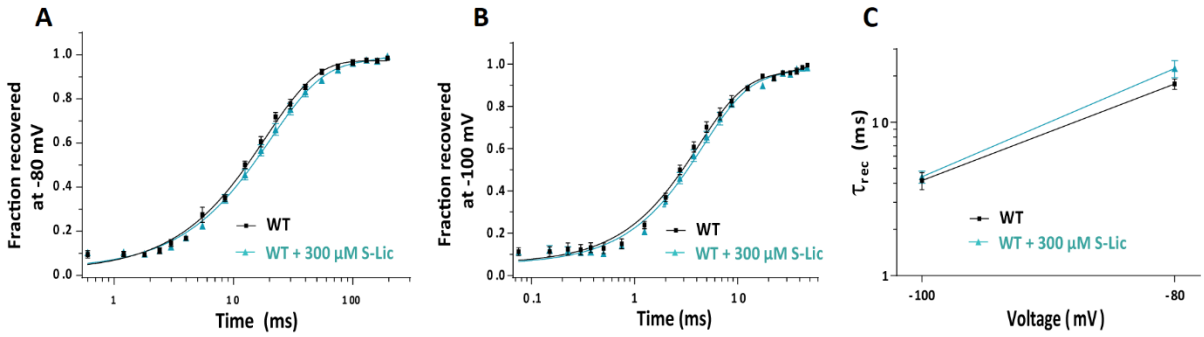

Figure 4.4. Effects of S-Lic on recovery from FI in WT $Na_v1.6$ Na^+ channels (A) at -80 mV and **(B)** at -100 mV, in order to fit the data points, a first-order exponential function with an initial delay was applied **(C)** average values of the τ_{rec} at both voltages. Administration of 300 µM of S-Lic did not cause a significant difference in the τ_{rec} from FI when compared to vehicle, n=7. Means ± SEM for the data points are displayed. n, number of recorded cells.

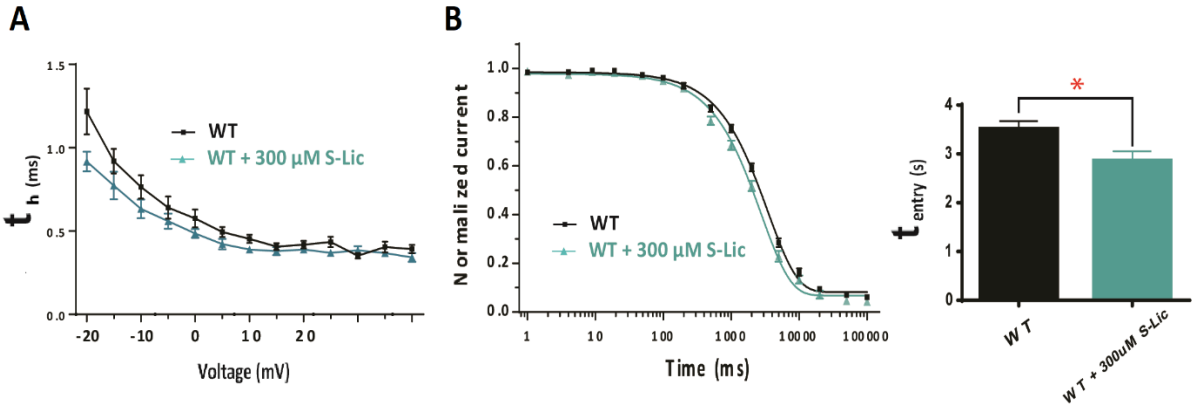

Figure 4.5. Effects of S-Lic on the kinetics of FI and SI in WT $Na_v1.6$ Na^+ channels. (A) Voltage-dependence of the τ_h of FI (n=10 for WT, and n=9 for WT+300 µM S-Lic. **(B)** Entry into SI. A first-order exponential function was applied. Administration of 300 µM of S-Lic accelerates the entry into SI (n=11) when compared to vehicle (n=10). Means ± SEM for the data points are displayed. n, number of recorded cells, *p<0.05 (un-paired *t*-test).

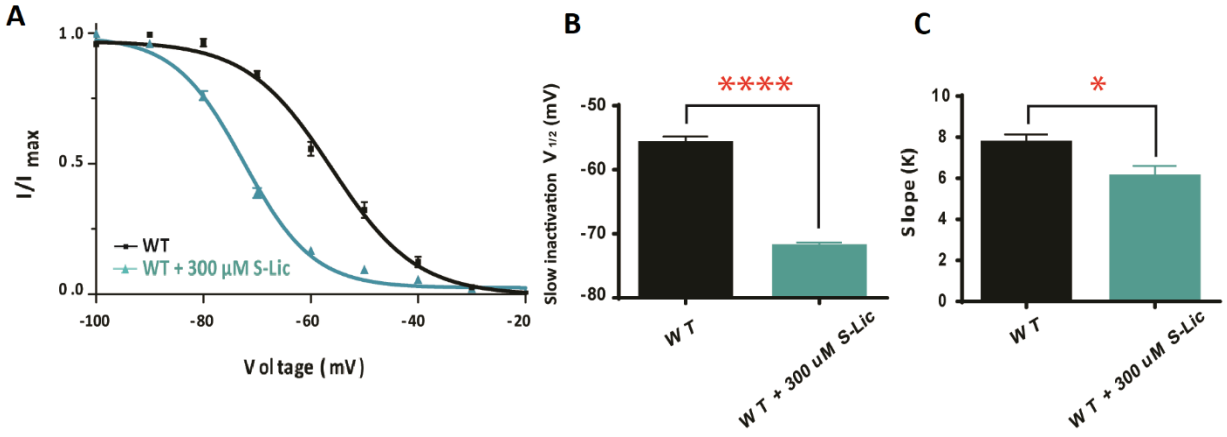

Figure 4.6. Effects of S-Lic on steady-state SI in WT $Na_v1.6$ Na^+ channels. (A) steady-state SI curves, a Boltzmann function was applied to fit the data points. Administration of 300 µM of S-Lic causes a hyperpolarizing shift **(B)** of the steady-state SI (n=7 for Vehicle, and n=7 for 300 µM S-Lic), and **(C)** decreased the slope of the steady-state SI when compared to vehicle (n=7). Means ± SEM for the data points are displayed. n, number of recorded cells, *p<0.05, ****p<0.0001 (un-paired *t*-test).

4.1.2. I-Clamp recordings in cultured hippocampal neurons

The recordings in cultured mouse neurons transfected with $Na_V1.6$ WT channels showed a reduction of maximal firing rates when treated with S-Lic (Figure 4.7). We recorded APs in neurons evoked after applying a series of current injections (-50 to 300 pA). Then, the area under the curve (AUC) across this range was calculated separately (for each neuron) and the corresponding values were significantly lower after the neurons were exposed to 300 µM S-Lic (1052±207.3 untreated versus 622.3±151.8 after treatment, n=9, p<0.05) (Figure 4.8). Administration of 300 µM S-Lic did not seem to affect otherwise tested neuronal properties and single AP parameters (Figure 4.9).

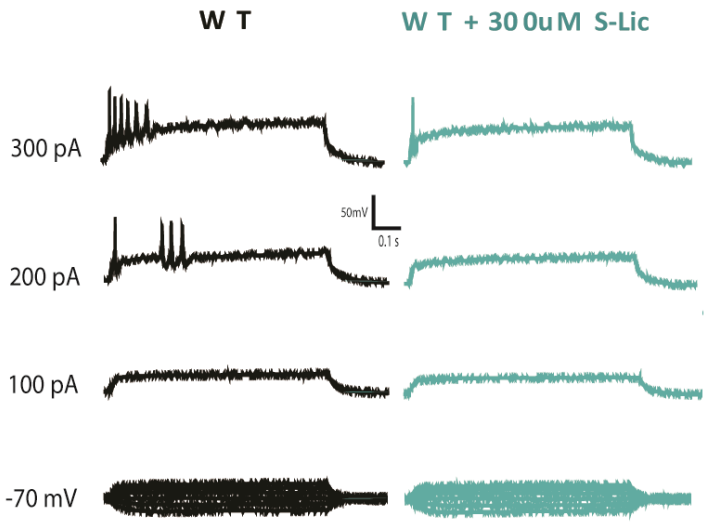

Figure 4.7. Illustrative traces of APs recorded in a neuron transfected with TTX-resistant $Na_v1.6$ WT before and after the addition of 300 µM S-Lic. WT (black), WT+300 µM S-Lic (turquoise).

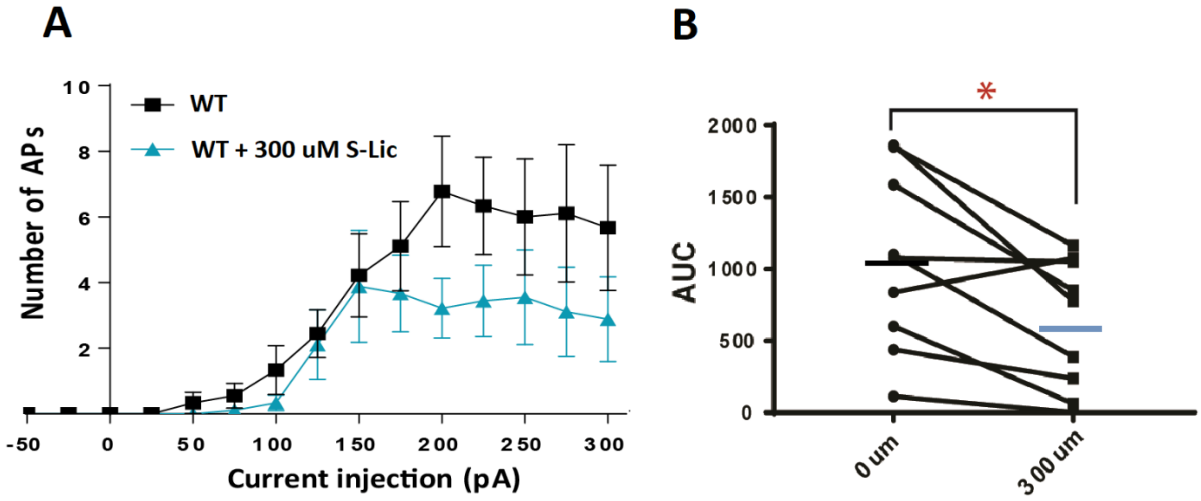

Figure 4.8. Effects of S-Lic on the firing properties of transfected WT $Na_v1.6$ Na^+ channels in primary cultured hippocampal mouse neurons. (A) Number of APs plotted versus injected current in transfected WT channels. **(B)** The AUC values were significantly lower when the neurons were exposed to 300 µM S-Lic (n=9). Means ± SEM for the data points are displayed. WT (black), WT+300 µM S-Lic (turquoise). *P<0.05, (paired *t*-test).

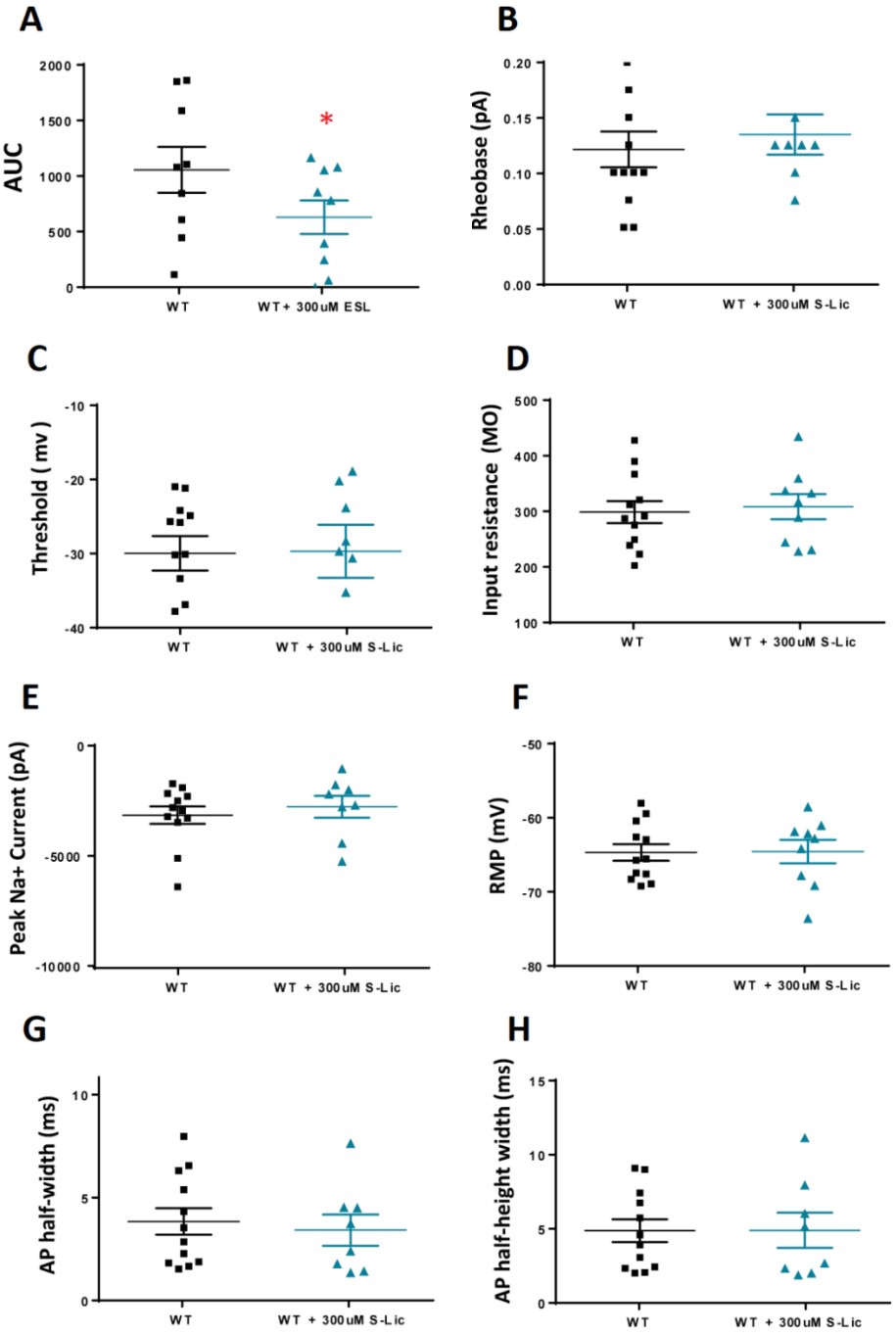

Figure 4.9. Effects of S-Lic on some inherent neuronal properties and AP parameters in WT $Na_v1.6$ Na^+ in the presence and absence of 300 µM of S-Lic. (A) The AUC for AP firing (n=9). **(B)** Rheobase (pA). **C)** Threshold (mV). **(D)** Input Resistance (MΩ). **(E)** Peak Na^+ current (pA). (F) Resting Membrane potential (mV). **(G)** AP Half-width (ms). **(H)** AP half-height-width (ms). Means ± SEM for the data points are displayed. WT (black), WT+300 µM S-Lic (turquoise). *P<0.05, (paired *t*-test).

4.2. Eslicarbazepine effects on M1760I variant VGSCs

4.2.1. V-Clamp recordings in ND7/23 cells

The current density and ramp currents for M1760I channels were statistically comparable with WT channels in ND7/23 cells (Figures 4.10 and 4.11). The recordings uncovered a hyperpolarizing shift of the activation curve in M1760I variant channels (WT, $V_{1/2}$ = -20.14±1.54 mV, n=10; M1760I, $V_{1/2}$ = -26.1±1.58 mV, n=12, p<0.05), however, the $V_{1/2}$ of steady-state FI and was not altered (Figure 4.12). Like-wise, the recovery from FI was comparable with WT channels (Figure 4.13). However, the kinetics of FI was altered since a delay in the transition from the activated to the FI state was detected (WT, τ at 10 mV; 0.45±0.02 ms, n=10, M1760I, τ at 10 mV; 0.67±0.03 ms, n=10, p<0.05, Figure 4.14A). Lastly, we evaluated the SI characteristics in this variant. Neither entry into SI (Figure 4.14 B), nor the $V_{1/2}$ of SI (Figure 4.15) were altered. However, the slope of the steady-state SI curve was steeper in M1760I variant when compared WT channels (M1760I; k=10.07±0.52, WT; k=7.69±0.44, p<0.01, Figure 4.15).

Administration of 300 µM S-Lic to transfected ND7/23 cells did not change the $V_{1/2}$ of activation and FI or current peaks of both transient and persistent Na^+ currents when compared to vehicle M1760I group (Figures 4.11 and 4.12). S-Lic did not alter the recovery from FI at -80 mV holding potential but an acceleration was observed at -100 mV (at -100 mV; WT τ=4.16±0.52; M1760I τ=3.95±0.35, M1760I+300 µM S-Lic τ=2.79±0.14, n=7, p<0.05, Figure 4.13). S-Lic slightly lowered the FI time constant of M1760I cells with respect to the M1760I group but abated the difference between M1760I and WT groups (Figure 4.14 A). S-Lic significantly sped up the entry into SI (M1760I+300 µM S-Lic; τ_{entry}=2984.18±355.44 ms, n=10; M1760I; τ_{entry}=4474.82±322.82 ms, n=12, p<0.01, Figure 4.14B). Finally, S-Lic triggered a hyperpolarizing shift of the steady-state SI (M1760I+300 µM; S-Lic $V_{1/2}$ =-70.66±1.35 mV, n=9; M1760I $V_{1/2}$= -54.98±1.28 mV, n=10; and WT $V_{1/2}$=-55.96±1.16 mV, n = 7; p<0.0001). It has also caused a decrease in the slope of the steady-state SI back to

the levels of WT (M1760I+300 µM S-Lic k=7.7±0.72; M1760I k=10.07±0.52, WT k=7.6±0.44, p<0.01, Figure 4.15 A, B and C).

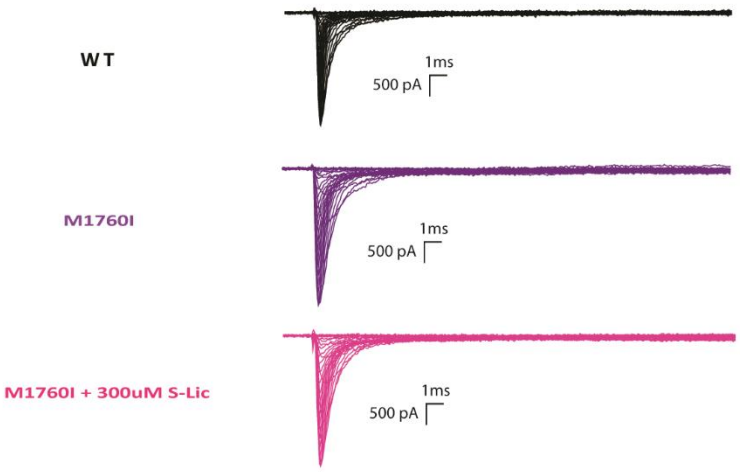

Figure 4.10. Representative Na^+ current traces from WT, M1760I and M1760I+300 µM S-Lic in ND7/23 cells.

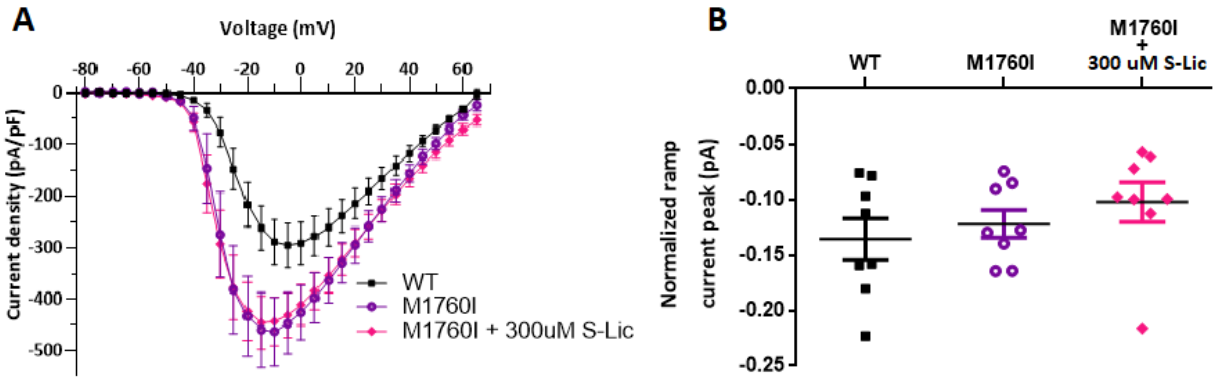

Figure 4.11. Effects of S-Lic on transient and persistent current in M1760I variant Na^+ channels. (A) Peak transient Na^+ currents (normalized to cell capacitances) versus voltage. WT, n=14. M1760I, n=12. M1760I+300 µM S-Lic, n=16. **(B)** Ramp current peaks normalized to I_{peak}, n=8. Means ± SEM for the data points are displayed. n, number of recorded cells.

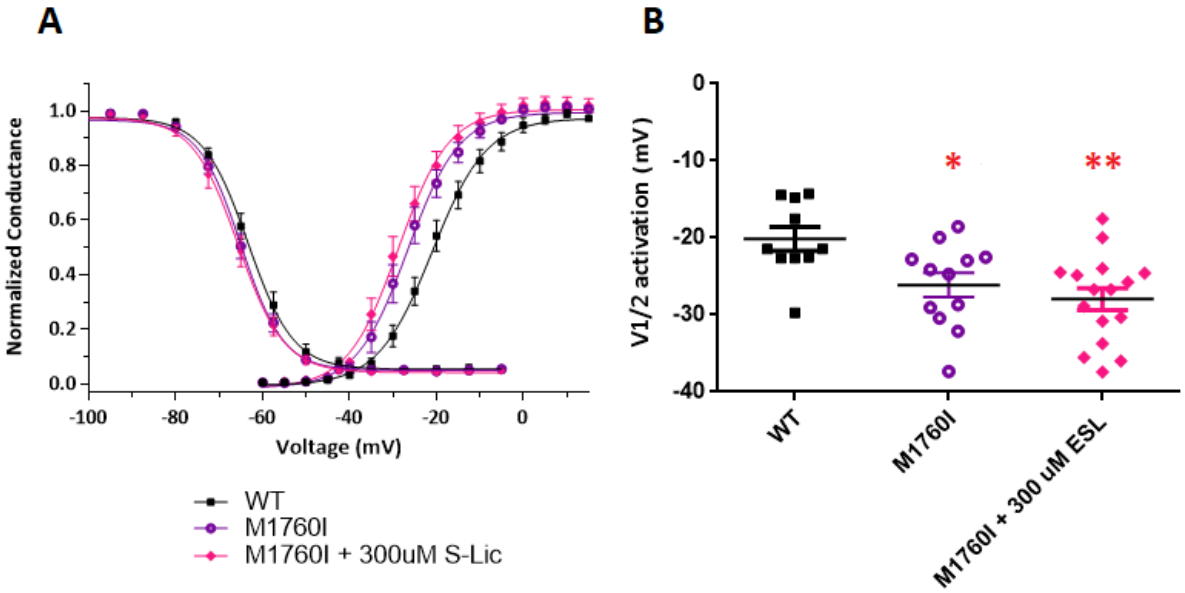

Figure 4.12. Steady-state activation and FI curves in M1760I variant Na^+ channels in the presence of 300 µM of S-Lic (pink) or vehicle (violet). (A) Steady-state activation and FI curves. A Boltzmann function was applied to fit the data points. **(B)** M1760I variant channels had a hyperpolarizing shift of the activation curve with respect to the WT, n = 12. Administration of 300 µM of S-Lic did not seem to alter the $V_{1/2}$ of activation and FI in M1760I variant. Means ± SEM for the data points are displayed. n, number of recorded cells. *p<0.05 versus WT, one-way ANOVA with Tukey´s *post-hoc* test.

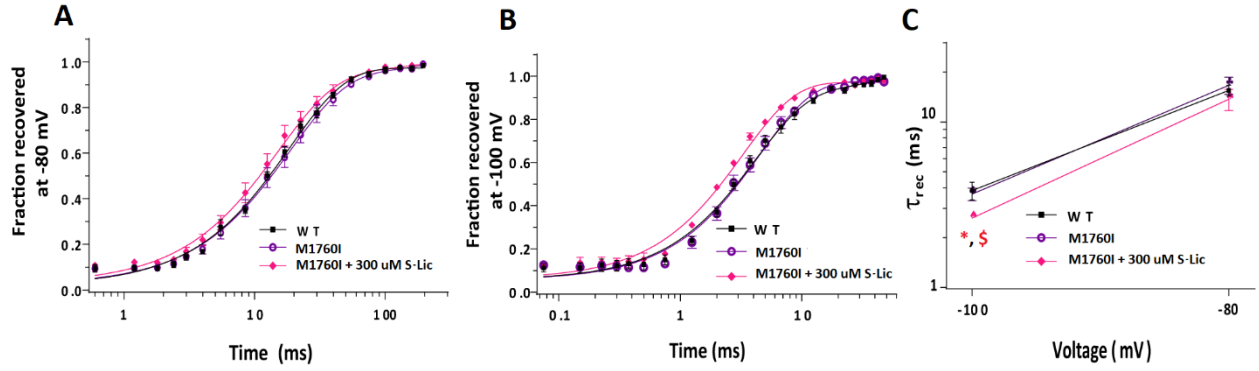

Figure 4.13. Effects of S-Lic on recovery from FI in M1760I variant Na^+ channels. (A) at -80 mV and **(B)** at -100 mV, a first-order exponential function with an initial delay was applied. **(C)** Average values of the τ_{rec} at both voltages. S-Lic did not alter the recovery from FI at -80 mV holding potential but an acceleration was observed at -100 mV, n=7. Means ± SEM for the data points are displayed. n, number of recorded cells.*p <0.05 versus WT and $^{\$}$p<0.05 versus untreated groups, Kruskal-Wallis test with Dunn's *post-hoc* test.

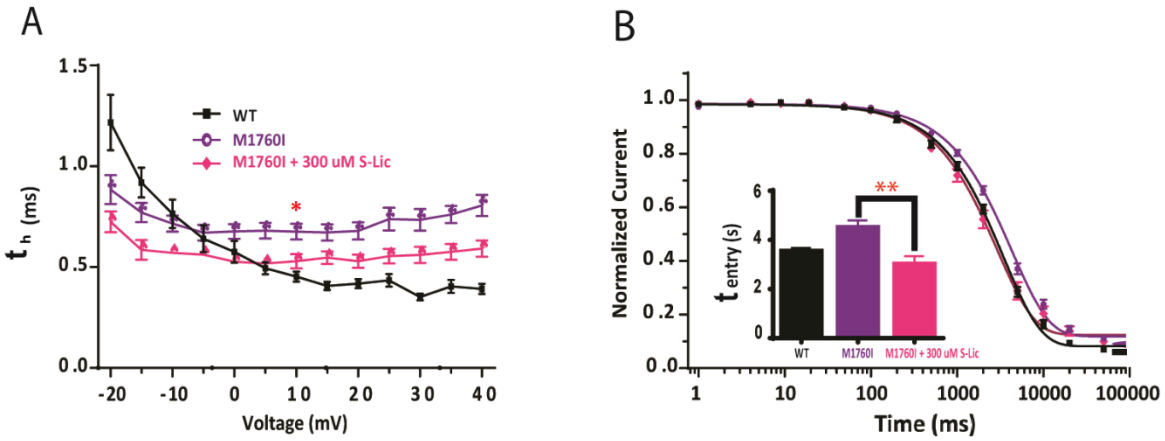

Figure 4.14. Effects of S-Lic on the kinetics of FI and SI in M1760I variant Na^+ channels. (A) Voltage-dependence of the τ_h of FI in mutated M1760I channels. Upon comparison, only untreated M1760I group have showed a significant delay in the transition from the activated to the FI state versus WT (n = 10, two-way ANOVA with Tukey's *post-hoc*, p<0.05 between WT and M1760I groups). **(B)** Entry into SI in variant M1760I channels. A first-order exponential function was applied. Administration of 300 µM of S-Lic in M1760I has accelerated the entry into SI (n=10) when compared to vehicle (n=12) **p<0.01; (one-way ANOVA with Tukey´s *post-hoc* test). Means ± SEM for the data points are displayed. n, number of recorded cells.

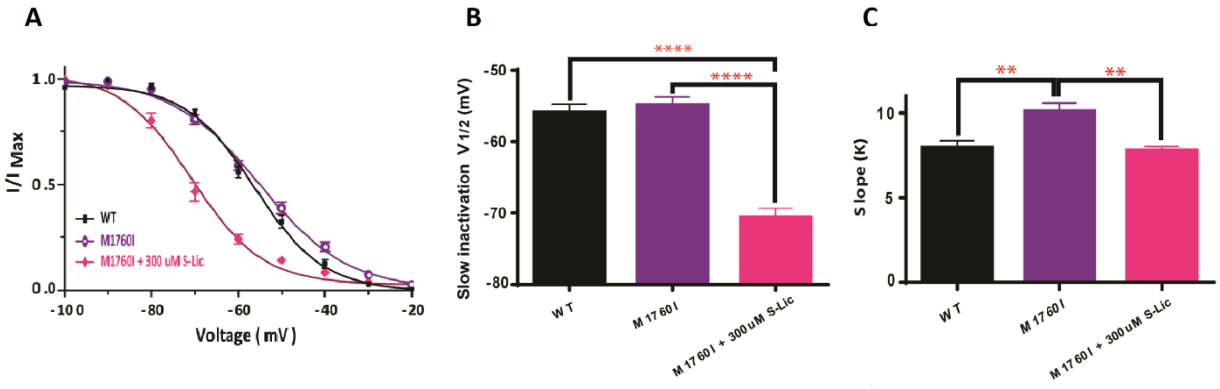

Figure 4.15. Effects of S-Lic on steady-state SI in WT $Na_v1.6$ Na^+ channels. (A) Steady-state SI curves, a Boltzmann function was applied to fit the data points. Administration of 300 µM of S-Lic in M1760I has caused **(B)** a hyperpolarizing shift of the steady-state SI when compared to vehicle and WT (n = 7), and **(C)** a decrease in the slope of the steady-state SI to a level comparable to WT (**p<0.01). M1760I; n=10, M1760I+300 µM S-Lic; n=9. Means ± SEM for the data points are displayed. n, number of recorded cells; **p<0.01; ****p<0.0001 (one-way ANOVA with Tukey´s *post-hoc* test or ANOVA on ranks with Dunn´s *post-hoc* test).

4.2.2. I-Clamp recordings in cultured neurons

The recordings showed a reduction of maximal firing rates with S-Lic (Figure 4.16). The AUC was significantly lower in the without S-Lic group (2240± 468.9 versus 1816.3±437 after treatment, n=9, p<0.05, Figure 4.17). M1760I variant channels had an increase in the AP firing frequency compared to WT channels and S-Lic brought it back to a level comparable to WT (AUC; WT, 904.3±174.2, n=12; M1760I, 2240±468.9, M1760I+300 µM S-Lic 1816.3±437, n=9; p<0.05 versus WT; Figure 4.18 A). Administration of 300 µM S-Lic did not seem to affect otherwise tested neuronal properties and single AP parameters (Figure 4.18).

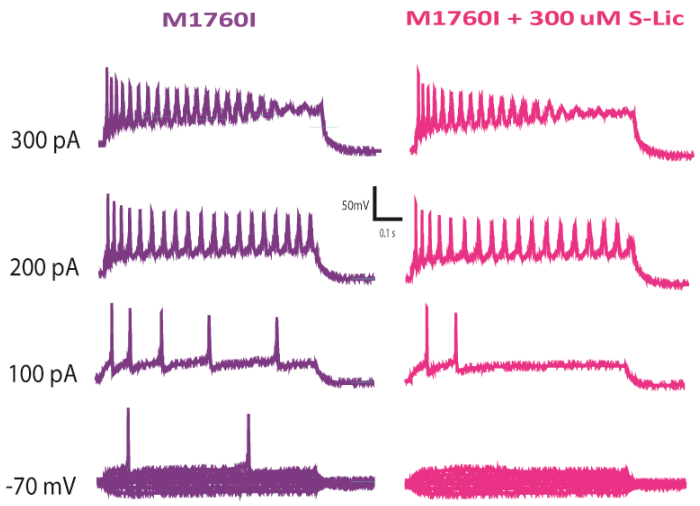

Figure 4.16. Illustrative traces of APs recorded in a neuron transfected with TTX-resistant M1760I variant before and after the addition of 300 µM S-Lic. M1760I (violet), M1760I+300 µM S-Lic (pink).

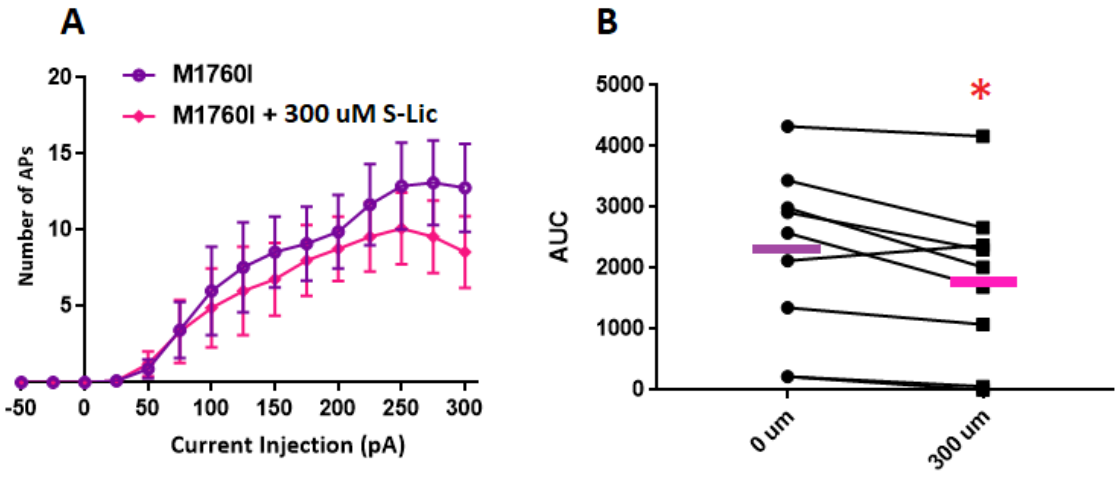

Figure 4.17. Effects of S-Lic on the firing properties of variant M1760I Na^+ channels in primary cultured hippocampal mouse neurons. (A) Number of APs plotted versus injected current in transfected variant M1760I channels. **(B**) The AUC was significantly lower when the neurons were exposed to 300 µM S-Lic (n=9). Means ± SEM for the data points are displayed. WT (black), M1760I (violet), M1760I+300 µM S-Lic (pink). *P<0.05, (paired *t*-test).

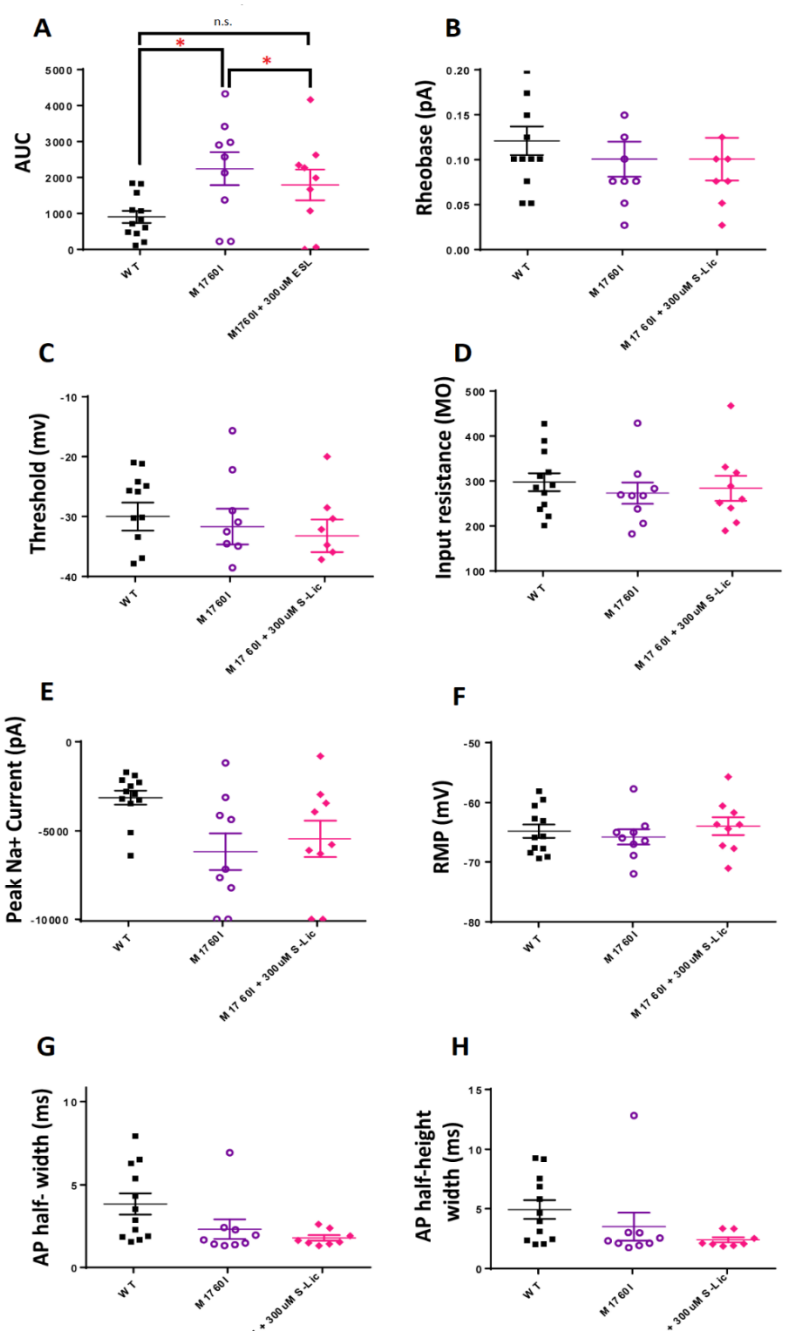

Figure 4.18. Effects of S-Lic on some neuronal features and AP parameters in variant M1760I Na^+ channels in the presence and absence of 300 µM of S-Lic. (A) The AUC for AP firing. M1760I variant channels significantly increase the AP firing frequency compared to WT channels and S-Lic brought it back to a level comparable to WT (WT, n=12; M1760I, M1760I+300 µM S-Lic n= 9) **(B)** Rheobase (pA). **(C)** Threshold (mV). **(D)** Input Resistance (MΩ). **(E)** Peak Na^+ current (pA). **(F)** Resting Membrane potential (mV). **(G)** AP Half-width (ms). **(H)** AP half-height-width (ms). Means ± SEM for the data points are displayed. WT (black), WT+300 µM S-Lic (turquoise). *P <0.05, (one-way ANOVA with Dunnett´s *post-hoc* test or ANOVA on ranks with Dunn´s *post-hoc* test for comparisons between groups and WT).

4.3. Eslicarbazepine effects on A1622D mutated channels

4.3.1. V-Clamp recordings in ND7/23 cells

The recordings revealed that the current density for A1622D channels was comparable with WT channels, but there was a large ramp current corresponding to a high persistent current in comparison to the WT (normalized ramp current peaks WT=-0.13± 0.01, n =8, M1760I=-0.25±0.03, n=8, p<0.01), (Figures 4.19 and 4.20). In addition, A1622D variant channels show a depolarizing shift of the activation curve (WT, $V_{1/2}$=-20.14±1.54 mV, n=10; A1622D, $V_{1/2}$ =-10.07±1.11 mV, n=9, p<0.0001, Figure 4.21 A and B). Steady-state FI curve was also shifted towards depolarized potentials for A1622D channels and the slope was increased compared to WT channels (WT, $V_{1/2}$ =-63.21±1.2 mV, k=4.79± 0.17 n=10; A1622D, $V_{1/2}$ =-56.31±1.41 mV, k=7.76±0.18 n=7, p<0.0001, Figure 4.21 A and C). A1622D channels displayed enhanced recovery from FI at both -80 and -100 mV holding potentials, (at -100 mV; WT τ=4.16±0.52; A1622D τ=0.71±0.1, n=9, p<0.0001; and at -80 mV; WT τ=17.75±1.39; A1622D τ=2.5±0.21, n=9, p<0.0001, Figure 4.22). The tau-voltage relationship for τ_h of FI in the variant group was reversed with respect to the WT group (WT; τ at 10 mV=0.45±0.02 ms, n=10, A1622D; τ at 10 mV=6.31±0.37 ms, n=9, p<0.05, Figure 4.23 A). Finally, A1622D variant channels cause an accelerated entry into SI in comparison with WT channels (A1622D τ_{entry}=1422.56±93.3 ms, n=8, WT τ_{entry}=3500.26±170.8 ms, n=10, p<0.0001, Figure 4.23 B). The $V_{1/2}$ of SI was not affected, but the slope of the steady-state SI was decreased in this variant (A1622D k=5.2±0.15, WT k=7.69±0.44, p<0.001, Figure 4.24 A and C).

In A1622D transfected ND7/23 cells, administration of 300 µM of S-Lic decreased the persistent current and this value got closer to that of WT group (Figure 4.20 B). S-Lic presence did not result in a significant difference in the $V_{1/2}$ of activation compared to the A1622D values. S-Lic further shifted the steady-state FI curve towards depolarized potentials of the A1622D cells (A1622D, $V_{1/2}$=-56.31± 1.41 mV, n=7; A1622D+300 µM S-Lic, $V_{1/2}$ =-51.85± 0.6 mV n=10, p<0.05, Figure 4.21). Administration of 300 µM of S-Lic did not cause a significant difference in the τ_{rec} from

FI when compared to vehicle-treated A1622D cells (Figure 4.22). Both S-Lic and without S-Lic A1622D groups exhibited substantially lower voltage-dependence of the τ_h of FI with respect to the WT. However, the S-Lic group has also shown a significant acceleration in the transition from the activated to the FI state in comparison to the without S-Lic group (at 10 mV: WT; τ=0.45±0.02 ms, n=10, A1622D; τ=6.31± 0.37 ms, n=9, A1622D+300 µM S-Lic; τ=4.35±0.23 ms, n=9, $p<0.05$, Figure 4.23 A). In addition, S-Lic accelerated the entry into SI versus without S-Lic group (A1622D τ_{entry}=1422.56±93.3 ms, n=8, A1622D+300 µM S-Lic τ_{entry}=871.1±53.5 ms, n=10, $p<0.05$, Figure 4.23B). S-Lic similarly triggered a hyperpolarizing shift of the steady-state SI (A1622D, $V_{1/2}$= -54.0± 1.11 mV, n = 7, A1622D+300 µM S-Lic, $V_{1/2}$ = -65.83± 1.8 mV, n = 9, $p < 0.01$), yet brought the slope back to WT levels (WT, k=7.69±0.44, n=7, A1622D, k=5.2±0.15, n=7, A1622D+300 µM S-Lic, k=7.46±0.4, n=9, Figure 4.24 A, B and C).

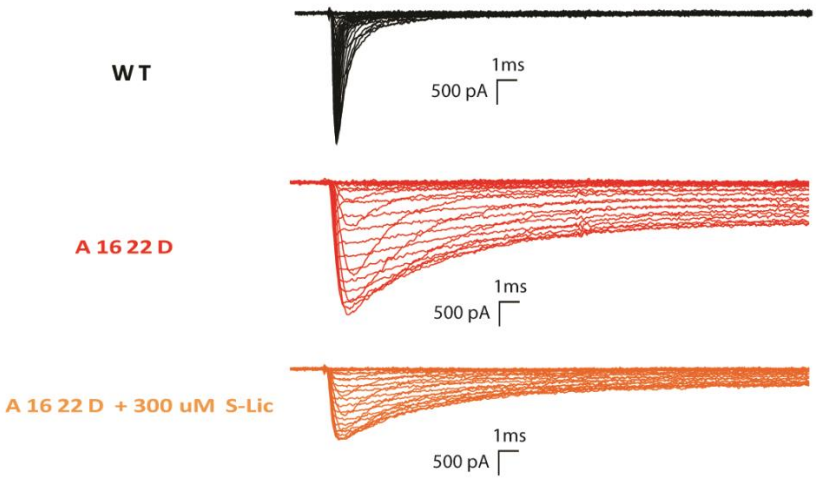

Figure 4.19. Representative Na^+ current traces from WT, A1622D and A1622D + 300 µM S-Lic in ND7/23 cells.

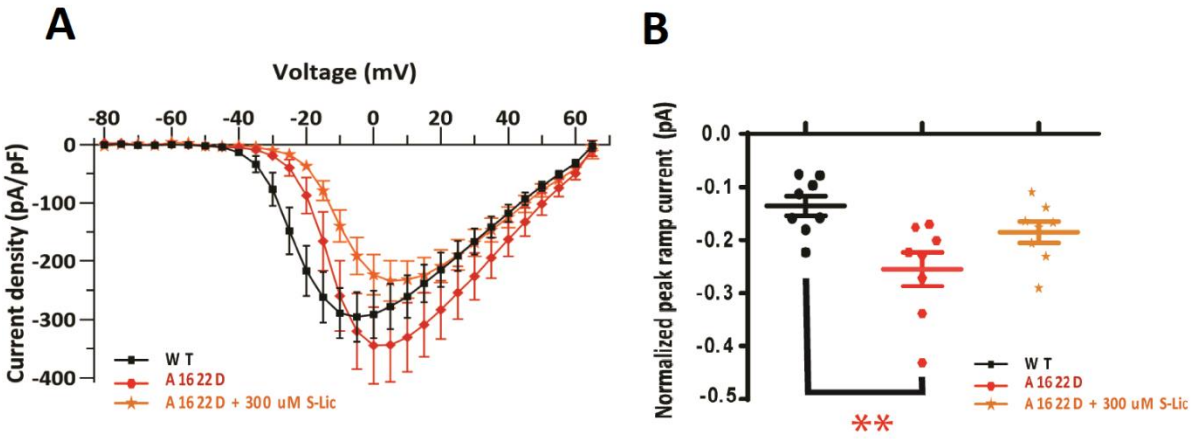

Figure 4.20. Effects of S-Lic on transient and persistent current in A1622D variant Na^+ channels. (A) Peak transient Na^+ currents (normalized to cell capacitances) versus voltage, A1622D, A1622D+300 µM S-Lic n=9. WT, n=14. **(B)** Ramp current peaks (persistent current) in variant A1622D channels normalized to I_{peak}. A huge persistent current for the A1622D variant was seen. Upon multiple comparison, only untreated A1622D group have shown a significant increase in the peak versus WT (n = 8, **p<0.01). Means ± SEM for the data points are displayed. n, number of recorded cells.

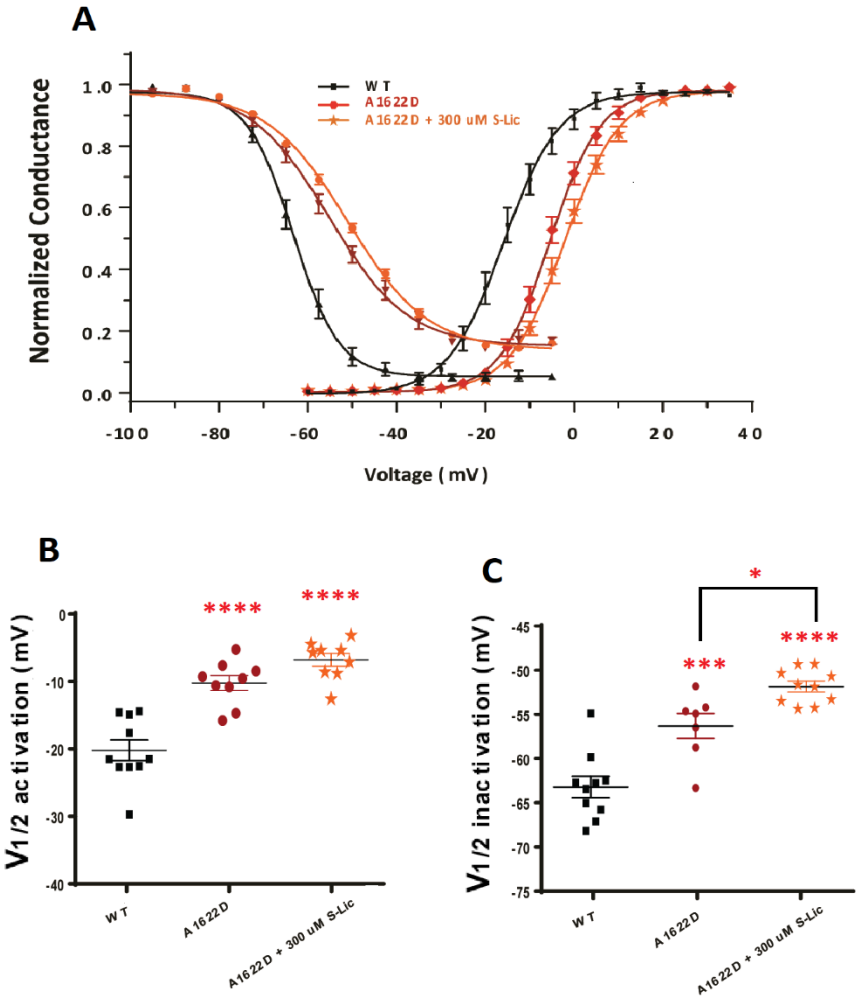

Figure 4.21. Steady-state activation and FI curves in A1622D variant Na^+ channels in the presence of 300 µM of S-Lic (orange) or vehicle (red). (A) Steady-state activation and FI curves. A Boltzmann function was applied to fit the data points. **(B)** Recordings revealed that A1622D channels show a depolarizing shift of the activation curve (WT, n=10; A1622D, n=9). **(C)** Steady-state FI curve was also shifted towards depolarized potentials for A1622D channels and the slope was increased compared to WT channels potentials (WT, n=10; A1622D, n=7). Administration of 300 µM of S-Lic has further shifted the steady-state FI curve towards depolarized potentials for A1622D (A1622D, n=7; A1622D+300 µM S-Lic, n=10). Means ± SEM for the data points are displayed. n, number of recorded cells. *p<0.05, ***p<0.001, ****p<0.0001, one-way ANOVA with Tukey´s *post-hoc* test.

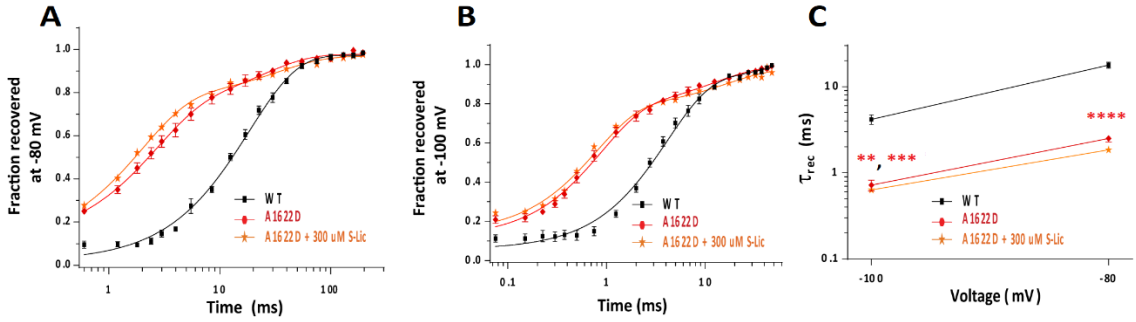

Figure 4.22. Effects of S-Lic on recovery from FI in A1622D variant Na^+ channels (A) at -80 mV and **(B)** at -100 mV, a second-order exponential function with an initial delay was applied. **(C)** Average values of the τ_{rec} at both voltages. A1622D variant channels significantly accelerated the recovery from FI at both -80 and -100 mV holding potentials, (n=9). 300 µM of S-Lic did not cause a significant difference in the τ_{rec} from FI when compared to vehicle. Means ± SEM for the data points are displayed. n, number of recorded cells. **p<0.01, ***p<0.001, ****p<0.0001 versus WT, one-way ANOVA with Tukey´s *post-hoc* test

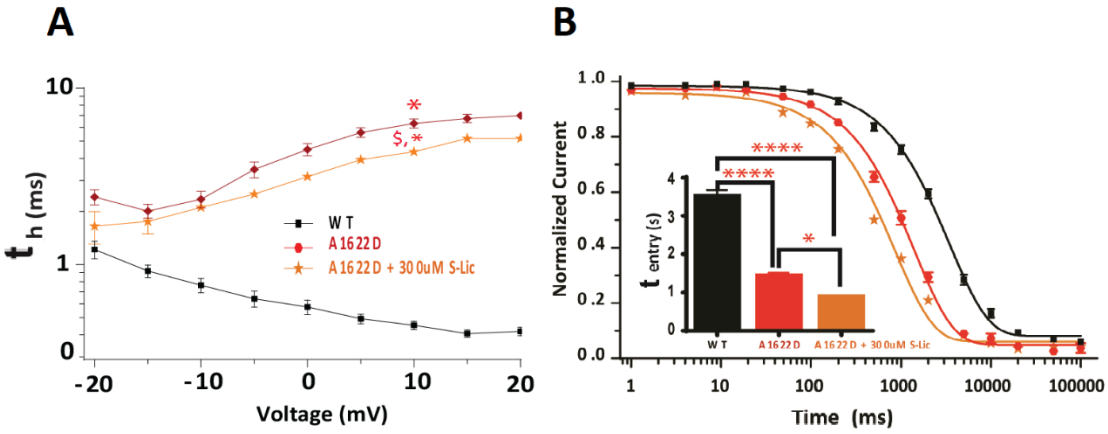

Figure 4.23. Effects of S-Lic on the kinetics of FI and SI in A1622D variant Na^+ channels. (A) Voltage-dependence of the τ_h of FI in variant A1622D channels. Both S-Lic and without S-Lic A1622D groups show a little voltage-dependence versus WT, however, the treated group shows a significant acceleration in the transition from the activated to the FI state in comparison to untreated group (n=10 for WT, n=9 for A1622D, and n=9 for A1622D+300 µM. *p<0.05 vs WT, $^{\$}$p<0.05 represents the difference between A1622D and A1622D+300 µM S-Lic groups, two-way ANOVA with Tukey's *post-hoc*). **(B)** Entry into SI in variant A1622D channels. A first-order exponential function was applied. A1622D channels had an accelerated entry into SI in comparison with WT and administration of 300 µM of S-Lic further accelerates the entry into SI versus vehicle (n=8 for A1622D, n=10 for A1622D+300 µM S-Lic, and n=10 for WT). *p<0.05; ****p<0.0001; one-way ANOVA with Tukey´s *post-hoc* test. Means ± SEM for the data points are displayed. n, number of recorded cells.

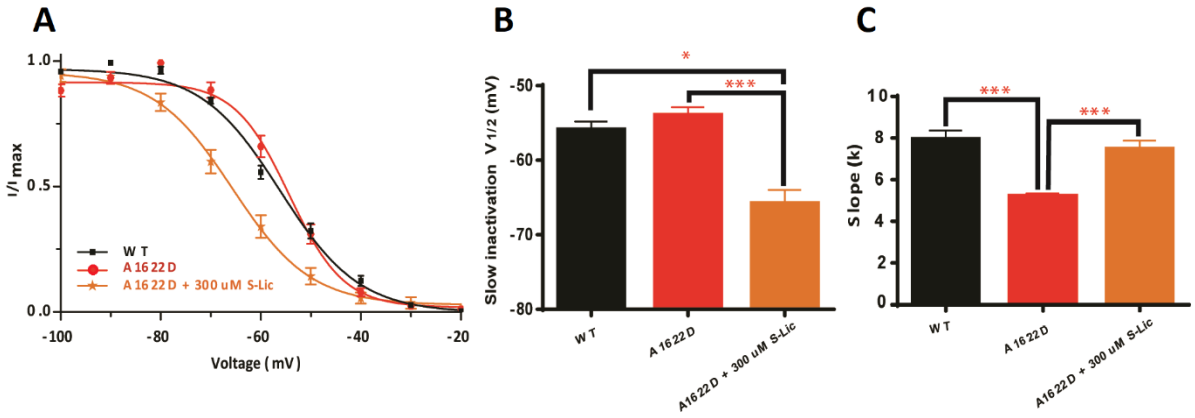

Figure 4.24. Effects of S-Lic on steady-state SI in A1622D $Na_v1.6$ Na^+ channels. (A) Steady-state SI curves, a Boltzmann function was applied to fit the data points. **(B)** Administration of 300 µM of S-Lic resulted in a hyperpolarizing shift of the steady-state SI (n=7 for A1622D, n=9 for A1622D+300 µM S-Lic, and n=7 for WT). **(C)** The A1622D variant results in an increase in the slope of the steady-state SI when compared to the WT but the treatment brings it back to WT levels (n=7 for A1622D, n=9 for A1622D+300 µM S-Lic, and n=7 for WT). Means ± SEM for the data points are displayed. n, number of recorded cells; *p<0.05; ***p< 0.001 (one-way ANOVA with Tukey´s *post-hoc* test or ANOVA on ranks with Dunn´s *post-hoc* test).

4.3.2. I-Clamp recordings in cultured neurons

In I-Clamp neuronal recordings, some neurons transfected with A1622D variant showed long-lasting depolarizations in AP firing (depolarization plateaus). Such depolarization plateaus were observed in 5 cells out of the 9 cells that were measured (Figure 4.25). Because of this phenomenon, A1622D neurons showed no change in AP firing rates when compared to that of WT, but a significant increase in AP half-height-width (the width at half-maximal spike amplitude) have been detected in this variant (WT 4.89±0.78 ms n=12; A1622D 47.64±17.5 ms, n=9, p<0.05, Figure 4.27 A and H).

Additionally, those neurons had an increase in the threshold to elicit an AP when compared to the WT (WT -29.97±2.324 mV; A1622D -18.79±1.35 mV, n=9, p<0.01), which echoes the depolarizing shift in the activation curve seen in this variant (Figure 4.27 C). Exposure to 300 µM of S-Lic showed no change in neuronal

firing rates, or in the AP threshold (Figures 4.26 and 4.27 C). However, a statistically non-significant decrease in AP half-height-width (in without S-Lic: 47.64±17.5 ms versus 12.28±4.78 ms in S-Lic, n=9) is seen specifically in the cells that had the depolarization plateaus (5 out of the 9 measured cells, Figure 4.27 I and J). Upon multiple group comparison, only untreated A1622D group have showed a significant increase in the AP half-height-width versus WT (WT=4.89±0.78 ms, n=11, A1622D without S-Lic: 47.64±17.5 ms versus 12.28±4.78 ms in S-Lic, n=9, Figure 4.21 H). Administration of 300 µM S-Lic did not seem to affect otherwise tested neuronal properties and single AP parameters (Figure 4.27).

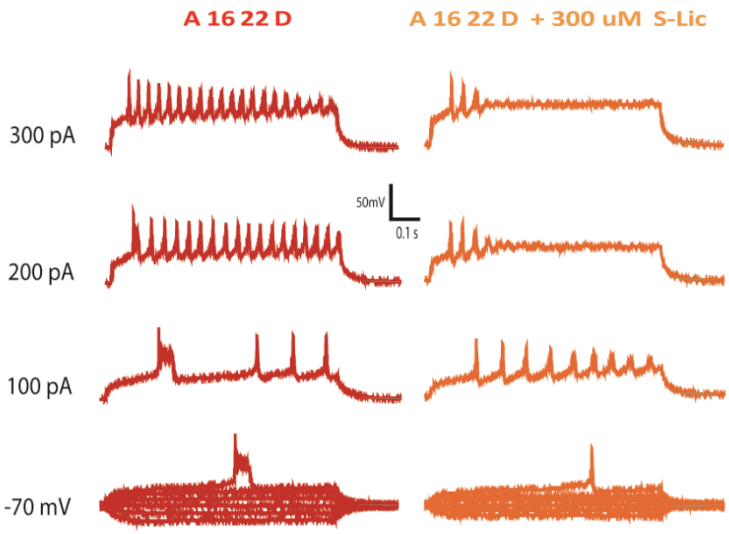

Figure 4.25. Illustrative traces of APs recorded in a neuron transfected with TTX-resistant A1622D variant before and after the addition of 300 µM S-Lic. In this variant, some transfected neurons showed long-lasting depolarizations in AP firing (depolarization plateaus). These depolarization plateaus were observed in 5 out of the 9 measured cells and S-Lic exposure seemed to resolve such depolarization plateaus. A1622D (red), A1622D + 300 µM of S-Lic (orange).

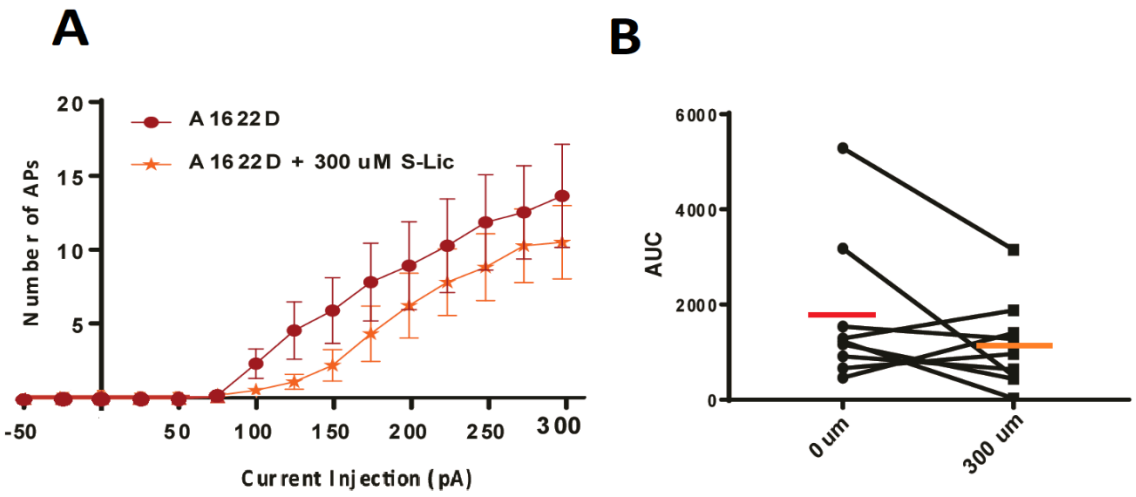

Figure 4.26. Effects of S-Lic on the firing properties of variant A1622D Na^+ channels in primary cultured hippocampal mouse neurons. (A) Number of APs plotted versus injected current in transfected A1622D channels. **(B)** The AUC values were not significantly different upon exposure to 300 µM S-Lic (n=9). Means ± SEM for the data points are displayed. WT (black), A1622D (red), A1622D + 300 µM of S-Lic (orange).

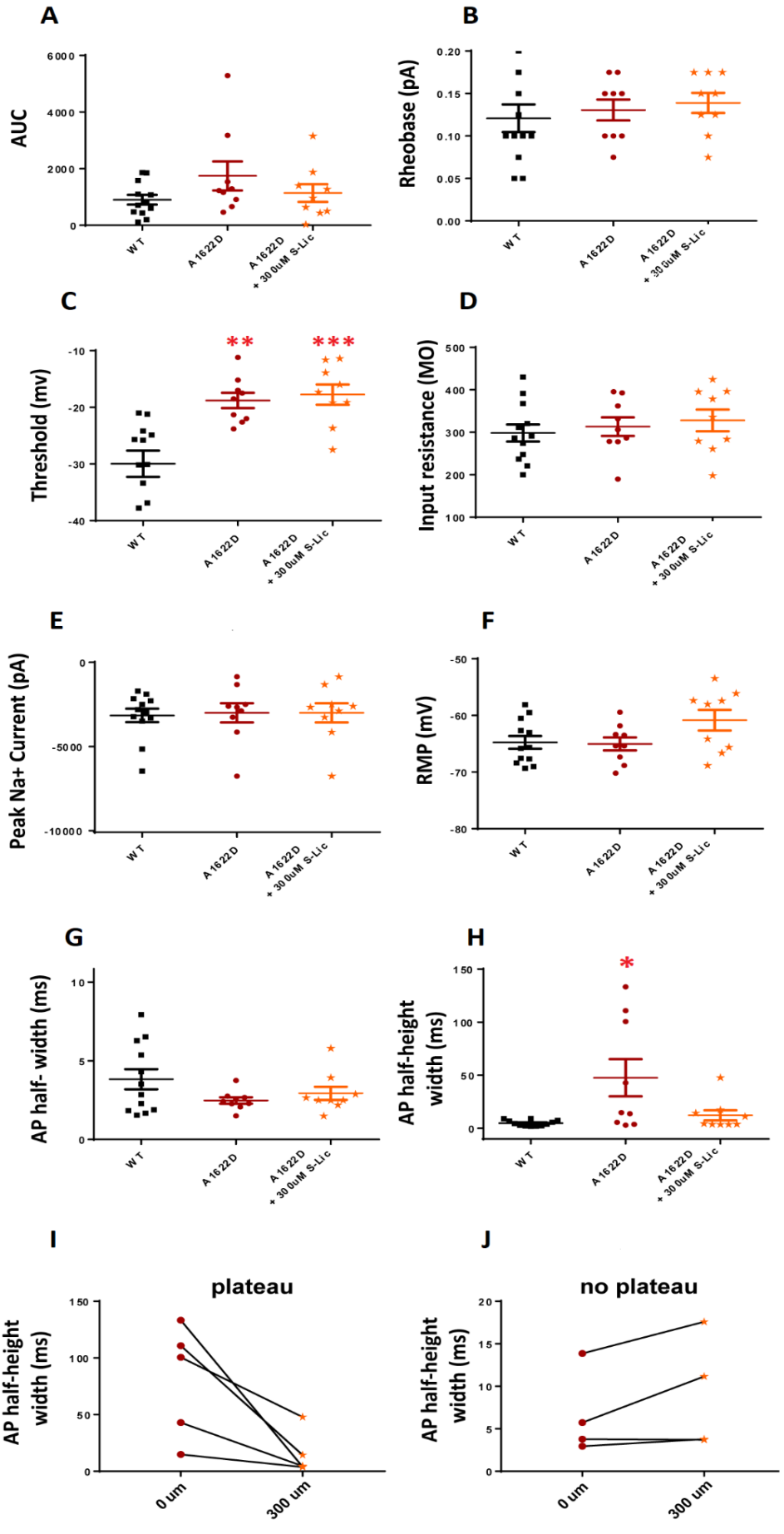
A
AUC
6000
4000
2000
0
WT
A1622D
A1622D + 30.0uM S-Lic
B
Rheobase (pA)
0.20
0.15
0.10
0.05
0.00
C
Threshold (mv)
-10
-20
-30
-40
**
***
D
Input resistance (MO)
500
400
300
200
100
E
Peak Na+ Current (pA)
0
-5000
-10000
F
RMP (mV)
-50
-60
-70
-80
G
AP half- width (ms)
10
5
0
H
AP half-height width (ms)
150
100
50
0
*
I
plateau
AP half-height width (ms)
0 um
300 um
J
no plateau
AP half-height width (ms)
20
15
10
5
0
0 um
300 um

Figure 4.27. Effects of S-Lic on some neuronal features and AP parameters in variant A1622D Na^+ channels in the presence and absence of 300 µM of S-Lic. (A) The AUC for AP firing. **(B)** Rheobase (pA). **(C)** Threshold (mV). A1622D variant neurons had an increase in the threshold to elicit an AP when compared to the WT (n=9, p<0.01). **(D)** Input Resistance (mΩ). **(E)** Peak Na^+ current (pA). **(F)** Resting Membrane potential (mV). **(G)** AP Half-width (ms). **(H)** AP half-height-width (ms), a significant increase in AP half-height-width have been detected in this variant when compared to WT (WT n=11; A1622D n=9), however, the difference against WT AP half-height-width was lost in the treated group. **(I and J)** Some A1622D variant neurons had APs with depolarization plateaus showing an increased half-height-width and the treatment with 300 µM S-Lic seemed to decrease it in those neurons. Means ± SEM for the data points are displayed. WT (black), A1622D (red), and A1622D + 300 µM of S-Lic (orange). *p<0.05, **p<0.01, ***p<0.001 versus WT (one-way ANOVA with Dunnett´s *post-hoc* test or ANOVA on ranks with Dunn´s *post-hoc* test).

4.4. Eslicarbazepine effects on G1475R mutated VGSCs

4.4.1. V-Clamp recordings in ND7/23 cells

The current density and persistent current in this variant were alike to the ones of the WT channels (Figures 4.28 and 4.29). The $V_{1/2}$ of steady-state activation was not affected, but G1475R channels displayed a depolarizing shift in their steady-state FI curve (WT, $V_{1/2}$ = -63.21± 1.2 mV, n = 10; G1475R, $V_{1/2}$ = -58.04± 0.87 mV, n = 8, p < 0.01, Figure 4.30). The recovery from FI was unaltered (Figure 4.31). Entry into both FI and SI (Figure 4.32) and $V_{1/2}$ of SI were found to be statistically comparable to WT, only the slope of the steady-state SI curve was decreased in this variant (WT k = 7.69 ± 0.44, G1475R k= 6.17±0.20, p<0.001, Figure 4.33).

Administration of 300 µM of S-Lic in ND7/23 cells speeded the entry into SI (G1475R τ_{entry}=3028.89±234.29 ms, n=13. G1475R+300 µM S-Lic τ_{entry}= 2182.25±202.39 ms, n=13, p<0.05, Figure 2.32B). A hyperpolarizing shift of the steady-state SI was observed with S-Lic (G1475R, $V_{1/2}$=-56.93± 1.8 mV, n=8. G1475R+300 µM S-Lic, $V_{1/2}$ =-66.93± 1.27 mV, n=9, p<0.001). The slope of the SI curve was further decreased with the S-Lic treatment (G1475R k=6.17±0.20, G1475R+300 µM S-Lic k=5.11±0.2, n=9. WT, k=7.69±0.44, n=7, p<0.001, Figure 2.33 A, B and C).

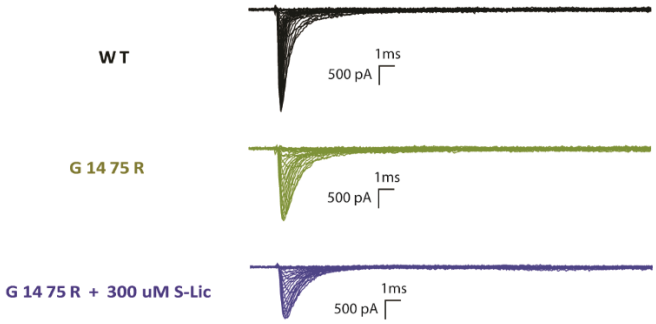

Figure 4.28. Representative Na^+ current traces from WT, G1475R and G1475R +300 µM S-Lic in ND7/23 cells.

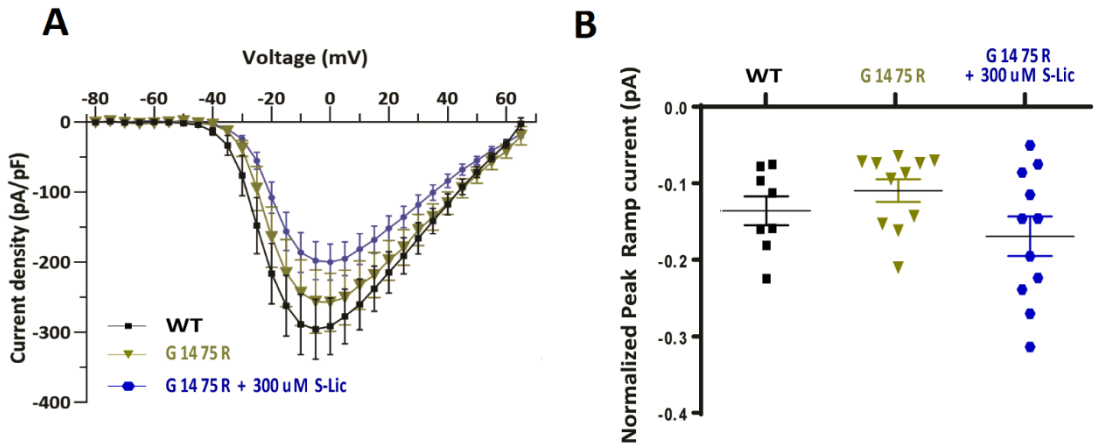

Figure 4.29. Effects of S-Lic on transient and persistent current in G1475R variant Na^+ channels. (A) Peak transient Na^+ currents (normalized to cell capacitances) versus voltage; G1475R n=10. G1475R+300 µM S-Lic, n=11 WT, n=14. **(B)** Ramp current peaks in variant G1475R channels normalized to I_{peak} (WT; n=8, G1475R and G1475R+300 µM S-Lic n=11). Means ± SEM for the data points are displayed. n, number of recorded cells.

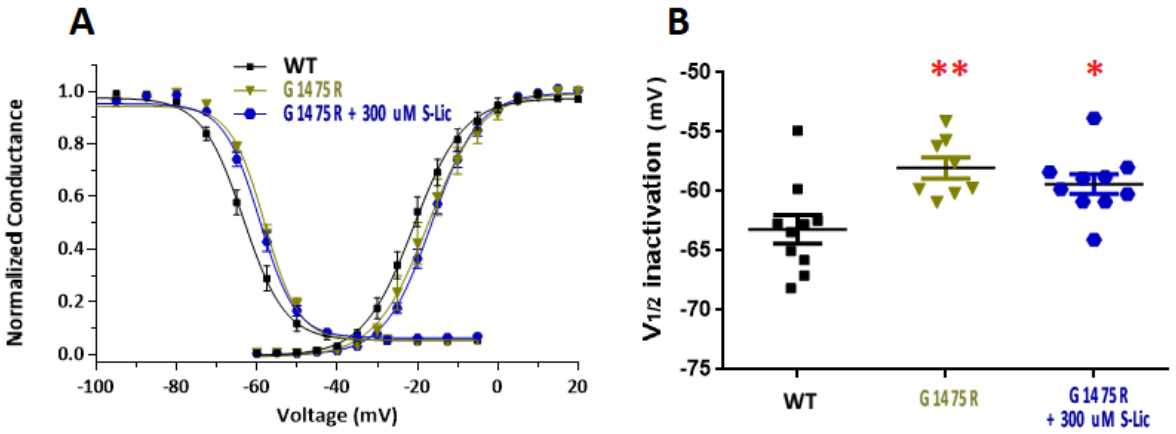

Figure 4.30. Steady-state activation and FI curves in G1475R variant Na^+ channels in the presence of 300 µM of S-Lic (blue) or vehicle (olive). (A) Steady-state activation and FI curves. A Boltzmann function was applied to fit the data points. **(B)** G1475R variant induced depolarizing a shift of the steady-state FI curve (WT, n=10; G1475R, n=8). Administration of 300 µM of S-Lic did not alter those parameters. Means ± SEM for the data points are displayed. n, number of recorded cells. *p<0.05, one-way ANOVA with Tukey´s *post-hoc* test.

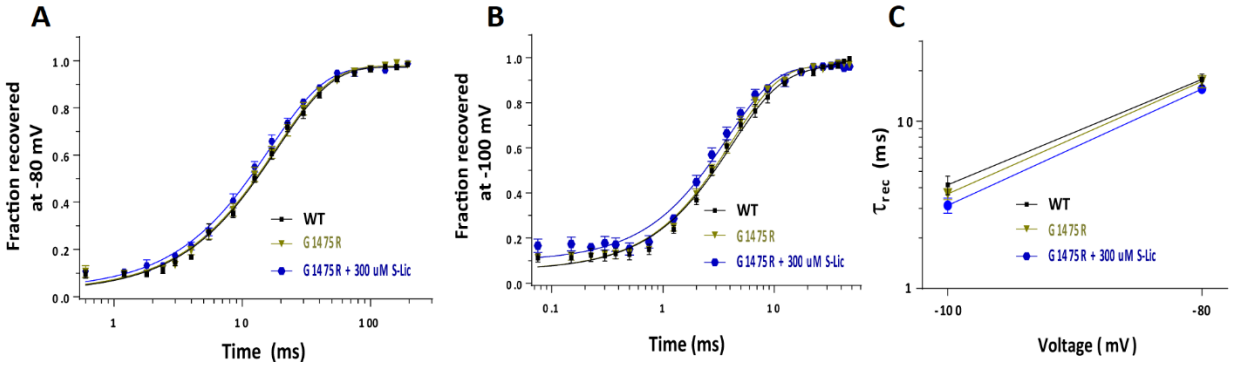

Figure 4.31. Effects of S-Lic on recovery from FI in G1475R variant Na^+ channels (A) at -80 mV and **(B)** at -100 mV, a first-order exponential function with an initial delay was applied. **(C)** average values of the τ_{rec} at both voltages. Administration of 300 µM of S-Lic did not cause a significant difference in the τ_{rec} from FI. Means ± SEM for the data points are displayed. n, number of recorded cells.

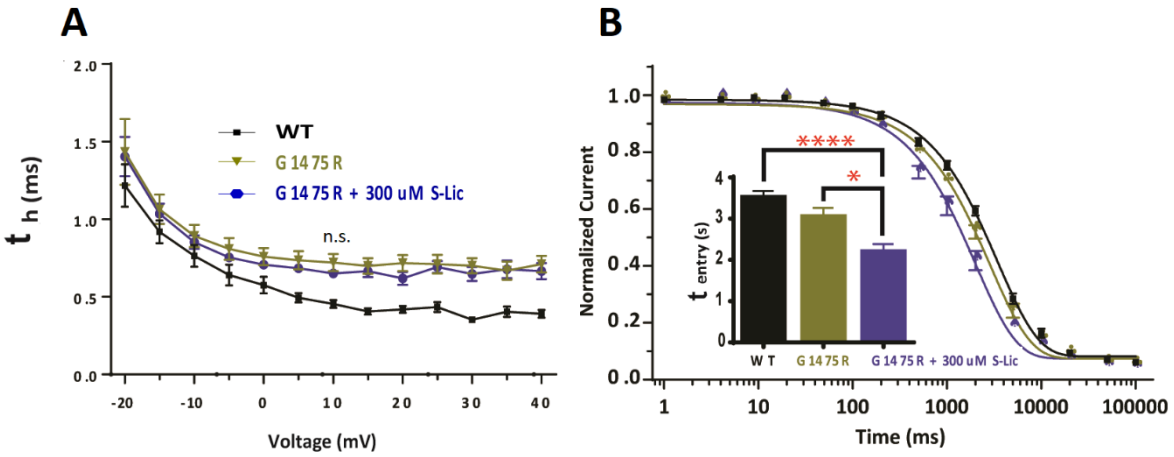

Figure 4.32. Effects of S-Lic on the kinetics of FI and SI in G1475R variant Na^+ channels. (A) Voltage-dependence of the τ_h of FI in variant G1475R channels. **(B)** Entry into SI in variant G1475R channels. a first-order exponential function was applied. Administration of 300 µM of S-Lic hastened the entry into SI (G1475R, n=13. G1475R+300 µM S-Lic n=13). Means ± SEM for the data points are displayed. n, number of recorded cells. *p<0.05, one-way ANOVA with Tukey´s *post-hoc* test.

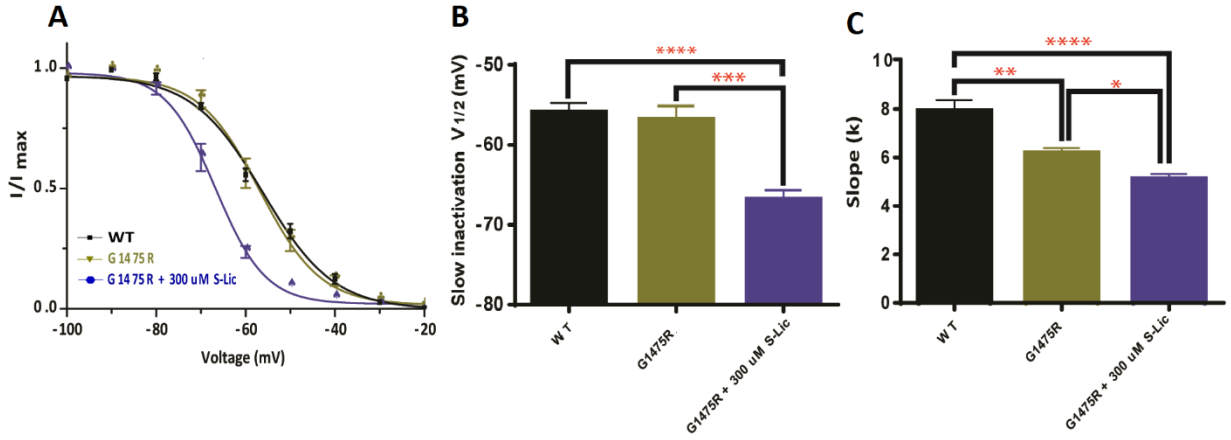

Figure 4.33. Effects of S-Lic on steady-state SI in G1475R $Na_v1.6$ Na^+ channels. (A) Steady-state SI curves, a Boltzmann function was applied to fit the data points. **(B)** Administration of 300 µM of S-Lic causes a hyperpolarizing shift of the SI curve (G1475R, n=8. G1475R+300 µM S-Lic, n=9). **(C)** The slope of the steady-state SI curve was decreased in this variant, with S-Lic the slope was further decreased (G1475R k=6.17±0.20, G1475R+300 µM S-Lic k=5.11±0.2, n=9. WT, k=7.69±0.44, n=7). Means ± SEM for the data points are displayed. n, number of recorded cells; *p < 0.05; **p < 0.01; ***P < 0.001; ****p < 0.0001 (one-way ANOVA with Tukey´s *post-hoc* test or ANOVA on ranks with Dunn´s *post-hoc* test).

4.4.2. I-Clamp recordings in cultured neurons

The recordings in primary neurons showed that the AP firing was not altered by the transfection of G1475R variant channels since no significant changes in the firing rates were detected (Figure 4.35A), or in the inherent neuronal features and single AP parameters (Figure 2.36). Administration of 300 µM S-Lic similarly did not seem to affect the AP firing or the tested neuronal properties and single AP parameters (n=11, Figures 4.34, 4.35 and 4.36).

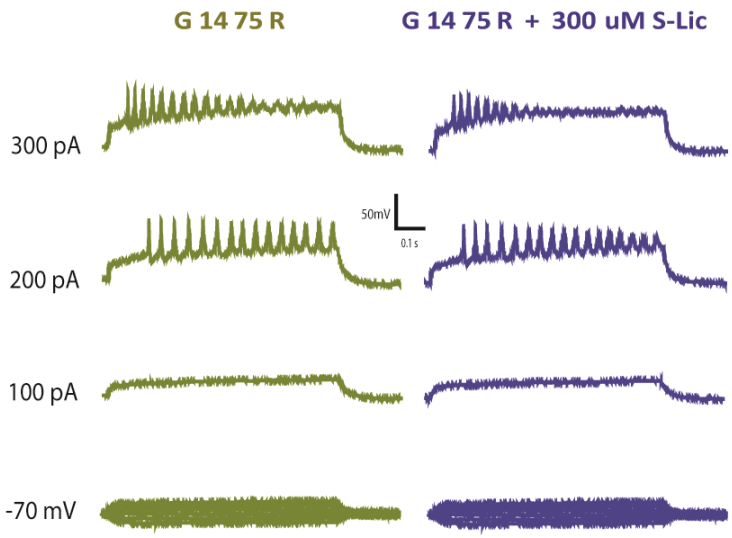

Figure 4.34. Illustrative traces of APs recorded in a neuron transfected with TTX-resistant G1475R variant before and after the addition of 300 µM S-Lic. G1475R (olive), and G1475R+300 µM of S-Lic (blue).

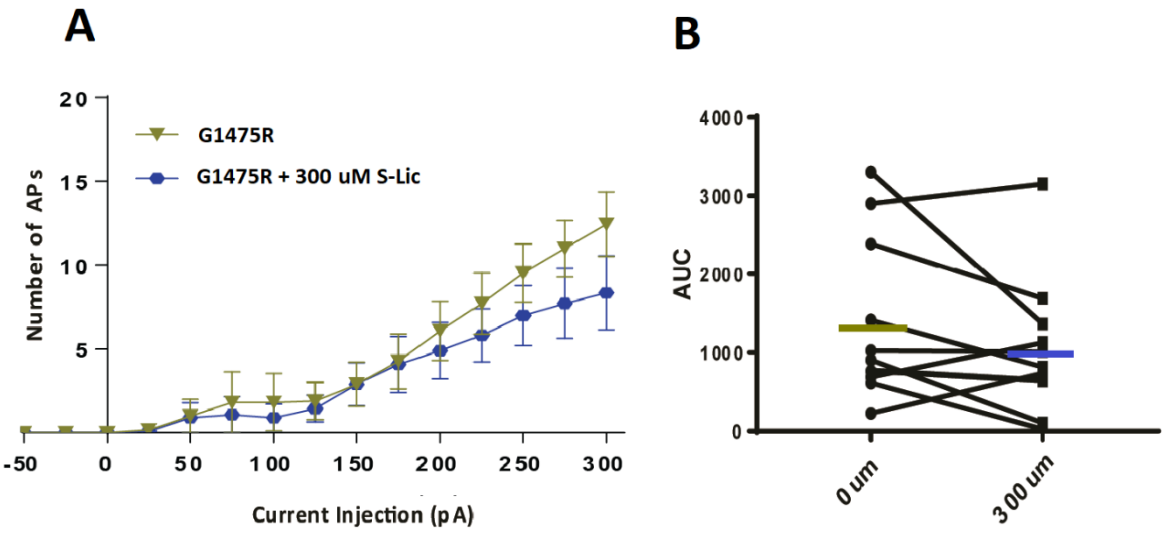

Figure 4.35. Effects of S-Lic on the firing properties of variant G1475R Na^+ channels in primary cultured hippocampal mouse neurons. (A) Number of APs plotted versus injected current in transfected G1475R channels. **(B)** The AUC values were not significantly different when the neurons were exposed to 300 µM S-Lic (n=11). Means ± SEM for the data points are displayed. WT (black), G1475R (olive), and G1475R+300 µM of S-Lic (blue).

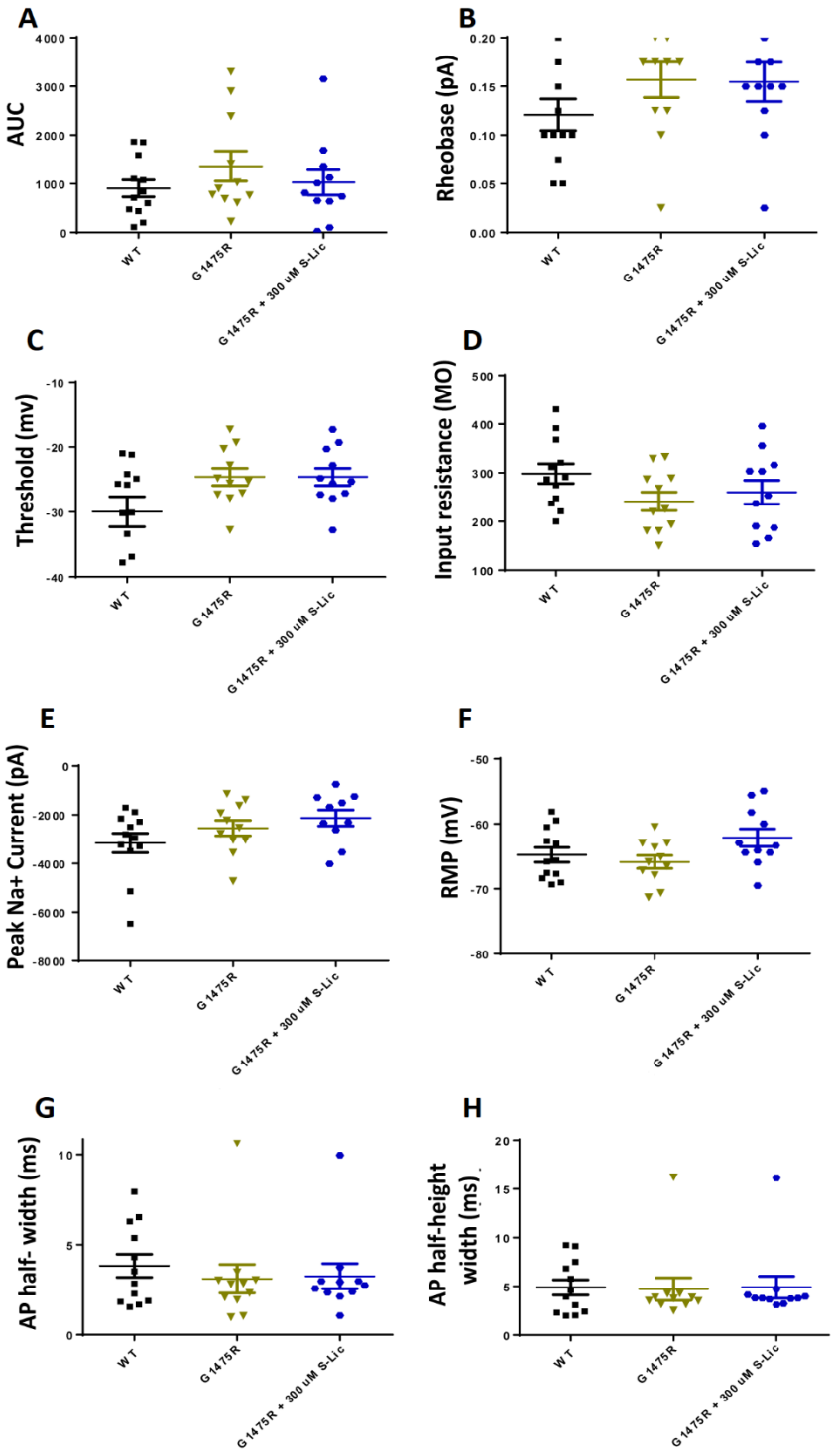

Figure 4.36. Effects of S-Lic some neuronal features and AP parameters in variant G1475R Na^+ channels in the presence and absence of 300 µM of S-Lic. (A) The AUC for AP firing. **(B)** Rheobase (pA). **(C)** Threshold (mV). **(D)** Input Resistance (mΩ). **(E)** Peak Na^+ current (pA). **(F)** Resting Membrane Potential (mV). **(G)** AP Half-width (ms). **(H)** AP half-height-width (ms). Shown are means ± SEM. WT (black), G1475R (olive), and G1475R+300 µM of S-Lic (blue).

4.5. Immunohistochemistry

Immunostaining studies of transfected hippocampal neurons have confirmed the successful transfection of excitatory neurons using CAMKII-GFP plasmid (Figure 4.1).

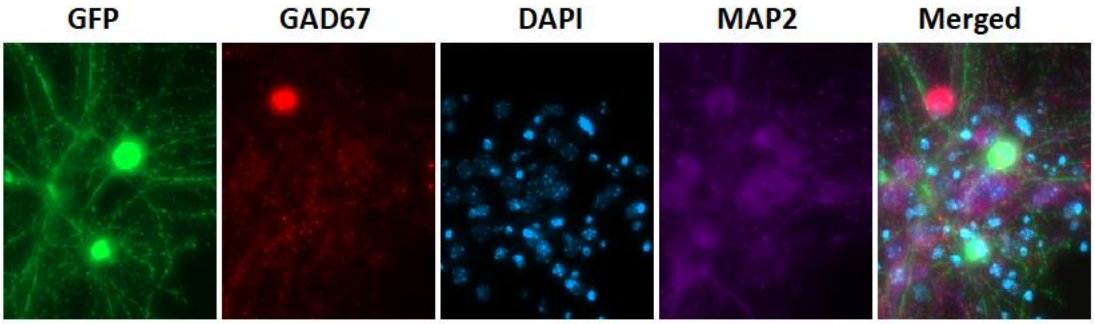

Figure 4.37. Immunostaining of a population of transfected hippocampal neurons. Transfected neurons were stained with a monoclonal anti-GFP antibody (green), a monoclonal anti-GAD67 antibody (red); the marker for inhibitory neurons in order to confirm the successful identification of excitatory neurons with CAMKII-GFP plasmid, the purple fluorescence indicated MAP2 (a neuronal marker), the blue fluorescence indicated DAPI staining in order to show the nucleus.

4.6. Summary Tables

Table 4.1. The $V_{1/2}$ of steady-state activation, FI and SI in WT and variant channels recorded in ND7/23 cells in the presence and absence of 300 µM of S-Lic.

Transfected Nav1.6 channel	n	Steady-state activation		n	Steady-state fast inactivation		n	Steady-state slow inactivation	
		$V_{1/2}$ (mV)	K		$V_{1/2}$ (mV)	K		$V_{1/2}$ (mV)	K
WT	10	-20.14±1.54	-6.06±0.48	10	-63.21±1.20	4.79±0.17	7	-55.97±1.16	7.69±0.44
WT + 300 uM S-Lic	9	-20.11±1.08	-5.59±0.38	7	-66.98±1.08 $	4.44±0.20	7	-72.06±0.71, $$$$	6.05±0.54 $
A1622D	9	-10.07±1.11****	-5.61±0.33	7	-56.31±1.41***	7.76±0.18****	7	-54.01±1.11	5.20±0.15 ***
A1622D + 300 uM S-Lic	9	-6.60±0.95****	-6.18±0.34	10	-51.85±0.60****,$	8.40±0.37****	9	-65.83±1.83 *, $$$	7.46±0.40 $$$
G1475R	10	-16.83±1.76	-5.50±0.49	8	-58.04±0.87**	4.15±0.06	8	-56.93±1.80	6.17±0.20 **
G1475R+300 uM S-Lic	11	-16.91±0.89	-5.36±0.22	10	-59.38±0.82*	4.20±0.15	9	-66.90±1.24 ****, $$$	5.11±0.21 ****, $
M1760I	12	-26.10±1.58*	-4.79±0.37	8	-65.04±0.90	4.63±0.24	10	-54.99±1.28	10.08±0.52 **
M1760I+300 uM S-Lic	16	-27.95±1.42**	-4.57±0.40	10	-65.77±1.35	4.80±0.18	9	-70.66±1.35 ****, $$$$	7.75±0.26 $$

Data are presented as means ± SEM. n, number of recorded cells. *p < 0.05; **p < 0.01; ***p < 0.001, ****p < 0.0001 versus WT, a similar pattern is used for $ sign but indicates a difference versus untreated respective group (un-paired *t*-test or Wilcoxon signed-rank test for WT or one-way ANOVA with Tukey´s *post-hoc* test or ANOVA on ranks with Dunn´s *post-hoc* test for the others).

Table 4.2. Some biophysical features of WT and variant channels recorded in ND7/23 cells in the presence and absence of 300 µM of S-Lic.

Transfected Nav1.6 channel	n	τ_{entry} (fast inactivation) at 10 mV (ms)	n	τ_{entry} (slow inactivation) (ms)	n	τ_{inac} (fast inactivation) at -100mV (ms)	n	Current density at peak (pA/pF)	n	Ramp current peak
WT	10	0.45±0.02	10	3500±170.8	9	4.16±0.52	14	-343.1±49.78	8	-0.13±0.01
WT + 300 uM S-Lic	9	0.38±0.01	11	2847±208.4 $	11	4.40±0.39	9	-232±35.63	8	-0.09±0.01
A1622D	9	6.31±0.37****	8	1423±93.3 ****	9	0.71±0.10 **	9	-349.4±65.49	8	-0.25±0.03 **
A1622D+300 uM S-Lic	9	4.35±0.23 ****, $$$$	10	871.1±53.58 ****, $	13	0.63±0.05 ***	9	-216±29.03	8	-0.18±0.01
G1475R	10	0.72±0.05 ***	13	3029±234.3	7	3.67±0.27	10	-268±44.87	11	-0.10±0.01
G1475R+300 uM S-Lic	10	0.65±0.02 **	13	2182±202.4 ***, $	8	3.14±0.32	11	-203.9±26.25	11	-0.16±0.02
M1760I	10	0.67±0.03 ***	12	4475±322.5	7	3.95±0.35	12	-478.6±71.8	8	-0.12±0.01
M1760I+300 uM S-Lic	10	0.52±0.03 $	10	2984±355.4 $$	7	2.79±0.14 *, $	16	-464±52.82	8	-0.10±0.01

Data are presented as means ± SEM. n, number of recorded cells. *p < 0.05; **p < 0.01; ***p < 0.001, **** p < 0.0001 versus WT, a similar pattern is used for $ sign but indicates a difference versus untreated respective group (un-paired *t*-test or Wilcoxon signed-rank test for WT and one-way ANOVA with Tukey´s *post-hoc* test or ANOVA on ranks with Dunn´s *post-hoc* test for the others).

Table 4.3. Some inherent neuronal features and single AP parameters in transfected neurons in the presence and absence of 300 µM of S-Lic.

Transfected Nav1.6 channel	n	Resting membrane potential (mV)	Input resistance (MΩ)	AP half-height-width (ms)	AP half-width (ms)	AP threshold (mV)	Rheobase (pA)	I/O area under the curve (nA)
WT	12	-64.76±1.13	298.4±20.25	4.89±0.78	3.83±0.63	-29.97±2.32	0.12±0.01	904.3±174.2
WT + 300 uM S-Lic	9	-64.65±1.58	308.2±23.11	4.92±1.21	3.41±0.75	-29.69±3.58	0.13±0.01	622.3±151.8$
A1622D	9	-65.03±1.13	313.4±21.83	47.64±17.5 *	2.47±0.20	-18.79±1.35 **	0.13±0.01	1746±513.3
A1622D + 300 uM S-Lic	9	-60.84±1.82	328.1±25.52	12.28±4.78	2.93±0.41	-17.74±1.79 ***	0.13±0.01	1140±313.9
G1475R	9	-65.87±1.00	241.5±18.95	4.72±1.15	3.10±0.79	-24.59±1.33	0.15±0.01	1363±309.2
G1475R + 300 uM S-Lic	9	-62.12±1.35	260.2±24.32	4.90±1.13	3.25±0.69	-24.59±1.33	0.15±0.02	1027±258.6
M1760I	11	-65.73±1.28	273.5±23.98	3.45±1.17	2.31±0.59	-31.63±2.97	0.10±0.01	2240±468.9 *
M1760I + 300 uM S-Lic	11	-63.93±1.49	284.4±28.17	2.34±0.21	1.78±0.16	-33.18±2.72	0.10±0.02	1816±437 $

Data are presented as means ± SEM. n, number of recorded cells. AP, action potential; I/O, input-output curve. The I/O area under the curve was determined for each neuron over the whole range of current injections. *p < 0.05; **p < 0.01; ***p < 0.001, ****p < 0.0001 versus WT, a similar pattern is used for $ sign but indicates a difference versus untreated respective group. (Paired *t*-test or Wilcoxon signed-rank test for before-after treatment and one-way ANOVA with Dunnett´s *post-hoc* test or ANOVA on ranks with Dunn´s *post-hoc* test for comparisons between groups and WT).

5. DISCUSSION

Nowadays, an increasing number of pediatric patients suffering from neurodevelopmental symptoms and drug resistant epilepsy are being diagnosed based on their underlying genetic variations with developmental and epileptic encephalopathies (DEEs). However, standard anticonvulsant treatment has a minor influence on the disease course, and there are no available therapeutic options to prevent the emergence of symptoms or slow the disease onset. Personalized therapeutic regimens targeting disease-causing pathophysiological machineries may offer the key to overcome intractability and a balance between the desired treatment effects with the potential side effects.

With this aim, we investigated the therapeutic potential of Eslicarbazepine (S-Lic), on selected gain of function $Na_V1.6$ variants linked to DEEs. S-Lic is a third-generation dibenzazepine that uniquely enhances the slow inactivation (SI) process of voltage-gated Na^+ channels (VGSC). We chose WT $Na_v1.6$ channels along with some *SCN8A* variants known to be causing DEEs. S-Lic-mediated modulation of biophysical properties and neuronal excitability was studied *in vitro* using neuroblastoma cells and mouse primary hippocampal neuron cultures. Our *in vitro* studies were conducted using a single concentration of S-Lic (300 µM). We chose this concentration putting into account its well-documented distinctive effects in literature in order to guarantee seeing its effects in our research. Although this concentration may seem high, it can be warranted considering the high lipid:water partition coefficient of S-Lic (50:1) and its low affinity for non-specific protein binding (93). Furthermore, previous estimates of the concentration of S-Lic at the organic fraction of brain tissue of epileptic patients resulted in peak values even higher to the concentration used for the *in vitro* experiments in this study (60). Our results demonstrated that S-Lic enhances both fast inactivation (FI) and SI of WT $Na_V1.6$ channels. In variant M1760I channels, S-Lic causes an earlier entry into both FI and SI, and a hyperpolarizing shift of the steady-state SI curve in ND7/23 cells, and rescues the increase seen in the AP firing rates in neurons caused by those channels. In

A1622D channels, S-Lic mainly causes an earlier entry into both FI and SI and a hyperpolarizing shift of the steady-state SI curve in ND7/23 cells and it shows a tendency to resolve the depolarization plateaus observed in some of those neurons. Likewise, in G1475R channels it leads to an earlier entry into SI and shifts steady-state SI to hyperpolarized potentials.

In WT ($Na_v1.6$) channels, we observed a slight reduction of peak transient I_{Na} current in ND7/23 neuroblastoma cells upon exposure to S-Lic. This can be explained by previous findings in TTX-sensitive native Na^+ channels of N1E-115 mouse neuroblastoma cells, where exposure to the same dose at the same holding potential reduced the peak Na^+ current only by 16% when compared with control. This reduction, however, has reached 50% when the cells were held at more depolarized potentials, indicating the low affinity of S-Lic for VGSCs in the resting state (94). Additionally, we observed a slight decrease in the conductance of persistent I_{Na} in our results. In literature, S-Lic was found to reduce maximal persistent I_{Na} conductance by around 20% in Na^+ channels of CA1 pyramidal neurons and dissociated rat dentate granule cells in hippocampal mice slices (66, 95). We found that the $V_{1/2}$ of activation of transient Na^+ current was unaltered by S-Lic treatment; which is in agreement with previous studies (65, 66, 93). As for the $V_{1/2}$ of inactivation, S-Lic caused a hyperpolarizing shift in the $V_{1/2}$ of FI. Our results are similar to the findings in TTX-sensitive native Na^+ channels of N1E-115 mouse neuroblastoma cells using the same concentration. However, this effect was not detected in the same cells using a lower concentration of 250 µM (93, 94). Furthermore, it was reported that 300 µM of S-Lic has influenced the $V_{1/2}$ of inactivation in dissociated rat dentate granule cells (66). The voltage-dependence of the major time constant (τ_h) of FI was generally not affected by S-Lic, as well as the time course of recovery from FI. Previous studies have shown that recovery from FI was not slowed by 250 µM of S-Lic in N1E-115 cells (93), however, it was slowed in the presence of 300 µM S-Lic in dissociated dentate granule cells taken from both sham-control and epileptic rats (66). Moreover, S-Lic has accelerated the entry into SI state, caused a hyperpolarizing shift of the steady-state SI, and decreased the slope of the steady-state SI curve when compared to vehicle

group. Those results are in agreement with the known mechanism of S-Lic of reducing VGSC availability through the enhancement of SI in literature. Furthermore, S-Lic effects on the voltage dependence of SI have shown subunit-specificity since a study assessing the effects of S-Lic on the various subunits of VGSCs has shown that S-Lic effects were only observed in $Na_v1.2$ and $Na_v1.6$ subunits, but not in $Na_v1.1$ and $Na_v1.3$ subunits, which agrees with our results (65, 93, 96). Finally, current-clamp recordings in cultured primary hippocampal mouse neurons transfected with $Na_V1.6$ WT channels showed a reduction of maximal firing rates when treated with S-Lic.

Our findings in the three *SCN8A* variants that we studied showed that S-Lic mainly caused an enhancement of SI; however, we noticed some distinct effects in some of those variants. Starting with the severe epilepsy phenotype variant (M1760) where hypotonia, severe intellectual disability, seizures *in utero*, epileptic encephalopathy, and blindness have been described (39). M1760I channels display a hyperpolarizing shift of the activation curve in ND7/23 cells and an increase of the maximal firing rate in neurons. Exposing those channels to S-Lic enhanced the entry into FI, enhanced the SI in ND7/23 cells. S-Lic treatment took the AP firing frequencies which is substantially increased in neurons with the variant M1760I channels back to normal rates. The intermediate epilepsy phenotype variant (G1475R), was reported in different publications (34, 39-42) with variating phenotypic expressivity ranging from treatment-responsive epilepsy to DEE with intellectual disabilities and motor manifestations. G1475R channels showed a shift of the steady-state FI curve towards more depolarized potentials in ND7/23 cells. S-Lic exposure had led to an earlier entry into SI in G1475R channels and shifted the steady-state SI to hyperpolarized potentials without affecting neuronal firing. The third variant included in this study (A1622D) is not an epilepsy variant (described in patients suffering from developmental delay, intellectual disability, autism, and motor manifestations) (39). This variant carries both gain and loss of function features manifested by a depolarizing shift of both the activation curve and FI curves and high persistent current in ND7/23 cells. In neuronal recordings, some neurons transfected with A1622D channels display long-lasting depolarizations in AP firing with a number of

APs comparable to that of WT. We have included this variant to our study since it has a huge gain of function that led to a functional loss of function (manifested by the AP firing rate that is comparable to WT contrary to what expected), putting into account the clinical evidence pointing towards using SCBs to treat patients with *SCN8A*-related channelopathies, especially if the mutations are known to cause GOF in Na^+ channels (97). In addition to its known and expected effects of enhancing SI, administration of 300 μM of S-Lic in transfected ND7/23 cells has further shifted the steady-state FI curve towards depolarized potentials, subsided the difference in persistent current between A1622D and WT groups, and caused a significant acceleration in the transition from the activated to the FI state in comparison to the without S-Lic group. In neurons, S-Lic displayed no significant effect on neuronal firing rate. But S-Lic treatment exhibited a tendency to resolve the depolarization plateaus during firing in the neurons.

In conclusion, our results have implications on contemporary clinical practices and highlight the necessity for the development of individualized and targeted therapies for DEE (since they demonstrate clear differential effects of S-Lic on WT and on three distinct genetic $Na_V1.6$ channel GOF variants), and support the idea that some effects of S-Lic can be variant-specific. This finding is of special interest since such data give emphasis to the importance of early diagnostic genetic workups, and can open in the doors for a variant-specific precision medicine approach, which will likely be the answer for successful treatment not only of *SCN8A*- related channelopathies but also for other treatment-resistant DEEs. Although further studies investigating additional doses and variants will be needed, our findings prompt the potential use of S-Lic-A, taking into account its unique effects on epileptogenesis and SI and its better safety and therapeutic index, as a good candidate against some *SCN8A*-related DEEs.

6. CONCLUSION AND FUTURE DIRECTIONS

- This study showed that:
    1- The major effect of S-Lic lies within slow inactivation kinetics.
    2- Some effects of S-Lic can be mutation-specific.
- Our findings can prompt the potential use of S-Lic-A as a good candidate against some *SCN8A*-related channelopathies.
- Future experiments testing various doses of S-Lic, using additional variants and comparing the data obtained with those of alternative AEDs will be needed.

7. REFERENCES

1. Yu FH, Catterall WA. Overview of the voltage-gated sodium channel family. Genome Biol. 2003;4(3):207.
2. Chen K, Godfrey DA, Ilyas O, Xu J, Preston TW. Cerebellum-related characteristics of Scn8a-mutant mice. Cerebellum. 2009;8(3):192-201.
3. Chahine M, O'Leary ME. Regulatory Role of Voltage-Gated Na Channel beta Subunits in Sensory Neurons. Front Pharmacol. 2011;2:70.
4. Meisler MH, O'Brien JE, Sharkey LM. Sodium channel gene family: epilepsy mutations, gene interactions and modifier effects. J Physiol. 2010;588(Pt 11):1841-8.
5. Gertler TS, Carvill GL. SCN8A: When Neurons Are So Excited, They Just Can't Hide It. Epilepsy Curr. 2019;19(4):269-71.
6. Gardella E, Moller RS. Phenotypic and genetic spectrum of SCN8A-related disorders, treatment options, and outcomes. Epilepsia. 2019;60 Suppl 3:S77-S85.
7. Bunton-Stasyshyn RKA, Wagnon JL, Wengert ER, Barker BS, Faulkner A, Wagley PK, et al. Prominent role of forebrain excitatory neurons in SCN8A encephalopathy. Brain. 2019;142(2):362-75.
8. Lerche H. New hope for the treatment of epilepsy. Brain. 2015;138(Pt 2):240-2.
9. Brodie MJ, Besag F, Ettinger AB, Mula M, Gobbi G, Comai S, et al. Epilepsy, Antiepileptic Drugs, and Aggression: An Evidence-Based Review. Pharmacol Rev. 2016;68(3):563-602.
10. Mula M. Recent and future antiepileptic drugs and their impact on cognition: what can we expect? Expert Rev Neurother. 2012;12(6):667-71.
11. Nadkarni S, Devinsky O. Psychotropic effects of antiepileptic drugs. Epilepsy Curr. 2005;5(5):176-81.
12. Billakota S, Devinsky O, Kim KW. Why we urgently need improved epilepsy therapies for adult patients. Neuropharmacology. 2019:107855.
13. Pressler RM, Lagae L. Why we urgently need improved seizure and epilepsy therapies for children and neonates. Neuropharmacology. 2019:107854.
14. Wang J, Ou SW, Wang YJ. Distribution and function of voltage-gated sodium channels in the nervous system. Channels (Austin). 2017;11(6):534-54.
15. Brunklaus A, Lal D. Sodium channel epilepsies and neurodevelopmental disorders: from disease mechanisms to clinical application. Dev Med Child Neurol. 2020.
16. Li ZM, Chen LX, Li H. Voltage-gated Sodium Channels and Blockers: An Overview and Where Will They Go? Curr Med Sci. 2019;39(6):863-73.

17. Huang W, Liu M, Yan SF, Yan N. Structure-based assessment of disease-related mutations in human voltage-gated sodium channels. Protein Cell. 2017;8(6):401-38.

18. Xu L, Ding X, Wang T, Mou S, Sun H, Hou T. Voltage-gated sodium channels: structures, functions, and molecular modeling. Drug Discov Today. 2019;24(7):1389-97.

19. Wood JN, Iseppon F. Sodium channels. Brain Neurosci Adv. 2018;2:2398212818810684.

20. Kwong K, Carr MJ. Voltage-gated sodium channels. Curr Opin Pharmacol. 2015;22:131-9.

21. Namadurai S, Yereddi NR, Cusdin FS, Huang CL, Chirgadze DY, Jackson AP. A new look at sodium channel beta subunits. Open Biol. 2015;5(1):140192.

22. Rogawski MA, Tofighy A, White HS, Matagne A, Wolff C. Current understanding of the mechanism of action of the antiepileptic drug lacosamide. Epilepsy Res. 2015;110:189-205.

23. Katz E, Stoler O, Scheller A, Khrapunsky Y, Goebbels S, Kirchhoff F, et al. Role of sodium channel subtype in action potential generation by neocortical pyramidal neurons. Proc Natl Acad Sci U S A. 2018;115(30):E7184-E92.

24. Meisler MH, Plummer NW, Burgess DL, Buchner DA, Sprunger LK. Allelic mutations of the sodium channel SCN8A reveal multiple cellular and physiological functions. Genetica. 2004;122(1):37-45.

25. Goldin AL. Evolution of voltage-gated Na(+) channels. J Exp Biol. 2002;205(Pt 5):575-84.

26. O'Brien JE, Meisler MH. Sodium channel SCN8A (Nav1.6): properties and de novo mutations in epileptic encephalopathy and intellectual disability. Front Genet. 2013;4:213.

27. Stafstrom CE. Persistent sodium current and its role in epilepsy. Epilepsy Curr. 2007;7(1):15-22.

28. Cannon SC, Bean BP. Sodium channels gone wild: resurgent current from neuronal and muscle channelopathies. J Clin Invest. 2010;120(1):80-3.

29. Veeramah KR, O'Brien JE, Meisler MH, Cheng X, Dib-Hajj SD, Waxman SG, et al. De novo pathogenic SCN8A mutation identified by whole-genome sequencing of a family quartet affected by infantile epileptic encephalopathy and SUDEP. Am J Hum Genet. 2012;90(3):502-10.

30. Steward CA, Roovers J, Suner MM, Gonzalez JM, Uszczynska-Ratajczak B, Pervouchine D, et al. Re-annotation of 191 developmental and epileptic encephalopathy-associated genes unmasks de novo variants in SCN1A. NPJ Genom Med. 2019;4:31.

31. El Kosseifi C, Cornet MC, Cilio MR. Neonatal Developmental and Epileptic Encephalopathies. Semin Pediatr Neurol. 2019;32:100770.

32. Scheffer IE, Liao J. Deciphering the concepts behind "Epileptic encephalopathy" and "Developmental and epileptic encephalopathy". Eur J Paediatr Neurol. 2020;24:11-4.

33. Musto E, Gardella E, Moller RS. Recent advances in treatment of epilepsy-related sodium channelopathies. Eur J Paediatr Neurol. 2020;24:123-8.

34. Gardella E, Marini C, Trivisano M, Fitzgerald MP, Alber M, Howell KB, et al. The phenotype of SCN8A developmental and epileptic encephalopathy. Neurology. 2018;91(12):e1112-e24.

35. Wagnon JL, Meisler MH. Recurrent and Non-Recurrent Mutations of SCN8A in Epileptic Encephalopathy. Front Neurol. 2015;6:104.

36. Schwarz N, Hahn A, Bast T, Muller S, Loffler H, Maljevic S, et al. Mutations in the sodium channel gene SCN2A cause neonatal epilepsy with late-onset episodic ataxia. J Neurol. 2016;263(2):334-43.

37. Butler KM, da Silva C, Shafir Y, Weisfeld-Adams JD, Alexander JJ, Hegde M, et al. De novo and inherited SCN8A epilepsy mutations detected by gene panel analysis. Epilepsy Res. 2017;129:17-25.

38. Larsen J, Carvill GL, Gardella E, Kluger G, Schmiedel G, Barisic N, et al. The phenotypic spectrum of SCN8A encephalopathy. Neurology. 2015;84(5):480-9.

39. Liu Y, Schubert J, Sonnenberg L, Helbig KL, Hoei-Hansen CE, Koko M, et al. Neuronal mechanisms of mutations in SCN8A causing epilepsy or intellectual disability. Brain. 2019;142(2):376-90.

40. Parrini E, Marini C, Mei D, Galuppi A, Cellini E, Pucatti D, et al. Diagnostic Targeted Resequencing in 349 Patients with Drug-Resistant Pediatric Epilepsies Identifies Causative Mutations in 30 Different Genes. Hum Mutat. 2017;38(2):216-25.

41. Wang J, Gao H, Bao X, Zhang Q, Li J, Wei L, et al. SCN8A mutations in Chinese patients with early onset epileptic encephalopathy and benign infantile seizures. BMC Med Genet. 2017;18(1):104.

42. Xiao Y, Xiong J, Mao D, Liu L, Li J, Li X, et al. Early-onset epileptic encephalopathy with de novo SCN8A mutation. Epilepsy Res. 2018;139:9-13.

43. Zaman T, Abou Tayoun A, Goldberg EM. A single-center SCN8A-related epilepsy cohort: clinical, genetic, and physiologic characterization. Ann Clin Transl Neurol. 2019;6(8):1445-55.

44. Zuliani V, Rapalli A, Patel MK, Rivara M. Sodium channel blockers: a patent review (2010 - 2014). Expert Opin Ther Pat. 2015;25(3):279-90.

45. Vohora D, Saraogi P, Yazdani MA, Bhowmik M, Khanam R, Pillai KK. Recent advances in adjunctive therapy for epilepsy: focus on sodium channel blockers as third-generation antiepileptic drugs. Drugs Today (Barc). 2010;46(4):265-77.

46. Rogawski MA, Loscher W. The neurobiology of antiepileptic drugs. Nat Rev Neurosci. 2004;5(7):553-64.

47. Dilena R, Striano P, Gennaro E, Bassi L, Olivotto S, Tadini L, et al. Efficacy of sodium channel blockers in SCN2A early infantile epileptic encephalopathy. Brain Dev. 2017;39(4):345-8.

48. Moller RS, Johannesen KM. Precision Medicine: SCN8A Encephalopathy Treated with Sodium Channel Blockers. Neurotherapeutics. 2016;13(1):190-1.

49. Ijff DM, Aldenkamp AP. Chapter 73 - Cognitive side-effects of antiepileptic drugs in children. In: Dulac O, Lassonde M, Sarnat HB, editors. Handbook of Clinical Neurology. 111: Elsevier; 2013. p. 707-18.

50. Hessen E, Lossius MI, Reinvang I, Gjerstad L. Influence of major antiepileptic drugs on attention, reaction time, and speed of information processing: results from a randomized, double-blind, placebo-controlled withdrawal study of seizure-free epilepsy patients receiving monotherapy. Epilepsia. 2006;47(12):2038-45.

51. Watkins L, O'Dwyer M, Oak K, Lawthom C, Maguire M, Thomas R, et al. The evidence for switching dibenzazepines in people with epilepsy. Acta Neurol Scand. 2020.

52. Fricke-Galindo I, A LL, Jung-Cook H, Lopez-Lopez M. Carbamazepine adverse drug reactions. Expert Rev Clin Pharmacol. 2018;11(7):705-18.

53. Helbig I, Ellis CA. Personalized medicine in genetic epilepsies - possibilities, challenges, and new frontiers. Neuropharmacology. 2020;172:107970.

54. Zuliani V, Fantini M, Rivara M. Sodium channel blockers as therapeutic target for treating epilepsy: recent updates. Curr Top Med Chem. 2012;12(9):962-70.

55. Stevens M, Peigneur S, Tytgat J. Neurotoxins and their binding areas on voltage-gated sodium channels. Front Pharmacol. 2011;2:71.

56. Benarroch EE. Sodium channels and pain. Neurology. 2007;68(3):233-6.

57. Lattanzi S, Brigo F, Cagnetti C, Verrotti A, Zaccara G, Silvestrini M. Eslicarbazepine acetate in the treatment of adults with partial-onset epilepsy: an evidence-based review of efficacy, safety and place in therapy. Core Evid. 2018;13:21-31.

58. Bialer M, Soares-da-Silva P. Pharmacokinetics and drug interactions of eslicarbazepine acetate. Epilepsia. 2012;53(6):935-46.

59. Willems LM, Zollner JP, Paule E, Schubert-Bast S, Rosenow F, Strzelczyk A. Eslicarbazepine acetate in epilepsies with focal and secondary generalised seizures: systematic review of current evidence. Expert Rev Clin Pharmacol. 2018;11(3):309-24.

60. Galiana GL, Gauthier AC, Mattson RH. Eslicarbazepine Acetate: A New Improvement on a Classic Drug Family for the Treatment of Partial-Onset Seizures. Drugs R D. 2017;17(3):329-39.

61. Singh RP, Asconape JJ. A review of eslicarbazepine acetate for the adjunctive treatment of partial-onset epilepsy. J Cent Nerv Syst Dis. 2011;3:179-87.

62. Elger C, Bialer M, Falcao A, Vaz-da-Silva M, Nunes T, Almeida L, et al. Pharmacokinetics and tolerability of eslicarbazepine acetate and oxcarbazepine at steady state in healthy volunteers. Epilepsia. 2013;54(8):1453-61.

63. Almeida L, Falcao A, Maia J, Mazur D, Gellert M, Soares-da-Silva P. Single-dose and steady-state pharmacokinetics of eslicarbazepine acetate (BIA 2-093) in healthy elderly and young subjects. J Clin Pharmacol. 2005;45(9):1062-6.

64. Falcao A, Fuseau E, Nunes T, Almeida L, Soares-da-Silva P. Pharmacokinetics, drug interactions and exposure-response relationship of eslicarbazepine acetate in adult patients with partial-onset seizures: population pharmacokinetic and pharmacokinetic/pharmacodynamic analyses. CNS Drugs. 2012;26(1):79-91.

65. Soares-da-Silva P, Pires N, Bonifacio MJ, Loureiro AI, Palma N, Wright LC. Eslicarbazepine acetate for the treatment of focal epilepsy: an update on its proposed mechanisms of action. Pharmacol Res Perspect. 2015;3(2):e00124.

66. Doeser A, Dickhof G, Reitze M, Uebachs M, Schaub C, Pires NM, et al. Targeting pharmacoresistant epilepsy and epileptogenesis with a dual-purpose antiepileptic drug. Brain. 2015;138(Pt 2):371-87.

67. Shorvon SD, Trinka E, Steinhoff BJ, Holtkamp M, Villanueva V, Peltola J, et al. Eslicarbazepine acetate: its effectiveness as adjunctive therapy in clinical trials and open studies. J Neurol. 2017;264(3):421-31.

68. Assenza G, Mecarelli O, Lanzone J, Assenza F, Tombini M, Di Lazzaro V, et al. The ROME (Retrospective Observational Multicenter study on Eslicarbazepine) study: Efficacy and behavioural effects of Eslicarbazepine acetate as adjunctive therapy for adults with partial onset seizures in real life. Seizure. 2018;58:35-40.

69. Jozwiak S, Veggiotti P, Moreira J, Gama H, Rocha F, Soares-da-Silva P. Effects of adjunctive eslicarbazepine acetate on neurocognitive functioning in children with refractory focal-onset seizures. Epilepsy Behav. 2018;81:1-11.

70. Klein P, Friedman A, Hameed MQ, Kaminski RM, Bar-Klein G, Klitgaard H, et al. Repurposed molecules for antiepileptogenesis: Missing an opportunity to prevent epilepsy? Epilepsia. 2020;61(3):359-86.

71. Pitkanen A, Lukasiuk K, Dudek FE, Staley KJ. Epileptogenesis. Cold Spring Harb Perspect Med. 2015;5(10).

72. Ho SN, Hunt HD, Horton RM, Pullen JK, Pease LR. Site-directed mutagenesis by overlap extension using the polymerase chain reaction. Gene. 1989;77(1):51-9.

73. Reikofski J, Tao BY. Polymerase chain reaction (PCR) techniques for site-directed mutagenesis. Biotechnol Adv. 1992;10(4):535-47.

74. Wood JN, Bevan SJ, Coote PR, Dunn PM, Harmar A, Hogan P, et al. Novel cell lines display properties of nociceptive sensory neurons. Proc Biol Sci. 1990;241(1302):187-94.

75. Felgner PL, Gadek TR, Holm M, Roman R, Chan HW, Wenz M, et al. Lipofection: a highly efficient, lipid-mediated DNA-transfection procedure. Proc Natl Acad Sci U S A. 1987;84(21):7413-7.

76. Hedrich UB, Liautard C, Kirschenbaum D, Pofahl M, Lavigne J, Liu Y, et al. Impaired action potential initiation in GABAergic interneurons causes hyperexcitable networks in an epileptic mouse model carrying a human Na(V)1.1 mutation. J Neurosci. 2014;34(45):14874-89.

77. Beaudoin GM, 3rd, Lee SH, Singh D, Yuan Y, Ng YG, Reichardt LF, et al. Culturing pyramidal neurons from the early postnatal mouse hippocampus and cortex. Nat Protoc. 2012;7(9):1741-54.

78. Moutin E, Hemonnot AL, Seube V, Linck N, Rassendren F, Perroy J, et al. Procedures for Culturing and Genetically Manipulating Murine Hippocampal Postnatal Neurons. Front Synaptic Neurosci. 2020;12:19.

79. Bean BP. The action potential in mammalian central neurons. Nat Rev Neurosci. 2007;8(6):451-65.

80. Hodgkin AL, Huxley AF. A quantitative description of membrane current and its application to conduction and excitation in nerve. J Physiol. 1952;117(4):500-44.

81. Cole KS, Moore JW. Potassium ion current in the squid giant axon: dynamic characteristic. Biophys J. 1960;1:1-14.

82. Neher E, Sakmann B. Single-channel currents recorded from membrane of denervated frog muscle fibres. Nature. 1976;260(5554):799-802.

83. Hamill OP, Marty A, Neher E, Sakmann B, Sigworth FJ. Improved patch-clamp techniques for high-resolution current recording from cells and cell-free membrane patches. Pflugers Arch. 1981;391(2):85-100.

84. Liem LK, Simard JM, Song Y, Tewari K. The patch clamp technique. Neurosurgery. 1995;36(2):382-92.

85. Bebarova M. Advances in patch clamp technique: towards higher quality and quantity. Gen Physiol Biophys. 2012;31(2):131-40.

86. Rubaiy HN. A Short Guide to Electrophysiology and Ion Channels. J Pharm Pharm Sci. 2017;20:48-67.

87. Brown AP, Greenberg HZ. Patch clamp. Br J Hosp Med (Lond). 2016;77(5):C74-7.